Electronic Supplementary Material (ESI) for Dalton Transactions.

Electronic Supplementary Information for

Variation in pnictogen–oxygen bonding unlocks greatly enhanced Brønsted basicity for the monomeric stibine oxide

John S. Wenger,[a] Addis Getahun,[a] and Timothy C. Johnstone[a]*

[a] Department of Chemistry and Biochemistry, University of California Santa Cruz, Santa Cruz, California 95064, United States.

CONTENTS

	Page
General methods	3
Discussion of intramolecular C–H activation product **3**	8
References	9
Figures S1 - S5: ^{1}H NMR, ^{13}C NMR, ^{19}F NMR, IR spectra, and PXRD of **2a**	10
Figures S6 - S10: ^{1}H NMR, ^{13}C NMR, ^{19}F NMR, IR spectra, and PXRD of **2b**·$CHCl_3$	12
Figures S11 - S14: ^{1}H NMR, ^{13}C NMR, ^{31}P NMR, and ^{19}F NMR spectra of **2c**	15
Figures S15 - S18: ^{1}H NMR, ^{13}C NMR, ^{31}P NMR, and ^{19}F NMR of a 1:1 mixture of **1c** and triflic acid	17
Figures S19 - S22: ^{1}H NMR, ^{13}C NMR, IR spectra, and PXRD of **4a**	19
Figures S23 - S26: ^{1}H NMR, ^{13}C NMR, IR spectra, and PXRD of **4b**·¾(C_6H_{12})	21
Figures S27 - S30: ^{1}H NMR, ^{13}C NMR, IR spectra, and PXRD of **5**·2($CHCl_3$)	23
Figures S31 - S34: ^{1}H NMR, ^{13}C NMR, IR spectra, and PXRD of **6**	25
Figures S35 - S42: ^{1}H NMR and ^{19}F NMR spectra of transesterification reaction mixtures	27
Figures S43 - S52: Thermal ellipsoid plots of **2a**-**c**, **3**, **4a**-**b**, **5**, **6**, and **6**·*p*-nitrophenol	32
Figures S53 - S54: Ball and stick representations of **1a**-**c**H^+ and phenols/oxides	42
Figures S55: Thermal ellipsoid plots of **3**	43
Figures S56: Ball and stick representations of **3**$^+$, **3**$^+$(As), and **3**$^+$(Sb)	44
Figures S57 - S59: Topological analysis of **1a**-**c**H^+	44
Figures S60: Non-covalent interaction (NCI) analysis of **1a**-**c**H^+	46
Figures S61: Space-filling diagrams of **1a**-**c**H^+	47
Table S1: Calculated reaction enthalpies and Gibbs free energies for H_2 elimination from **1a**-**c**H^+	47
Tables S2 - S4: Crystallographic parameters	48
Tables S5 - S7: Select data from NMR monitoring of titration of **2a** with triethylamine	51
Tables S8 - S10: Select data from NMR monitoring of titration of **2b** with acridine	54
Table S11: Natural population analysis of **1a**-**c**H^+	57
Tables S12 - S24: Optimized coordinates of **1a**-**c**H^+, phenols/oxides, **3**$^+$, **3**$^+$(As), **3**$^+$(Sb), and H_2	57

General methods. Reagents and solvents were purchased from commercial vendors and used as received unless otherwise specified. 1-Bromo-2,6-diisopropylbenzene, *p*-nitrophenyl acetate, iodosobenzene, $Dipp_3SbO$ (**1a**), $Dipp_3AsO$ (**1b**), and $Dipp_3PO$ (**1c)** were prepared using established procedures.[1-3] **Picric acid is explosive and should be handled with caution**. Triethylamine was freshly distilled before use. Dichloromethane (DCM) was purified using an Innovative Technology PURE-SOLV solvent purification system. All solvents were dried over 3-Å molecular sieves. NMR spectra were collected using a Bruker Avance III HD 500 spectrometer equipped with a multinuclear Smart Probe. Signals in the ^{1}H and ^{13}C NMR spectra are reported in ppm as chemical shifts from tetramethylsilane and were referenced using the $CHCl_3$ (^{1}H, 7.26 ppm), CHD_2CN (^{1}H, 1.94 ppm), $CDCl_3$ (^{13}C, 77.16 ppm), and CD_3CN (^{13}C, 118.26 ppm) solvent signals. The frequencies of ^{19}F NMR signals are reported in ppm as chemical shifts from $CFCl_3$ (referenced to $BF_3{\cdot}Et_2O$ at –152.8 ppm). ^{31}P NMR spectra were reported as chemical shifts from 85% H_3PO_4 and were referenced using triphenylphosphine (–5.35 ppm). Infrared (IR) spectra were collected on KBr pellets using a PerkinElmer Spectrum One FT-IR spectrometer. Mass spectrometry measurements were collected using an LTQ-Orbitrap Velos Pro MS instrument.

Synthesis of tris(2,6-diisopropylphenyl)hydroxystibonium trifluoromethanesulfonate ($[Dipp_3SbOH][O_3SCF_3]$) (2a). Triflic acid (9.3 µL, 0.11 mmol) was added to a solution of **1a** (66 mg, 0.11 mmol) in DCM (2 mL). The reaction mixture was transferred under a layer of hexanes. Colorless crystals suitable for X-ray diffraction formed overnight, and the mixture was cooled to –20 °C for 1 h to drive crystallization. The mother liquor was decanted and the product was washed with pentane (3 x 5 mL). Yield: 69 mg (85%). M.p. 308 °C (decomposed). **MS (*m/z*) $[M–O_3SCF_3]^+$** 621.305 (calc 621.305). **^{1}H NMR (500 MHz, CD_3CN)** δ 7.72 (t, *J* = 7.7 Hz, 3H), 7.59 (dd, *J* = 7.7, 1.1 Hz, 3H), 7.53 (dd, *J* = 7.7, 1.1 Hz, 3H), 4.71 (br s, 1H), 2.87 (sept, *J* = 6.4 Hz, 3H), 2.78 (sept, *J* = 6.3 Hz, 3H), 1.37 (d, *J* = 6.4 Hz, 9H), 1.25 (d, *J* = 6.5 Hz, 9H), 1.03 (d, *J* = 6.5 Hz, 9H), 0.90 (d, *J* = 6.4 Hz, 9H). **$^{13}C\{^{1}H\}$ NMR (125 MHz, CD_3CN)** δ 155.76, 153.75, 137.78, 135.49, 129.58, 128.43, 40.56, 37.81, 26.21, 25.26, 24.73, 24.22. **^{19}F NMR (470 MHz, $CDCl_3$)** δ –77.88.

Synthesis of tris(2,6-diisopropylphenyl)hydroxyarsonium trifluoromethanesulfonate chloroform solvate ($[Dipp_3AsOH][O_3SCF_3]{\cdot}CHCl_3$) (2b·$CHCl_3$). Triflic acid (8.3 µL, 0.093 mmol) was added to a solution of **1b** (53.7 mg, 0.093 mmol) in $CHCl_3$ (1 mL). Pentane was allowed to transfer into the reaction mixture by vapor diffusion. Colorless crystals suitable for X-ray diffraction formed overnight. The mother liquor was decanted and the product was washed with pentane (3 x 3 mL). Yield: 44 mg (56%). M.p. 249 °C (decomposed). **MS (*m/z*) $[M–O_3SCF_3]^+$** 575.323 (calc 575.323). **^{1}H NMR (500 MHz, $CDCl_3$)** δ 7.63 (t, *J* = 7.8 Hz, 3H), 7.48 (d, *J* = 7.8 Hz, 3H), 7.34 (d, *J* = 7.7 Hz, 3H), 7.01 (s, 1H), 3.09 (sept, *J* = 6.3 Hz, 3H), 2.90 (sept, *J* = 6.4 Hz, 3H), 1.41 (d, *J* = 6.4 Hz, 9H), 1.19 (d, *J* = 6.6 Hz, 9H), 0.97 (d, *J* = 6.5 Hz, 9H), 0.83 (d, *J* = 6.4 Hz, 9H). **$^{13}C\{^{1}H\}$ NMR (125 MHz, $CDCl_3$)** δ 154.26, 150.80, 135.69, 134.33, 129.06, 126.99, 35.42, 33.88, 26.07, 25.32, 24.88, 23.82. **^{19}F NMR (470 MHz, $CDCl_3$)** δ –77.80.

Crystal growth of tris(2,6-diisopropylphenyl)hydroxyphosphonium trifluoromethanesulfonate (2c). Triflic acid (8 µL, 0.09 mmol) was added to a solution of **1c** (49.2 mg, 0.09 mmol) in DCM (0.7 mL). Colorless crystals of **2c** were grown by allowing the solution to slowly concentrate by evaporation, but not to dryness. The product was characterized by single-crystal X-ray diffraction. A portion of the crystals of **2c** grown in this manner were dissolved in $CDCl_3$ and characterized by NMR spectroscopy. **^{1}H NMR (500 MHz, $CDCl_3$)** δ 7.61 (td, *J* = 7.8, 1.6 Hz, 3H), 7.46 (ddd, *J* = 7.8, 4.5, 1.1 Hz, 3H), 7.37 – 7.30 (m, 3H), 5.12 (s, 4H), 3.26 (sept, *J* = 6.4 Hz, 3H), 2.82 (sept, *J* = 6.4 Hz, 3H), 1.36 (d, *J* = 6.5 Hz, 9H), 1.14 (d, *J* = 6.6 Hz, 9H), 0.96 (d, *J* = 6.5 Hz, 9H), 0.75 (d, *J* = 6.4 Hz, 9H). **$^{13}C\{^{1}H\}$ NMR (125 MHz, $CDCl_3$)** δ 156.26 (d, *J* = 9.0 Hz), 152.23 (d, *J* = 15.5 Hz), 134.35 (d, *J* = 2.6 Hz), 130.52 (d, *J* = 95.5 Hz), 128.30 (d, *J* = 11.2 Hz),

126.52 (d, *J* = 12.2 Hz), 33.85 (d, *J* = 7.6 Hz), 33.16 (d, *J* = 4.3 Hz), 26.08, 25.19, 24.85, 23.91. **^{19}F NMR (470 MHz, $CDCl_3$)** δ –78.09. **^{31}P NMR (470 MHz, $CDCl_3$)** δ 52.15. NMR spectra were also collected on a mixture of **1c** (5 mg, 9 μmol) and triflic acid (0.8 μL, 9 μmol) in $CDCl_3$ (550 μL) and are consistent with the formation of **2c** in solution. When pentane was allowed to diffuse into a solution of triflic acid (7.8 μL, 0.089 μmol) and **1c** (47 mg, 0.089 mmol) in chloroform (1 mL), an oil was produced. The oil was redissolved in DCM and addition of hexanes produced a small batch of crystals of **3**, which were characterized by single-crystal X-ray diffraction.

Synthesis of tris(2,6-diisopropylphenyl)hydroxystibonium 2,4,6-trinitrophenoxide ([$Dipp_3SbOH$][$OPh(NO_2)_3$]) (4a). Picric acid (20 mg, 0.088 mmol) was added to a solution of **1a** (55 mg, 0.088 mmol) in $CHCl_3$ (1 mL) to form a bright yellow solution. Pentane was allowed to transfer into the reaction mixture by vapor diffusion. Yellow crystals suitable for X-ray diffraction formed overnight. The mother liquor was decanted and the product was washed with pentane (3 x 3 mL). Yield: 51 mg (71%). The melting point was not measured because of the known exothermic reactivity of picric acid and picrate salts. **MS (*m/z*) [M–$(O_2N)_3PhO$]$^+$** 621.305 (calc 621.305). **^{1}H NMR (500 MHz, $CDCl_3$)** δ 8.75 (s, 2H), 7.59 (t, *J* = 7.7 Hz, 3H), 7.39 (dd, *J* = 7.7, 1.2 Hz, 3H), 7.35 (dd, *J* = 7.7, 1.2 Hz, 3H), 3.19 (sept, *J* = 6.3 Hz, 3H), 2.86 (sept, *J* = 6.4 Hz, 3H), 1.31 (d, *J* = 6.3 Hz, 9H), 1.24 (d, *J* = 6.6 Hz, 9H), 0.96 (d, *J* = 6.5 Hz, 9H), 0.91 (d, *J* = 6.4 Hz, 9H). **^{13}C{^{1}H} NMR (125 MHz, $CDCl_3$)** δ 161.04, 155.98, 152.35, 141.71, 137.67, 133.93, 128.33, 126.89, 126.75, 126.42, 39.05, 36.65, 26.27, 25.29, 24.94, 24.23.

Synthesis of tris(2,6-diisopropylphenyl)hydroxyarsonium 2,4,6-trinitrophenoxide cyclohexane solvate ([$Dipp_3AsOH$][$OPh(NO_2)_3$]·¾(C_6H_{12})) (4b·¾(C_6H_{12})). Picric acid (24 mg, 0.11 mmol) was added to a solution of **1b** (60 mg, 0.11 mmol) in DCM (2 mL) to form a bright yellow solution. The reaction mixture was transferred under a layer of cyclohexane. Yellow crystals suitable for X-ray diffraction formed overnight. The mother liquor was decanted and the product was washed with pentane (3 x 3 mL). Yield: 45 mg (50%). The melting point was not measured because of the known exothermic reactivity of picric acid and picrate salts. **MS (*m/z*) [M–$(O_2N)_3PhO$]$^+$** 575.323 (calc 575.323). **^{1}H NMR (500 MHz, $CDCl_3$)** δ 8.76 (s, 2H), 7.57 (t, *J* = 7.7 Hz, 3H), 7.38 (d, *J* = 7.2 Hz, 3H), 7.34 (d, *J* = 7.7 Hz, 3H), 3.15 (sept, *J* = 6.3 Hz, 3H), 3.12 (sept, *J* = 6.3 Hz, 3H), 1.42 (s, 8H), 1.27 (d, *J* = 6.4 Hz, 9H), 1.19 (d, *J* = 6.6 Hz, 9H), 0.89 (d, *J* = 6.5 Hz, 9H), 0.85 (d, *J* = 6.4 Hz, 9H). **^{13}C{^{1}H} NMR (125 MHz, $CDCl_3$)** δ 160.23, 154.67, 150.77, 141.55, 136.35, 133.82, 128.45, 127.51, 126.83, 126.36, 35.09, 33.44, 27.06, 26.05, 25.41, 25.16, 23.84.

Synthesis of tris(2,6-diisopropylphenyl)hydroxystibonium 2,4-dinitrophenoxide chloroform disolvate ([$Dipp_3SbOH$][$OPh(NO_2)_2$]·2($CHCl_3$)) (5·2($CHCl_3$)). 2,4-Dinitrophenol (14.8 mg, 0.080 mmol) and **1a** (50 mg, 0.080 mmol) were dissolved in $CHCl_3$ (1.5 mL). The bright yellow solution was transferred under a layer of cyclohexane (18 mL). Yellow crystals suitable for X-ray diffraction grew overnight. The solvent was decanted and the crystals were washed with pentane (5 mL). Yield: 41 mg (49%). M.p. 186 °C (decomposed). **MS (*m/z*) [M–$(O_2N)_2PhO$]$^+$** 621.305 (calc 621.305). **^{1}H NMR (500 MHz, $CDCl_3$)** δ 8.80 (d, *J* = 3.0 Hz, 1H), 7.86 (dd, *J* = 9.6, 3.0 Hz, 1H), 7.57 (t, *J* = 7.7 Hz, 3H), 7.40 (d, *J* = 6.9 Hz, 3H), 7.32 (d, *J* = 7.6 Hz, 3H), 6.30 (d, *J* = 9.6 Hz, 1H), 3.40 (sept, *J* = 5.9 Hz, 3H), 2.88 (sept, *J* = 6.3 Hz, 3H), 1.34 (d, *J* = 6.3 Hz, 9H), 1.23 (d, *J* = 6.5 Hz, 9H), 0.96 (d, *J* = 6.5 Hz, 9H), 0.86 (d, *J* = 6.4 Hz, 9H). **^{13}C{^{1}H} NMR (125 MHz, $CDCl_3$)** δ 156.25, 152.32, 138.28, 136.55, 133.57, 128.41, 128.26, 126.51, 124.92, 124.35, 38.51, 36.28, 27.06, 26.52, 25.17, 24.73, 24.48.

Synthesis of tris(2,6-diisopropylphenyl)stibine oxide 4-nitrophenol adduct ($Dipp_3SbO$·$HOPhNO_2$) (6). 4-Nitrophenol (3.3 mg, 0.024 mmol) and **1a** (15 mg, 0.024 mmol) were dissolved in $CHCl_3$ (1 mL). The bright yellow solution was transferred under a layer of cyclohexane (18 mL). Yellow crystals suitable for

X-ray diffraction grew overnight. The solvent was decanted and the crystals were washed with pentane (5 mL). Yield: 6 mg (32%). M.p. 224 °C (decomposed). **MS (*m/z*) [M–O_2NPhO]$^+$** 621.305 (calc 621.305). **^{1}H NMR (500 MHz, $CDCl_3$)** δ 8.00 (d, *J* = 9.2 Hz, 2H), 7.48 (t, *J* = 7.7 Hz, 3H), 7.36 (d, *J* = 7.5 Hz, 3H), 7.23 (d, *J* = 7.6 Hz, 3H), 6.90 (d, *J* = 9.2 Hz, 2H), 3.99 (br sept, *J* = 6.3 Hz, 3H), 2.95 (sept, *J* = 6.3 Hz, 3H), 1.35 (d, *J* = 5.7 Hz, 9H), 1.19 (d, *J* = 6.1 Hz, 9H), 0.96 (d, *J* = 6.3 Hz, 9H), 0.77 (d, *J* = 6.0 Hz, 9H). **^{13}C{^{1}H} NMR (125 MHz, $CDCl_3$)** δ 156.69, 152.21, 140.38, 138.32, 132.43, 128.23, 127.52, 126.22, 125.82, 116.58, 37.48, 34.77, 26.78, 25.07, 24.69.

Titration of 2a with triethylamine. A solution of **2a** (2.5 mg, 4.0 μmol) in d_3-MeCN (600 μL) was prepared. Triethylamine (100 μL) was diluted in d_3-MeCN (900 μL). NMR spectra were collected after addition of aliquots of the triethylamine solution or pure triethylamine (Tables S5 - S7). The experiment was performed in triplicate.

Titration of 2b with acridine. A solution of **2b** (1.5 mg, 2.6 μmol) in d_3-MeCN (500 μL) was prepared. A separate solution of acridine (37.1 mg, 0.2 mmol) in d_3-MeCN (750 μL) was prepared. NMR spectra were collected after addition of aliquots of the acridine solution (Table S8 - S10). For the final data points, solid acridine was added to the sample. The experiment was performed in triplicate.

General transesterification reaction. A solution of *p*-nitrophenyl acetate (13.4 mg, 0.074 mmol), 2,2,2-trifluoroethanol (10 equiv, 53.2 μL, 0.74 mmol), and catalyst (0.2 equiv, 0.015 mmol) in $CDCl_3$ (500 μL) was prepared and transferred to an NMR tube. The NMR tube was heated to 50 °C in an oil bath. ^{1}H and ^{19}F NMR spectra were collected on the samples to monitor the reaction after 26 h (Figures S35 - S42).

X-ray crystallography: Independent Atom Model (IAM). Crystals of **2a**, **2b**·$CHCl_3$, **2c**, **3**, **4a**, **4b**·¾(C_6H_{12}), **5**·2($CHCl_3$), **6**, and **6**·*p*-nitrophenol were grown as described above, selected under a microscope, loaded onto a MiTeGen polyimide sample loop using Paratone-N, and mounted onto a Rigaku XtaLAB Synergy-S single-crystal diffractometer. Each crystal was cooled to 100 K under a stream of nitrogen. Diffraction of Mo Kα or Cu Kα radiation from a PhotonJet-S microfocus source was detected using a HyPix6000HE hybrid photon counting detector. Screening, indexing, data collection, and data processing were performed with CrysAlisPro.[4] The structures were solved using SHELXT and refined using SHELXL following established strategies.[5-7] All non-H atoms were refined anisotropically. C-bound H atoms were placed at calculated positions and refined with a riding model and coupled isotropic displacement parameters (1.2 × U_{eq} for aryl and methylene groups and 1.5 × U_{eq} for methyl groups). O-bound H atoms were located in the Fourier difference map and refined semi-freely, employing distance restraints. Disordered atoms were treated with distance, similarity, and rigid-bond restraints.

X-ray crystallography: Hirshfeld atom refinement (HAR). The IAM results for **6** and **6**·*p*-nitrophenol were used as input for the *NoSpherA2* implementation of HAR in *Olex2* (version 1.5).[8] The quantum chemistry calculations were performed by ORCA (version 5.0.1).[9, 10] A wavefunction was calculated with high integration accuracy and tight SCF convergence criteria using the PBE0 hybrid functional and the x2c-TZVPP all-electron relativistically contracted basis set.[11-14] The effects of relativity were introduced using the second-order Douglass-Kroll-Hess formalism.[15] Least-squares crystallographic refinement was carried out with the *olex2.refine* engine.[16] The ADPs and positions of non-H atoms were freely refined using the aspherical atomic form factors obtained from Hirshfeld stockholder partitioning of the theoretical electron density obtained from the computed wavefunction.[17] C-bound H-atom positions were refined semi-freely; distance restraints were applied to chemically similar C–H bond lengths. H-atom isotropic thermal parameters were refined freely. The positional and isotropic thermal parameters of O-bound H atoms were refined freely. The newly refined atomic coordinates were used as the input

for a new density functional theory (DFT) calculation, from which new aspherical form factors were obtained. This procedure was iterated until it had converged.

Powder X-ray diffraction (PXRD). Bulk samples of were ground using an agate mortar and pestle. The fine white powders were each loaded onto a MiTeGen polyimide sample loop using Paratone-N and mounted onto a Rigaku XtaLAB Synergy-S single-crystal diffractometer. The powder was cooled to 100 K under a stream of nitrogen. The diffraction of Cu Kα radiation was collected while the sample underwent a Gandolfi scan. Data collection and processing were performed using CrysAlisPro. Simulated PXRD diffractograms were generated from the crystal structures of **2a**, **2b**·$CHCl_3$ triclinic, **2c**, **3**, **4a**, **4b**·¾(C_6H_{12}), **5**·2($CHCl_3$), and **6** using Mercury and compared to the experimentally determined diffractograms.

Computational experiments. Geometry optimizations were performed on **1a**-**c**, **1a**-**c**H^+, *p*-nitrophenol, *p*-nitrophenoxide, 2,4-dintrophenol, 2,4-dinitrophenoxide, picric acid, picrate, **3**$^+$, **3**$^+$(As), and **3**$^+$(Sb) at the PBE0/def2-TZVPP level of theory with the RIJCOSX approximation and def2/J auxiliary basis set in the gas phase.[11-13, 18, 19] Frequency calculations were performed at the same level of theory for **1a**-**c**, **1a**-**c**H^+, **3**$^+$, **3**$^+$(As), and **3**$^+$(Sb) in the gas phase. Proton affinities of **1a**-**c** were calculated by subtracting the enthalpy of the deprotonated species from that of the protonated species. Frequency calculations were then performed on **1a**-**c**, **1a**-**c**H^+, *p*-nitrophenol, *p*-nitrophenoxide, 2,4-dintrophenol, 2,4-dinitrophenoxide, picric acid, and picrate at the same level of theory including implicit DCM solvation. Isodesmic reaction free energies in DCM were calculated by subtracting the sum of the free energies of the products from that of the reactants. Energetic analysis of the elimination of H_2 from cations **1a**-**c**H^+ to form cyclized alkoxypnictonium cations **3**$^+$(Sb), **3**$^+$(As), and **3**$^+$, respectively, were performed by subtracting the sum of the Gibbs free energies of the cyclized alkoxyphosphonium and H_2 from that of the corresponding hydroxypnictonium cation. Single point energy calculations were performed using ORCA 5.0.0 or ORCA 5.0.1 on the optimized structures using the PBE0 hybrid functional and the old-DKH-TZVPP all-electron basis set using the RIJCOSX approximation and the SARC/J auxiliary basis set.[20-23] The effects of relativity were introduced using the second-order Douglass-Kroll-Hess formalism (DKH).[15] Single point energy calculations were used to generate wavefunctions that were subject to topological and Natural Bond Orbital (NBO) analyses. Topological analysis of the electron density was performed in MultiWFN (version 3.7).[24] Bond paths were visualized in MultiWFN (version 3.7). The values of the real space functions ρ, $\nabla^2\rho$, and ε along interatomic vectors were visualized using R (version 4.0.2) through RStudio (version 1.3.1073). The following R packages were used for analysis and visualization: ggplot2, tidyverse, gridExtra, ggtext, scales, ggbreak, and grid.[25] NBO analysis was performed using the NBO program (version 7.0.7).[26] Non-covalent interactions (NCI) were calculated using MultiWFN and the results were visualized in VMD.[27, 28]

pK_a determination from titration data. The observed chemical shift of the Pn-proximal benzylic proton resonance (the benzylic proton resonance that appears most downfield in pure pnictine oxide) was used to determine the percentage of deprotonated pnictine oxide in solution according to Equation 1. The percentage of pnictine oxide in solution, the initial moles of hydroxypnictonium in the sample, and the total volume can be used to determine the concentrations of pnictine oxide, hydroxypnictonium, free base titrant, and protonated titrant in the sample according to Equations 2-7. The equilibrium constant of Equations 8 and 9 (K_8) was obtained by non-linear regression of the data by the nls function in R of Equation 10. The known pK_a value of the titrant was then used to determine the pK_a of hydroxypnictonium, following equations 11-20.

1. $\frac{[\mathrm{PnO}]}{[\mathrm{PnO}]+[\mathrm{PnOH^+}]} = \frac{\delta(\mathrm{observed})-\delta(\mathrm{PnOH^+})}{\delta(\mathrm{PnO})-\delta(\mathrm{PnOH^+})}$

2. $\mathrm{Base} + \mathrm{PnOH^+} \rightleftharpoons \mathrm{PnO} + \mathrm{BaseH^+}$

3. $\text{mole PnO} = \text{mole PnOH}^+{}_0 * \frac{[\mathrm{PnO}]}{[\mathrm{PnO}]+[\mathrm{PnOH^+}]}$

4. $[\mathrm{PnO}] = \frac{\text{mole PnO}}{\text{Total Volume}}$

5. $[\mathrm{PnOH^+}] = \frac{\text{mole PnOH}^+{}_0 - \text{mole PnO}}{\text{Total Volume}}$

6. $[\mathrm{Base}] = \frac{\text{mole Based added} - \text{mole PnO}}{\text{Total Volume}}$

7. $[\mathrm{BaseH^+}] = [\mathrm{PnO}]$

8. $K_8 = \frac{[\mathrm{PnO}]\,[\mathrm{BaseH^+}]}{[\mathrm{Base}][\mathrm{PnOH^+}]}$

9. $K_8 = \frac{[\mathrm{PnO}]^2}{[\mathrm{Base}][\mathrm{PnOH^+}]}$

10. $[\mathrm{PnO}] = \sqrt{K_8[\mathrm{Base}][\mathrm{PnOH^+}]}$

11. $\mathrm{PnOH^+} \rightleftharpoons \mathrm{PnO} + \mathrm{H^+}$

12. $\mathrm{Base} + \mathrm{H^+} \rightleftharpoons \mathrm{BaseH^+}$

13. $\Delta G_8 = \Delta G_{11} + \Delta G_{12}$

14. $-RT\ln K_8 = -RT\ln K_{11} + (-RT\ln K_{12})$

15. $\ln K_8 = \ln(K_{11}K_{12})$

16. $K_8 = K_{11}K_{12}$

17. $\frac{K_8}{K_{12}} = K_{11}$

18. $K_\mathrm{a} = 10^{-\mathrm{p}K_\mathrm{a}}$

19. $K_{12} = \frac{1}{10^{-\mathrm{p}K_\mathrm{a}\text{ of base}}}$

20. $\mathrm{p}K_\mathrm{a}\text{ of PnO} = -\log(K_{11})$

Discussion of intramolecular C–H activation product 3. Compound **3** (Figure S55) is the result of the formal elimination of H_2 from **2c**. Although we were unable to independently synthesize **3**, its formation prompted a further investigation of the computationally optimized structures **1a**-**c**H^+. As noted in the main text, the hydroxy groups of **1a**-**c**H^+ are buried to a greater or lesser extent within the pocket created by the Dipp groups. A close inspection of the intramolecular interactions in which these hydroxyl groups engage revealed that a dihydrogen bond between the protic H atom and a methyl H atom is present in each case; **1c**H^+ features the shortest computed OH···HC distance at 1.786 Å, suggesting a bond strength comparable to conventional hydrogen bonds.[29] Although the heavier congeners engage in similar hydroxy-methyl interactions, the OH group of **1c**H^+ uniquely features a bifurcated dihydrogen bonding interaction in which the benzylic H atom appears at 1.833 Å. Topological analysis of the theoretical electron density (DKH-PBE0/old-DKH-TZVPP) of the isolated **1a-c**H^+ cations confirms the presence of a bond critical point between the dihydrogen-bonding H atoms in each case. The magnitude of ρ at the bond critical point becomes smaller as the pnictogen becomes heavier (Figures S57-S59). Furthermore, non-covalent interaction analysis[28] of **1a-c**H^+ reveals singularities in the reduced density gradient between the dihydrogen-bonding H atoms, but only in **1c**H^+ do the dihydrogen bonds appear at a negative sign(λ_2)ρ, indicating the strongest dihydrogen-bonding interaction in the series (Figure S60). As noted in the main text, natural population analysis reveals a systematic increase in the charge of the protic H atom from **1a**H^+ < **1b**H^+ < **1c**H^+. The increasing trend in dihydrogen bond strength from **1a**H^+ < **1b**H^+ < **1c**H^+ can be rationalized by multiple factors. First, the lower Brønsted basicity of the O atom in **1c** attenuates charge transfer to the proton, thus the corresponding O–H group of **1c**H^+ is a more polarized, potent H-bond donor. Second, as the pnictogen becomes smaller, the Dipp groups impose greater steric pressure on the hydroxyl group, shielding the hydroxyl group from intermolecular, stabilizing H-bonding interactions and positioning the isopropyl substituents in close contact with the protic H atom. Importantly, we verified that the dihydrogen bonding is not only present in the computed structures, but that it is borne out in the crystallography as well. Specifically, in the structure of **2c**, the triflate anion cannot donate to the extremely protic H atom because of the steric shielding from the Dipp groups, but an isopropyl substituent is poised to act as an H-bond acceptor. It is noteworthy that this arrangement is observed in both of the crystallographically independent units of the hydroxyphosphonium cation present in the crystal structure. The dihydrogen bond can be thought of as a pre-arrangement necessary for the reaction whereby **2c** produces **3** and H_2. Energetic analysis of the elimination of H_2 from cations **1a**-**c**H^+ to form cyclized alkoxypnictonium cations **3**$^+$(Sb), **3**$^+$(As), and **3**$^+$, respectively, was performed computationally (Table S1). In all cases, $\Delta G_{rxn} > 0$, but the lowest positive number was obtained in the case of **1c**H^+, consistent with the crystallographic observation of **3** but not the As or Sb analogs. Although the variations in Brønsted basicity/acidity that are the focus of this paper have informed our initial interpretation of this result as arising from a closed-shell process, we highlight that the final product could also be obtained via an open-shell mechanism. We have tried repeatedly to effect this transformation on a preparative scale without success, but efforts in this direction are ongoing.

References

1. M. Warsitz and S. Doye, *Chem.–Eur. J.*, 2020, **26**, 15121-15125.
2. K. Li, A. E. Weber, L. Tseng and S. J. Malcolmson, *Org. Lett.*, 2017, **19**, 4239-4242.
3. D. Chakraborty and R. Das, *Synthesis*, 2011, **2011**, 1621-1625.
4. Rigaku Oxford Diffraction, *CrysAlis^{Pro}*, 2020.
5. G. M. Sheldrick, *Acta Crystallogr. Sect. A*, 2015, **71**, 3-8.
6. G. M. Sheldrick, *Acta Crystallogr. Sect. C*, 2015, **71**, 3-8.
7. P. Müller, *Crystallogr. Rev.*, 2009, **15**, 57-83.
8. F. Kleemiss, O. V. Dolomanov, M. Bodensteiner, N. Peyerimhoff, L. Midgley, L. J. Bourhis, A. Genoni, L. A. Malaspina, D. Jayatilaka, J. L. Spencer, F. White, B. Grundkötter-Stock, S. Steinhauer, D. Lentz, H. Puschmann and S. Grabowsky, *Chem. Sci.*, 2021, **12**, 1675-1692.
9. F. Neese, *Wiley Interdiscip. Rev.-Comput. Mol. Sci*, 2012, **2**, 73-78.
10. F. Neese, *WIREs Comput. Mol. Sci*, 2018, **8**, e1327.
11. F. Weigend and R. Ahlrichs, *Phys. Chem. Chem. Phys.*, 2005, **7**, 3297-3305.
12. J. P. Perdew, M. Ernzerhof and K. Burke, *J. Chem. Phys.*, 1996, **105**, 9982-9985.
13. J. P. Perdew, K. Burke and M. Ernzerhof, *Phys. Rev. Lett.*, 1996, **77**, 3865-3868.
14. P. Pollak and F. Weigend, *J. Chem. Theory Comput.*, 2017, **13**, 3696-3705.
15. A. Wolf, M. Reiher and B. A. Hess, *J. Chem. Phys.*, 2002, **117**, 9215-9226.
16. O. V. Dolomanov, L. J. Bourhis, R. J. Gildea, J. A. K. Howard and H. Puschmann, *J. Appl. Crystallogr.*, 2009, **42**, 339-341.
17. F. L. Hirshfeld, *Theor. Chim. Acta*, 1977, **44**, 129-138.
18. F. Weigend, *Phys. Chem. Chem. Phys.*, 2006, **8**, 1057.
19. F. Neese, F. Wennmohs, A. Hansen and U. Becker, *Chem. Phys.*, 2009, **356**, 98-109.
20. D. A. Pantazis, X.-Y. Chen, C. R. Landis and F. Neese, *J. Chem. Theory Comput.*, 2008, **4**, 908-919.
21. D. A. Pantazis and F. Neese, *J. Chem. Theory Comput.*, 2009, **5**, 2229-2238.
22. D. A. Pantazis and F. Neese, *J. Chem. Theory Comput.*, 2011, **7**, 677-684.
23. D. A. Pantazis and F. Neese, *Theor. Chem. Acc.*, 2012, **131**, 1292.
24. T. Lu and F. Chen, *J. Comput. Chem.*, 2012, **33**, 580-592.
25. S. Xu, M. Chen, T. Feng, L. Zhan, L. Zhou and G. Yu, *Front. Genet.*, 2021, **12**, 774846.
26. E. D. Glendening, C. R. Landis and F. Weinhold, *J. Comput. Chem.*, 2019, **40**, 2234-2241.
27. W. Humphrey, A. Dalke and K. Schulten, *J. Mol. Graph.*, 1996, **14**, 33-38.
28. E. R. Johnson, S. Keinan, P. Mori-Sánchez, J. Contreras-García, A. J. Cohen and W. Yang, *J. Am. Chem. Soc.*, 2010, **132**, 6498-6506.
29. H. Cybulski, E. Tymińska and J. Sadlej, *ChemPhysChem*, 2006, **7**, 629-639.

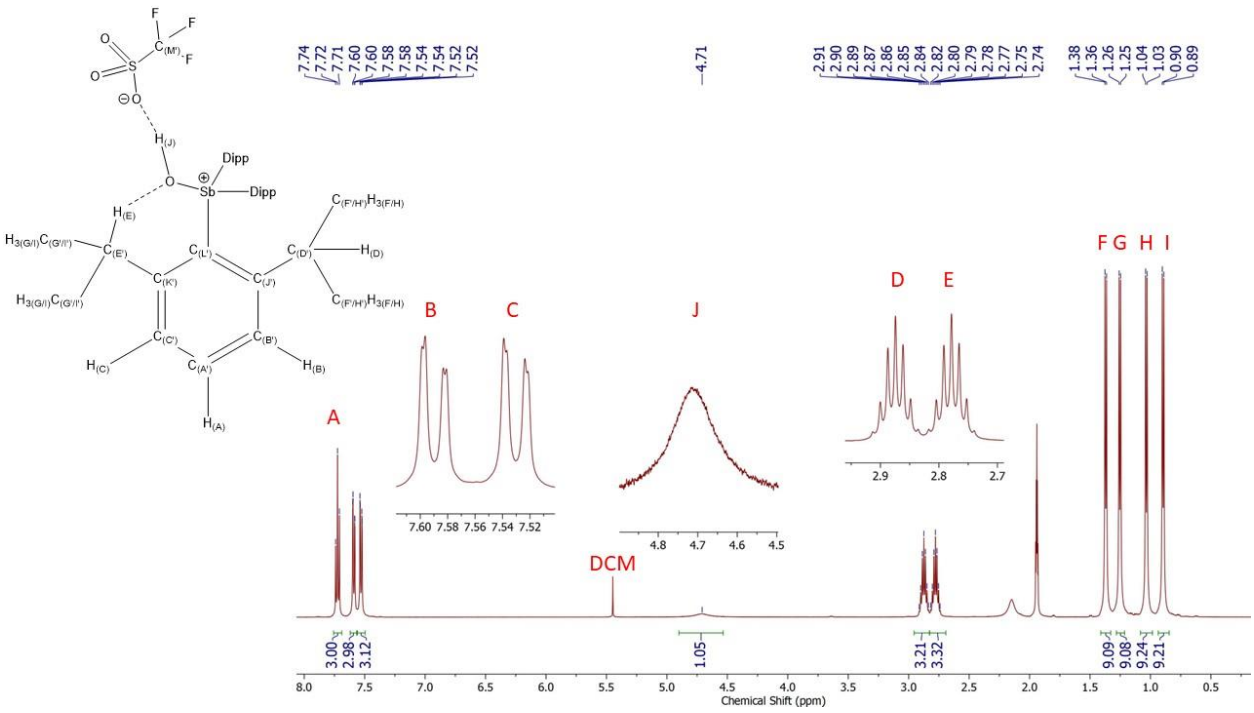

Figure S1. ^{1}H NMR spectrum (CD_3CN, 500 MHz) of **2a** at room temperature.

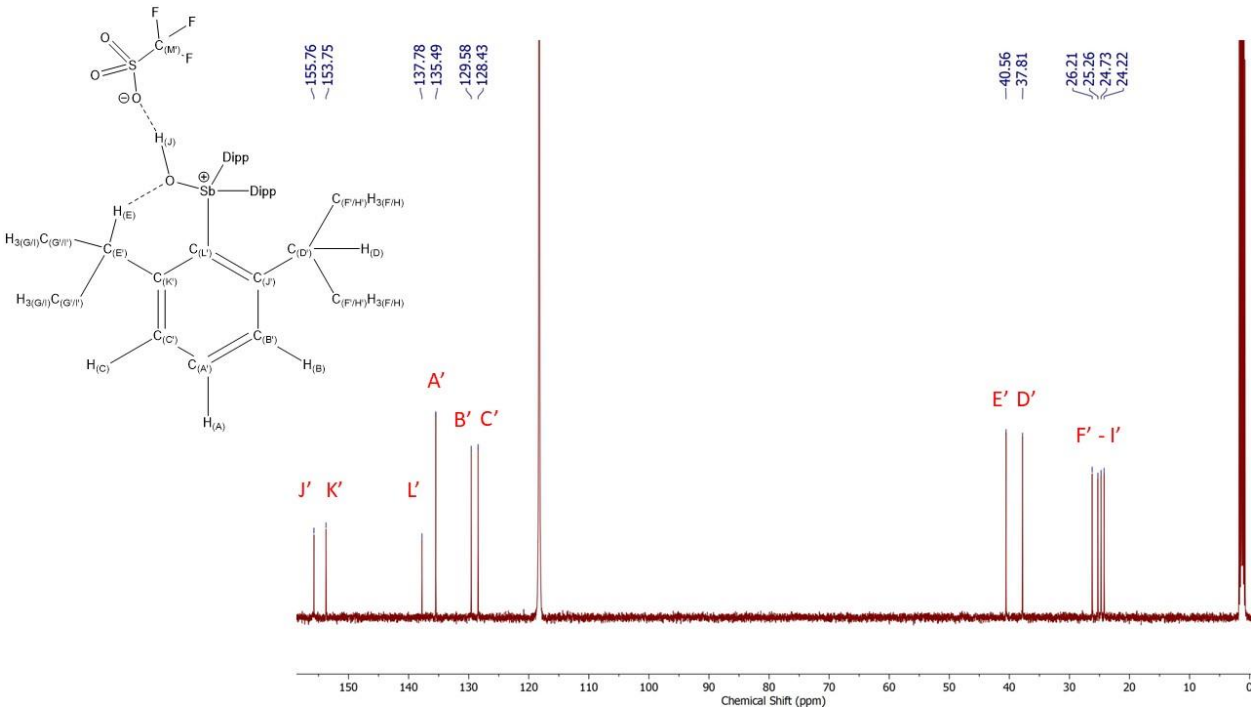

Figure S2. $^{13}C\{^{1}H\}$ NMR spectrum (CD_3CN, 125 MHz) of **2a** at room temperature.

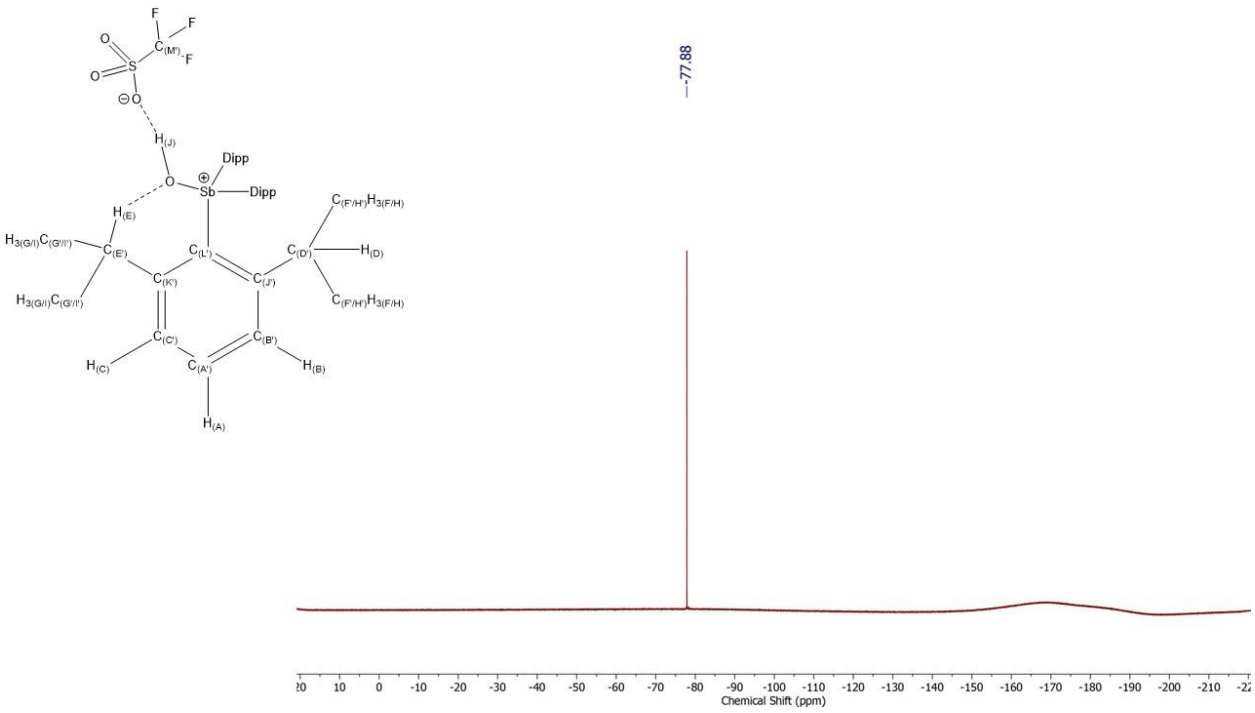

Figure S3. ^{19}F NMR spectrum ($CDCl_3$, 470 MHz) of **2a** at room temperature.

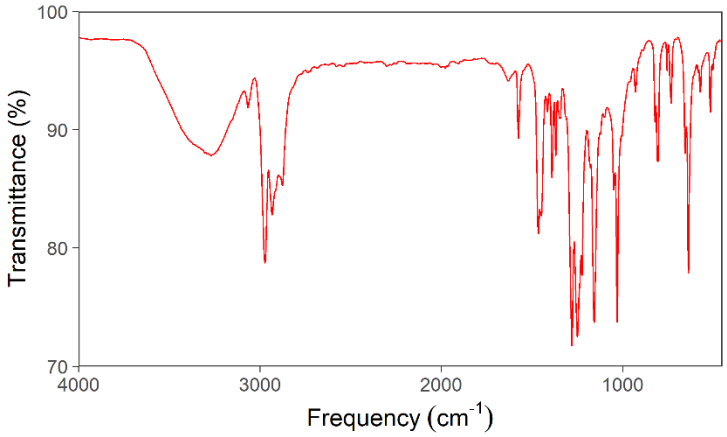

Figure S4. Experimental IR spectrum (KBr pellet) of **2a**.

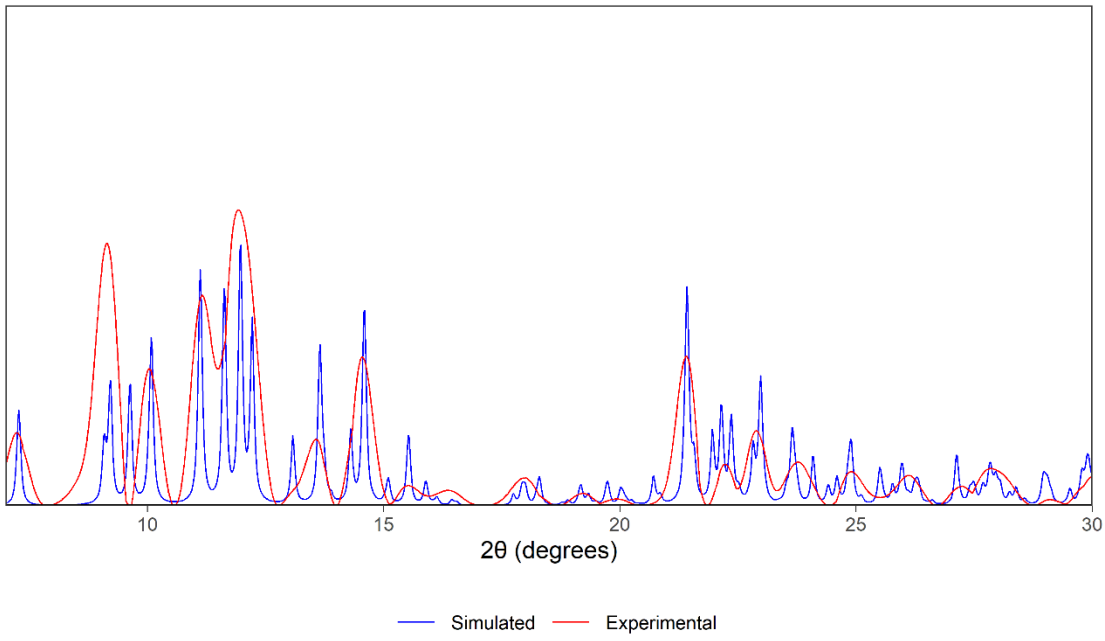

Figure S5. Simulated and experimental PXRD diffractograms of **2a**.

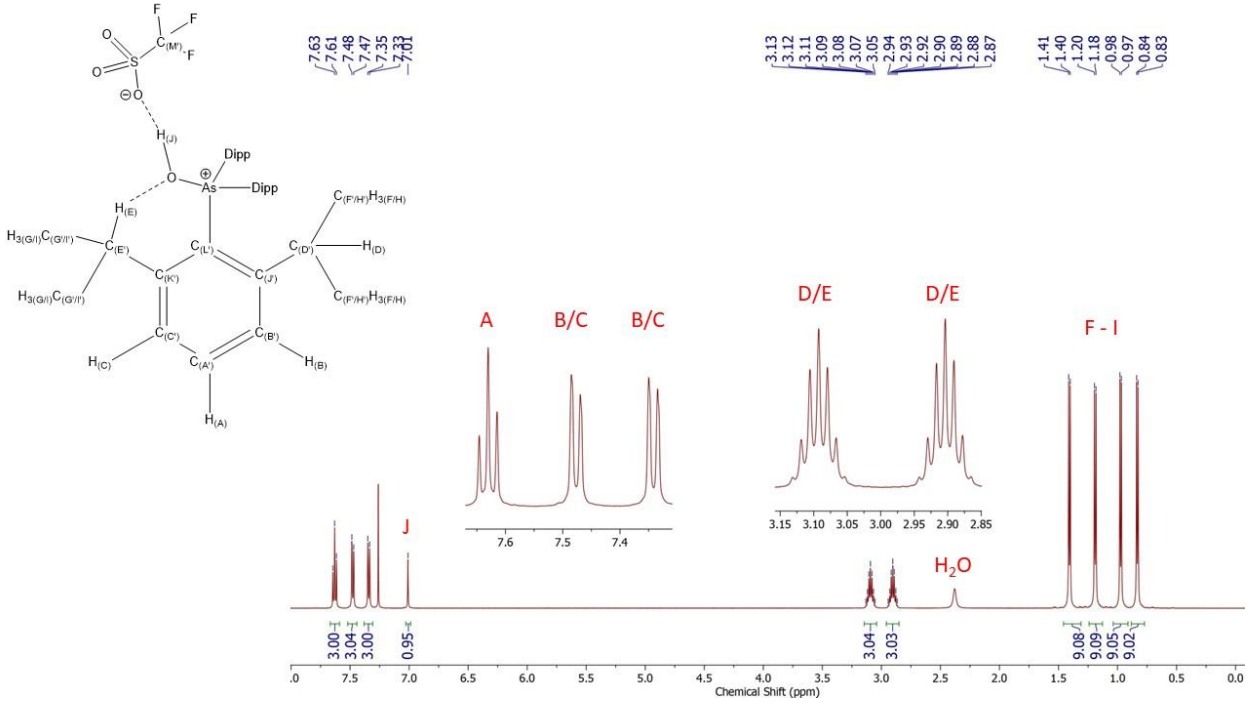

Figure S6. ^{1}H NMR spectrum ($CDCl_3$, 500 MHz) of **2b**·$CHCl_3$ at room temperature.

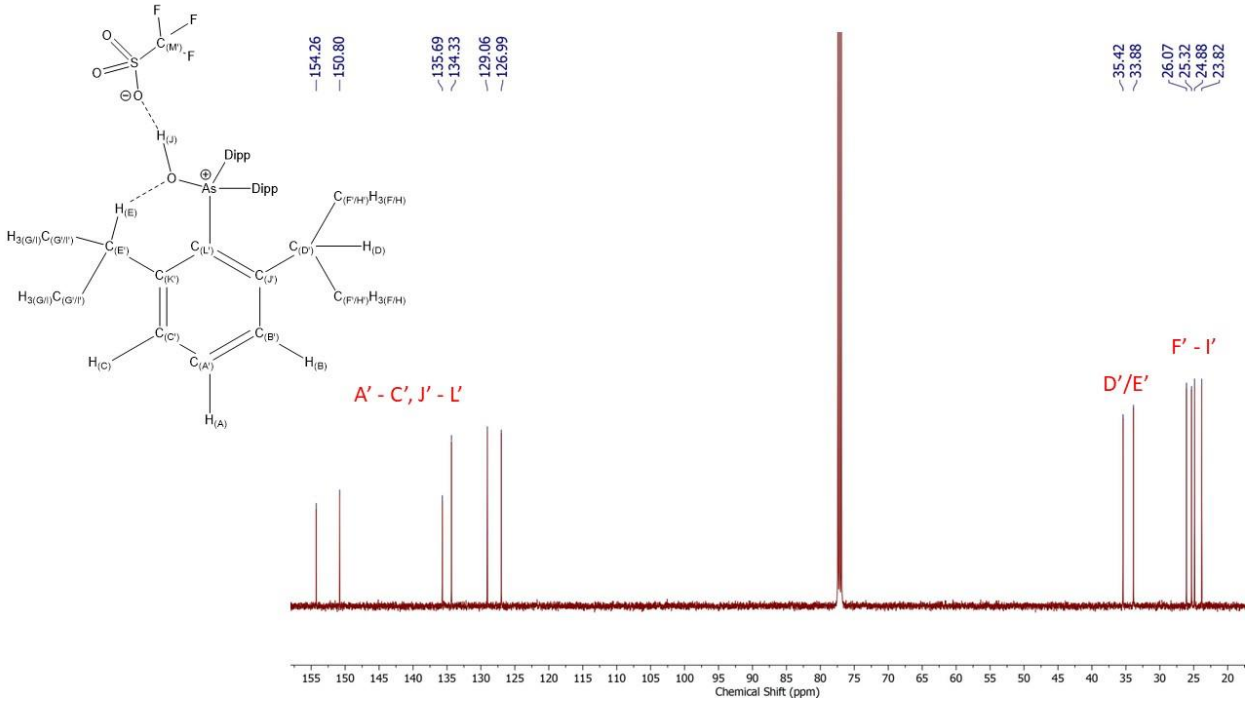

Figure S7. $^{13}C\{^{1}H\}$ NMR spectrum ($CDCl_3$, 125 MHz) of **2b**·$CHCl_3$ at room temperature.

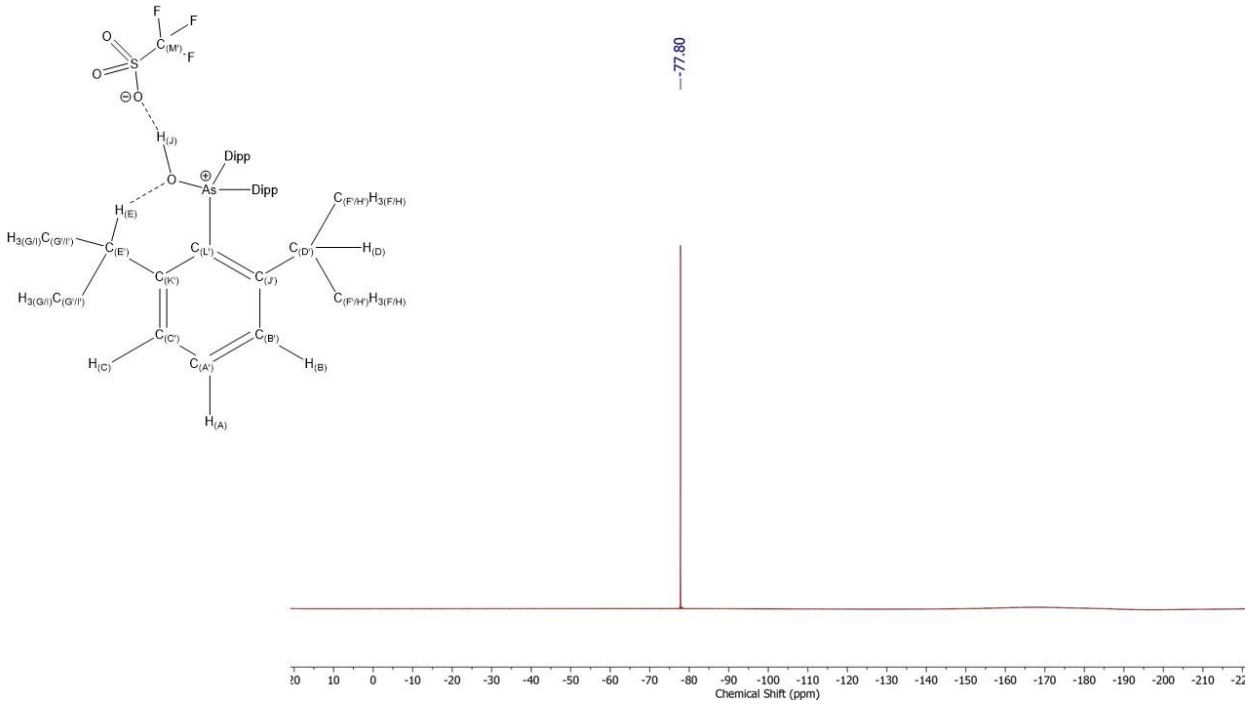

Figure S8. ^{19}F NMR spectrum ($CDCl_3$, 470 MHz) of **2b**·$CHCl_3$ at room temperature.

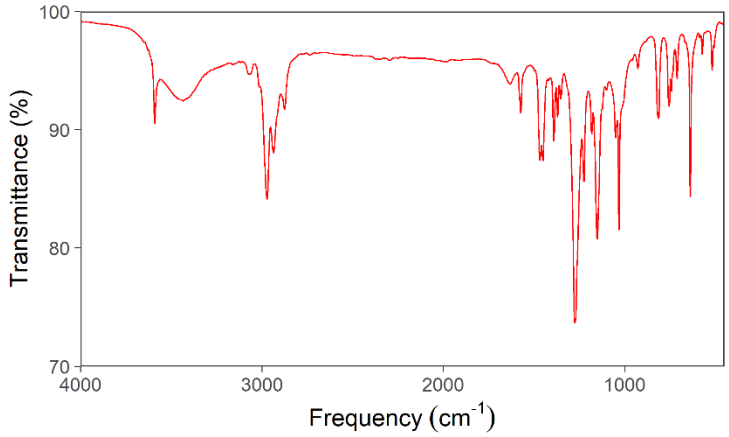

Figure S9. Experimental IR spectrum (KBr pellet) of **2b**·$CHCl_3$.

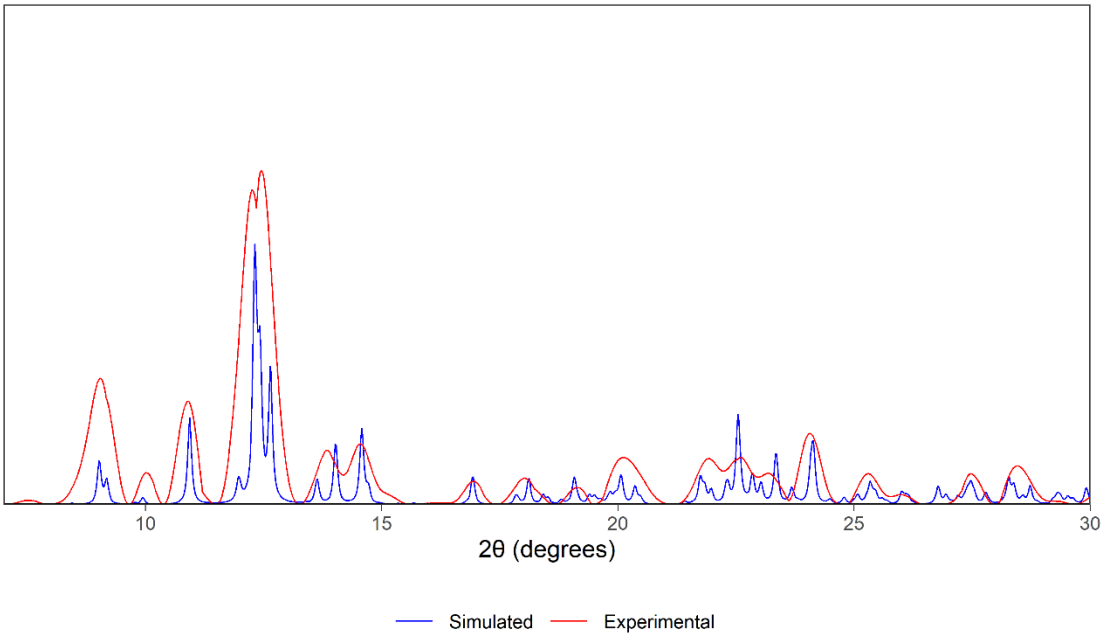

Figure S10. Simulated and experimental PXRD diffractogram of **2b**·$CHCl_3$. The simulated diffractogram is of the triclinic polymorph of **2b**·$CHCl_3$.

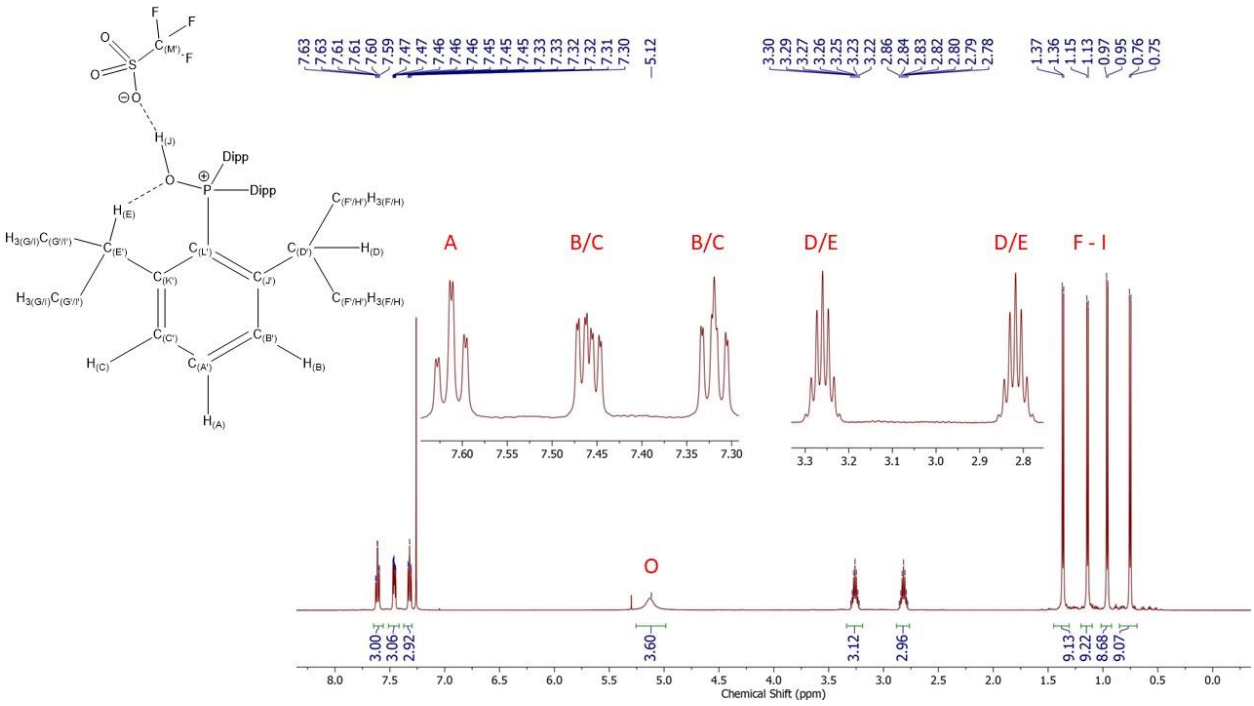

Figure S11. ^{1}H NMR spectrum ($CDCl_3$, 500 MHz) of **2c** at room temperature.

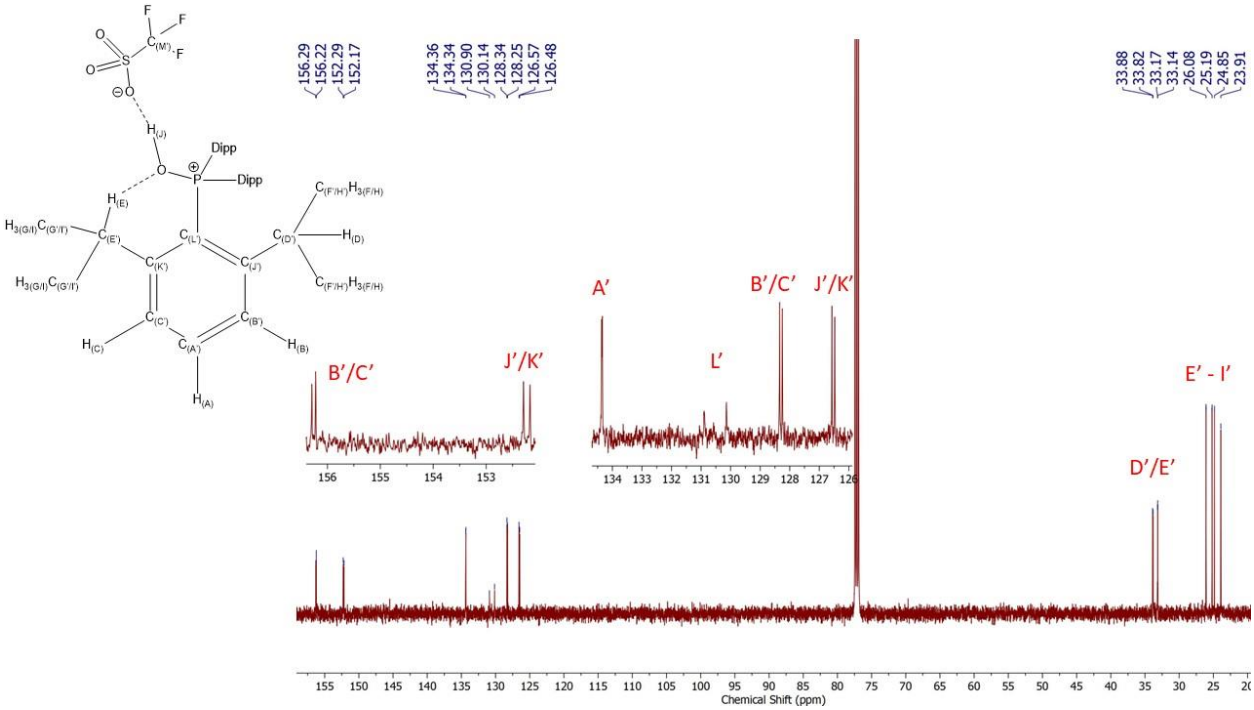

Figure S12. $^{13}C\{^{1}H\}$ NMR spectrum ($CDCl_3$, 125 MHz) of **2c** at room temperature. Aryl signals were assigned positions relative to ^{31}P nucleus based on coupling constants.

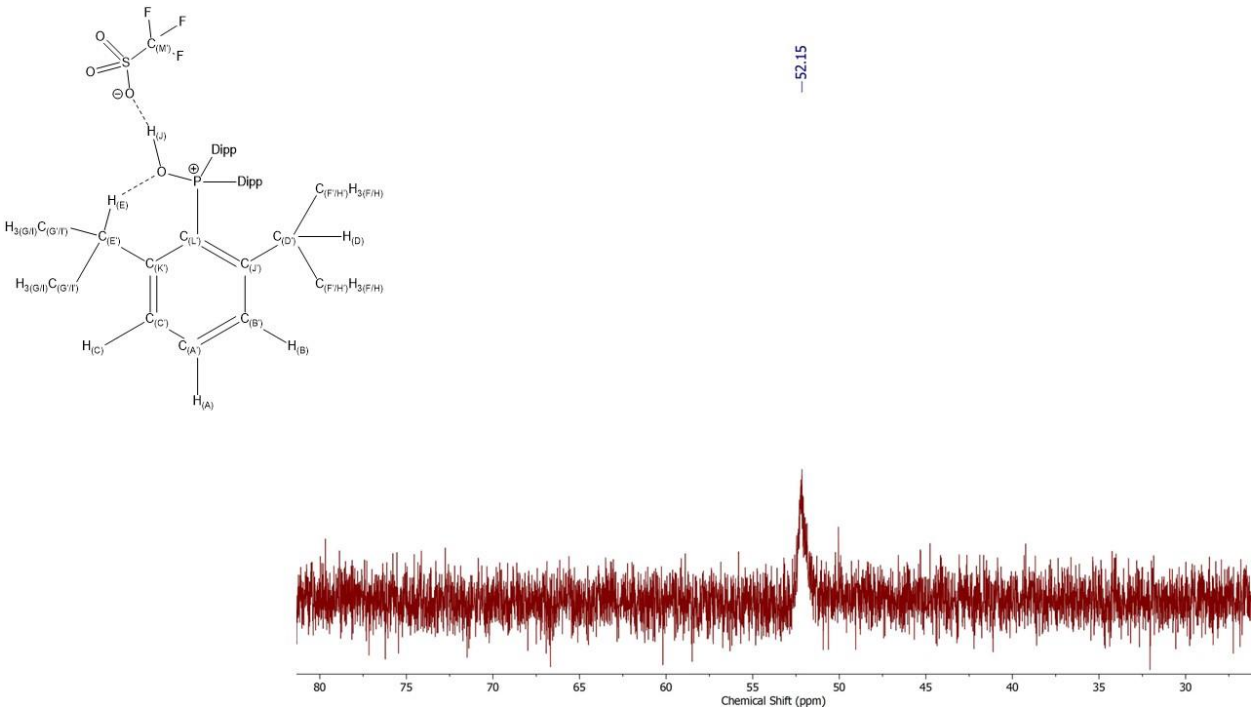

Figure S13. ^{31}P NMR spectrum ($CDCl_3$, 470 MHz) of **2c** at room temperature.

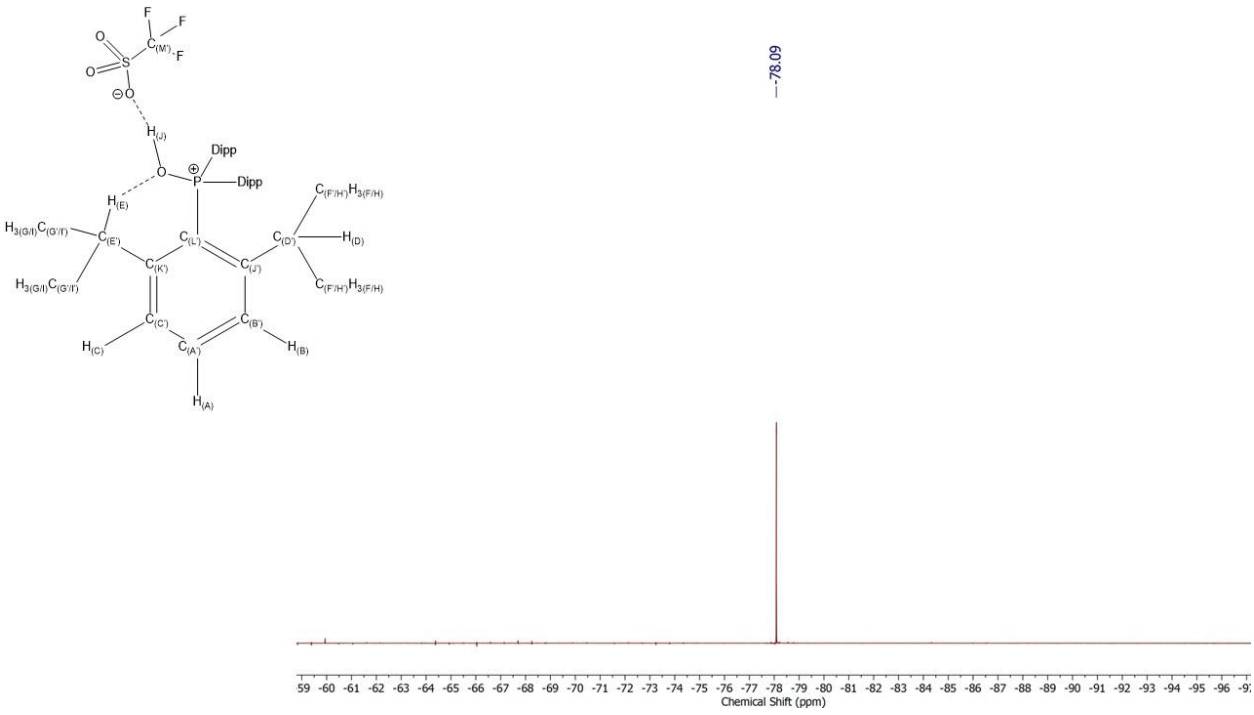

Figure S14. ^{19}F NMR spectrum ($CDCl_3$, 470 MHz) of **2c** at room temperature.

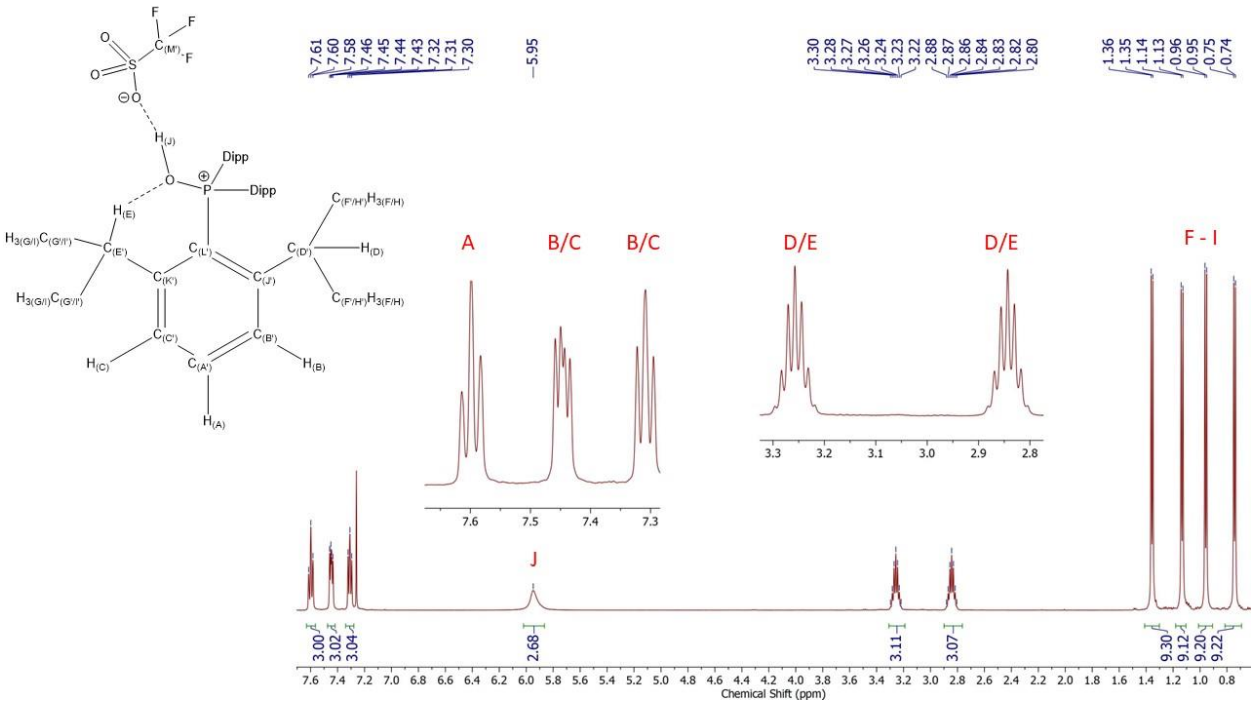

Figure S15. ^{1}H NMR spectrum ($CDCl_3$, 500 MHz) of a 1:1 mixture of **1c** and triflic acid at room temperature.

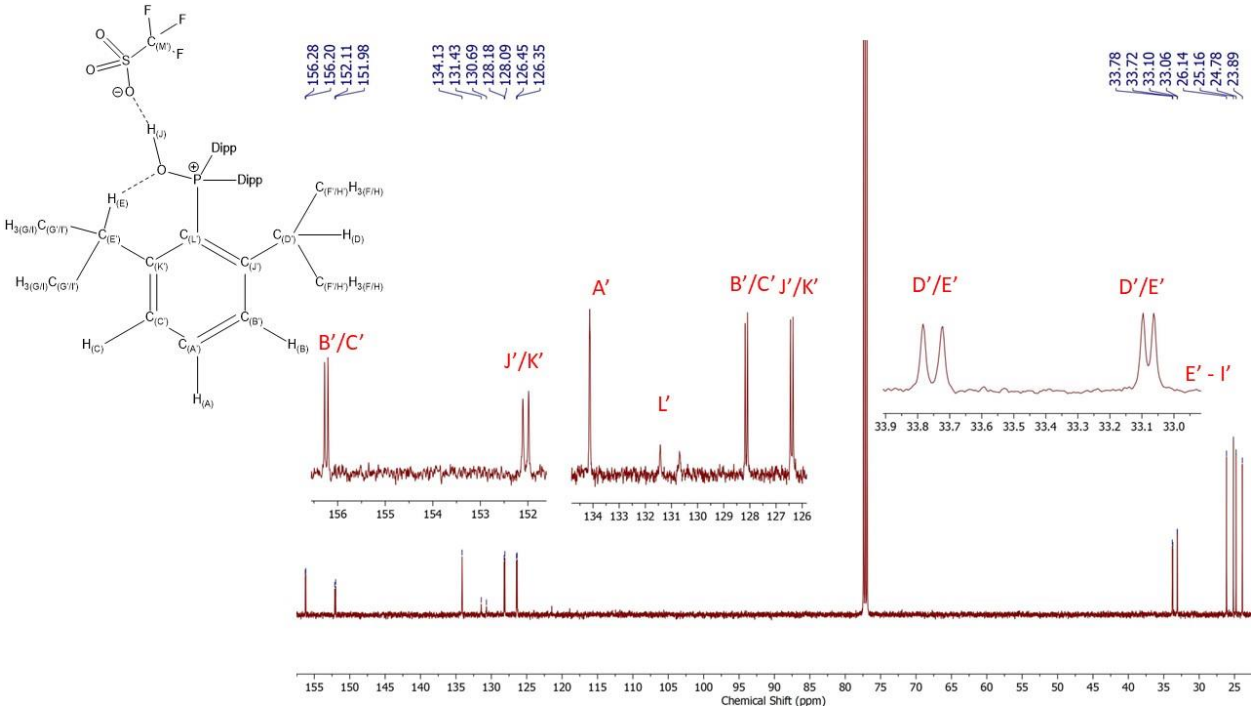

Figure S16. $^{13}C\{^{1}H\}$ NMR spectrum ($CDCl_3$, 125 MHz) of a 1:1 mixture of **1c** and triflic acid at room temperature. Aryl signals were assigned positions relative to ^{31}P nucleus based on coupling constants.

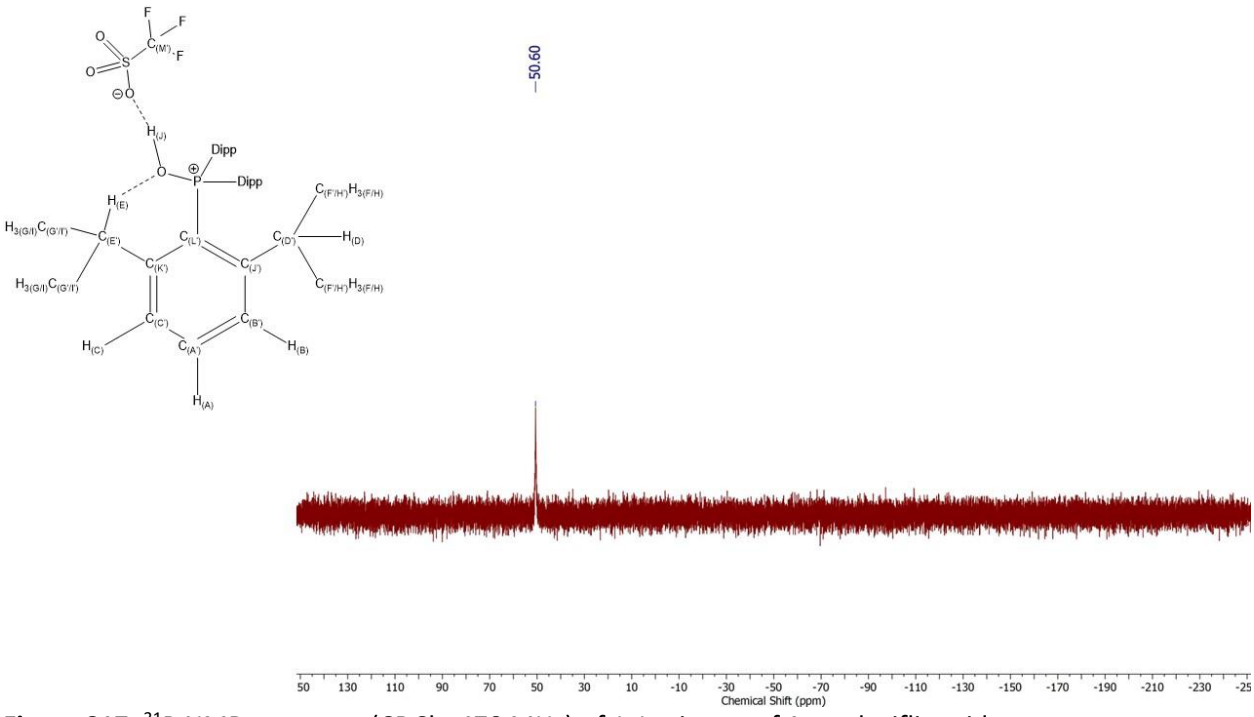

Figure S17. ^{31}P NMR spectrum ($CDCl_3$, 470 MHz) of 1:1 mixture of **1c** and triflic acid at room temperature.

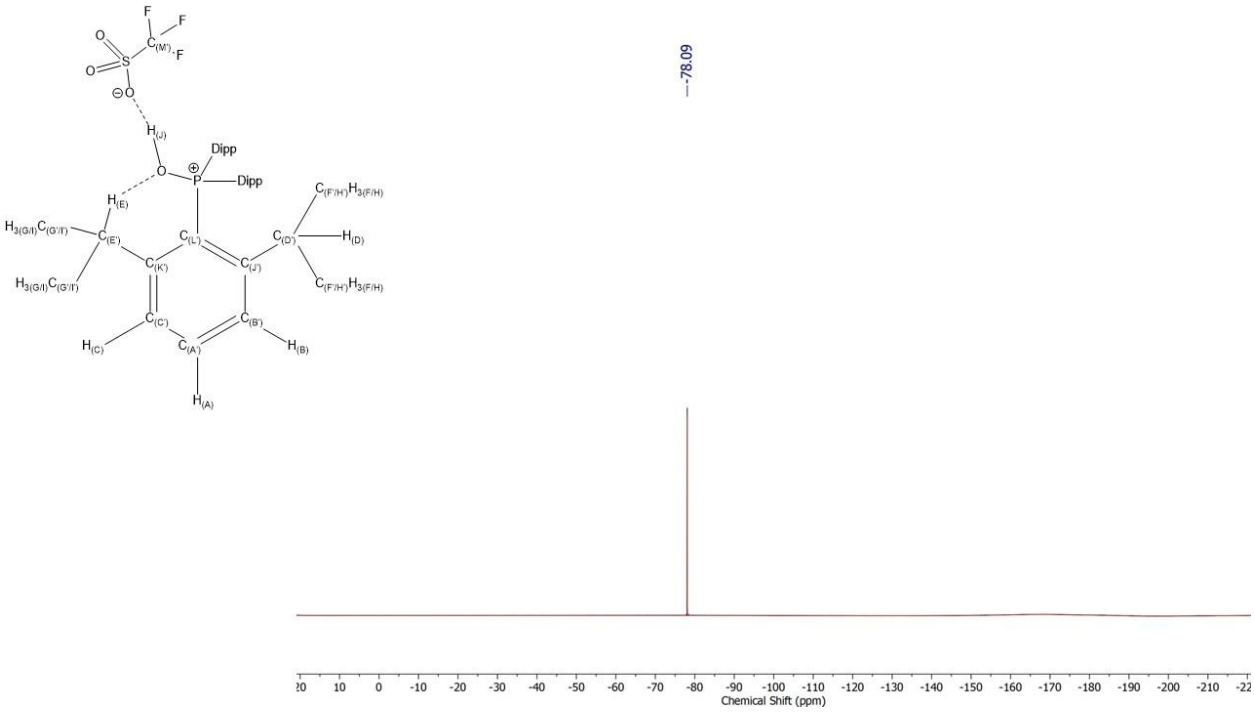

Figure S18. ^{19}F NMR spectrum ($CDCl_3$, 470 MHz) of a 1:1 mixture of **1c** and triflic acid at room temperature.

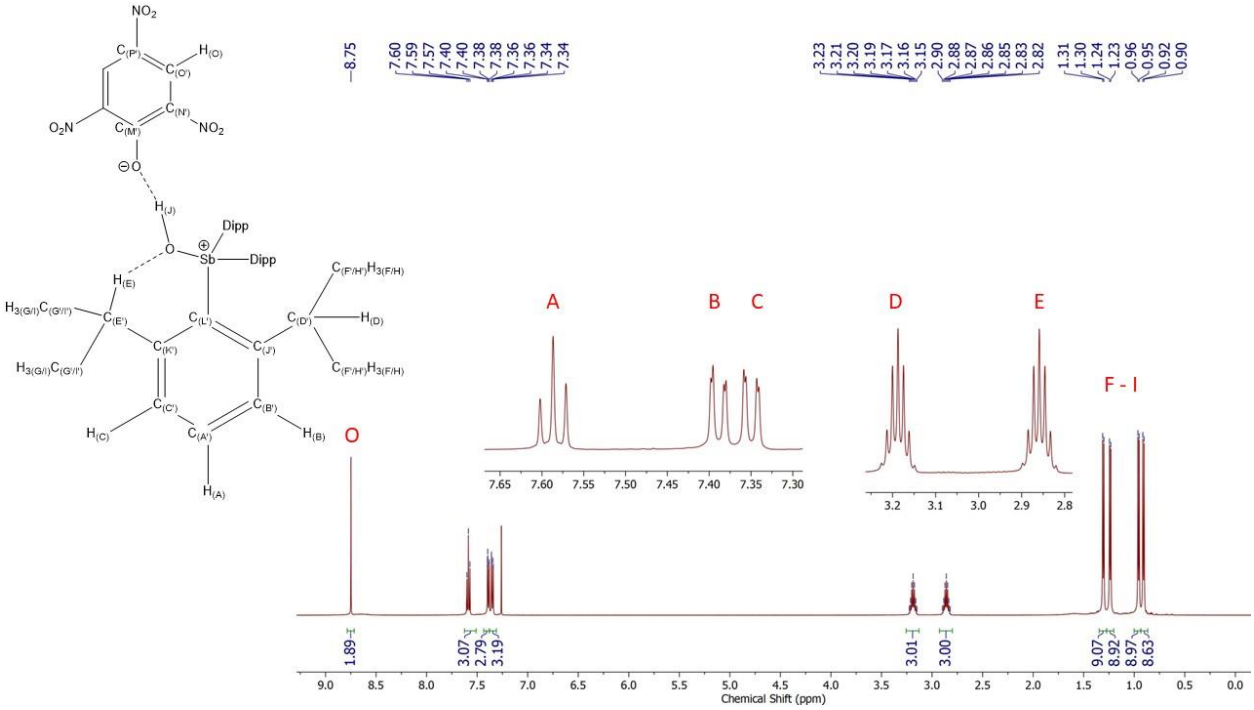

Figure S19. ^{1}H NMR spectrum ($CDCl_3$, 500 MHz) of **4a** at room temperature.

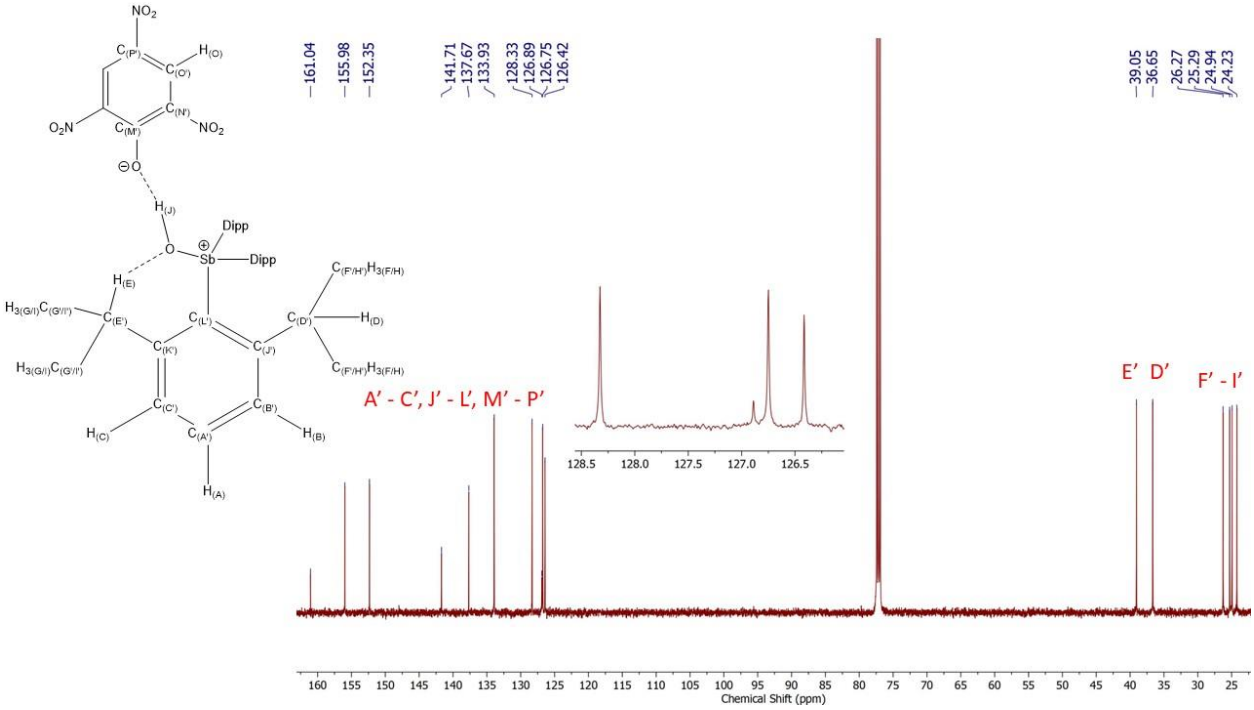

Figure S20. $^{13}C\{^{1}H\}$ NMR spectrum ($CDCl_3$, 125 MHz) of **4a** at room temperature.

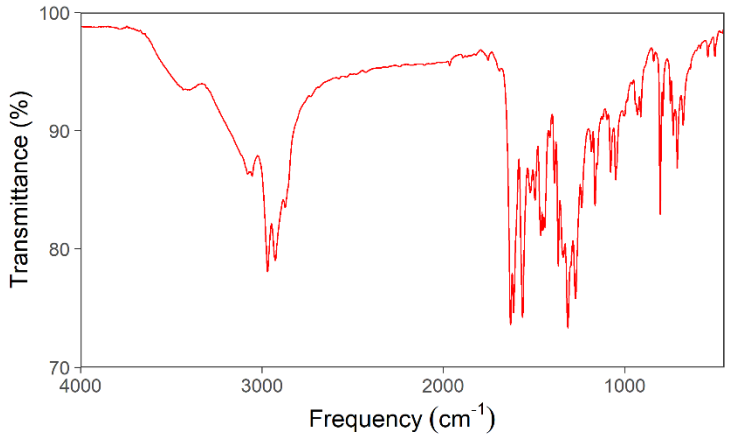

Figure S21. Experimental IR spectrum (KBr pellet) of **4a**.

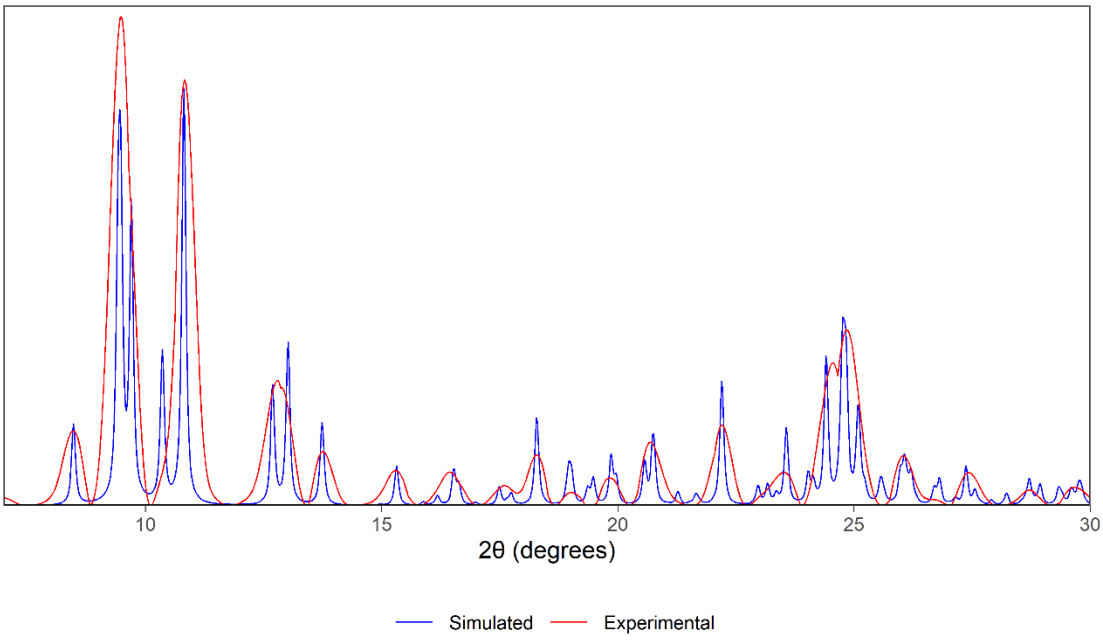

Figure S22. Simulated and experimental PXRD diffractogram of **4a**.

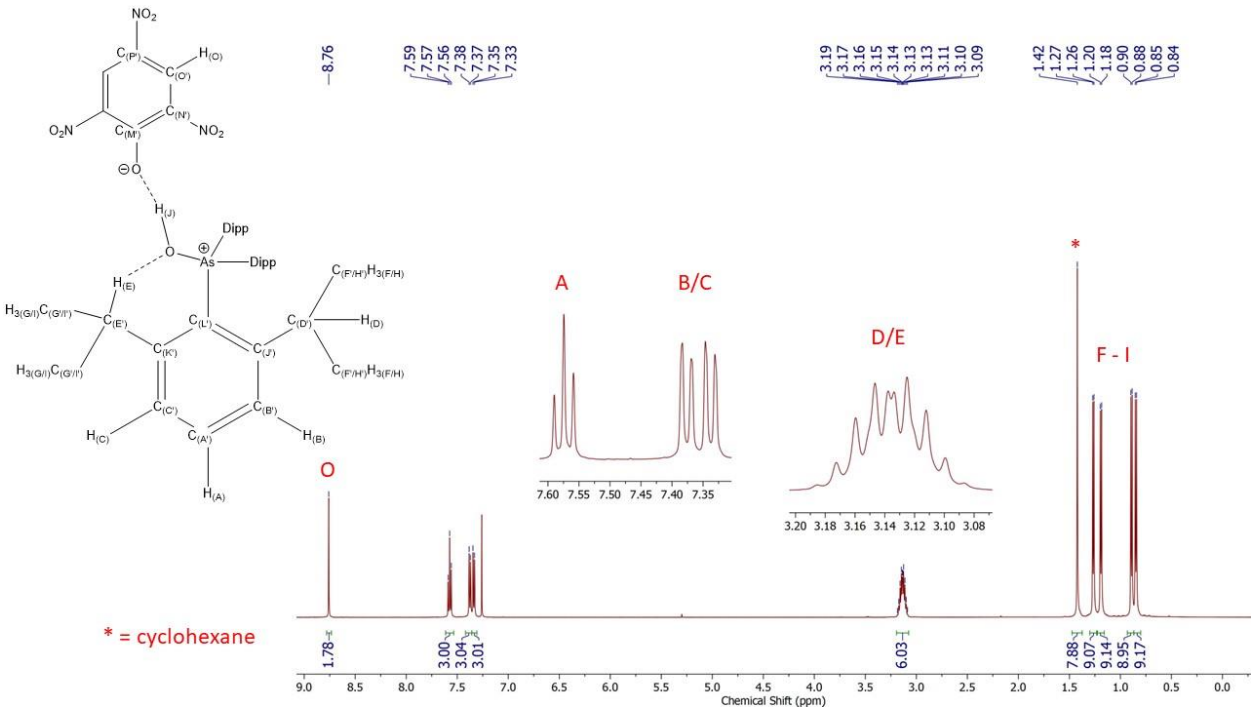

Figure S23. ^{1}H NMR spectrum ($CDCl_3$, 500 MHz) of **4b**·¾(C_6H_{12}) at room temperature.

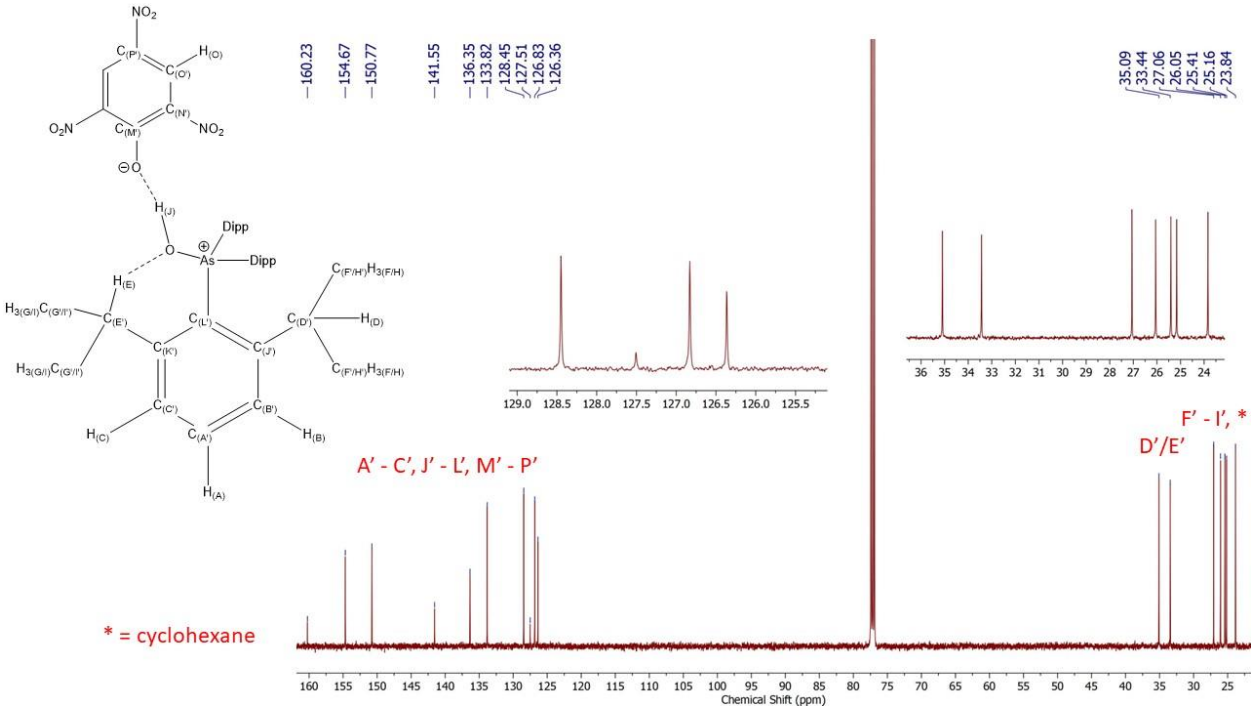

Figure S24. $^{13}C\{^{1}H$ NMR spectrum ($CDCl_3$, 125 MHz) of **4b**·¾(C_6H_{12}) at room temperature.

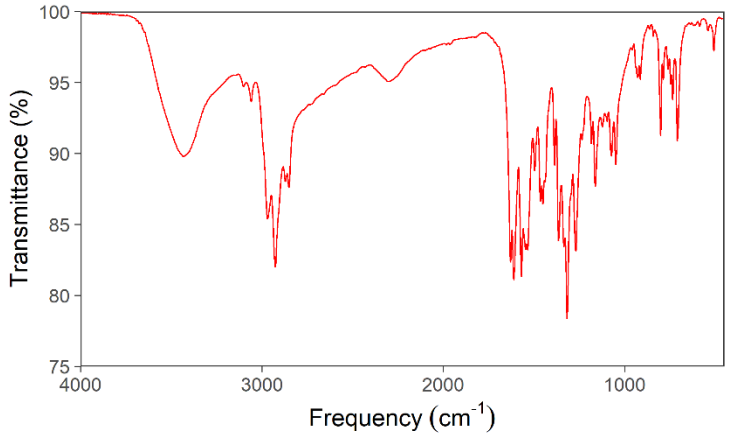

Figure S25. Experimental IR spectrum (KBr pellet) of **4b**·¾(C_6H_{12}).

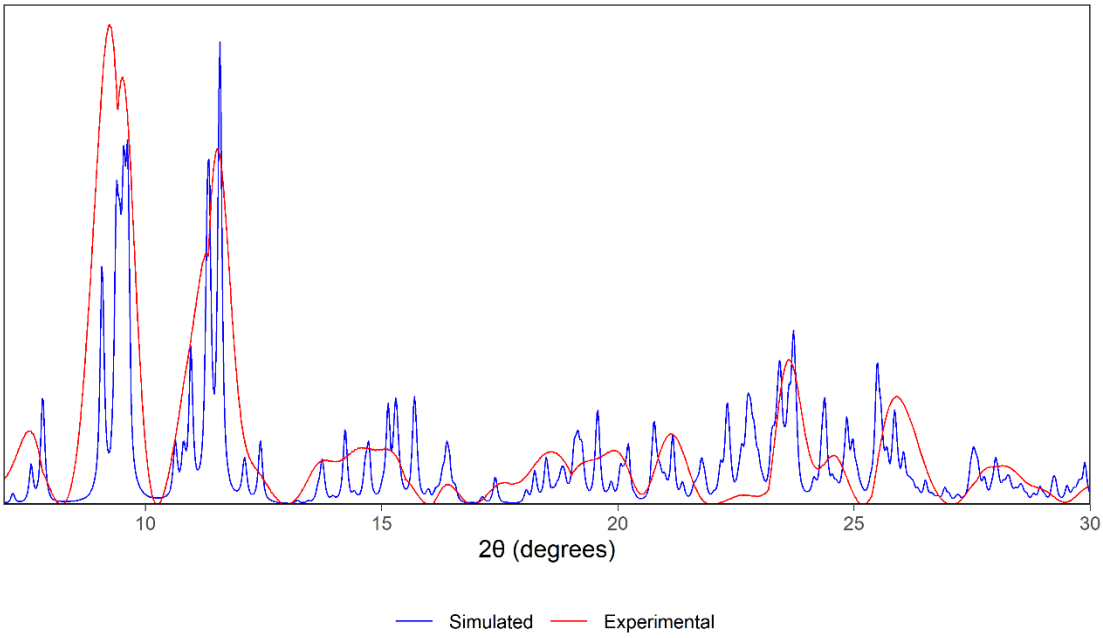

Figure S26. Simulated and experimental PXRD diffractogram of **4b**·¾(C_6H_{12}).

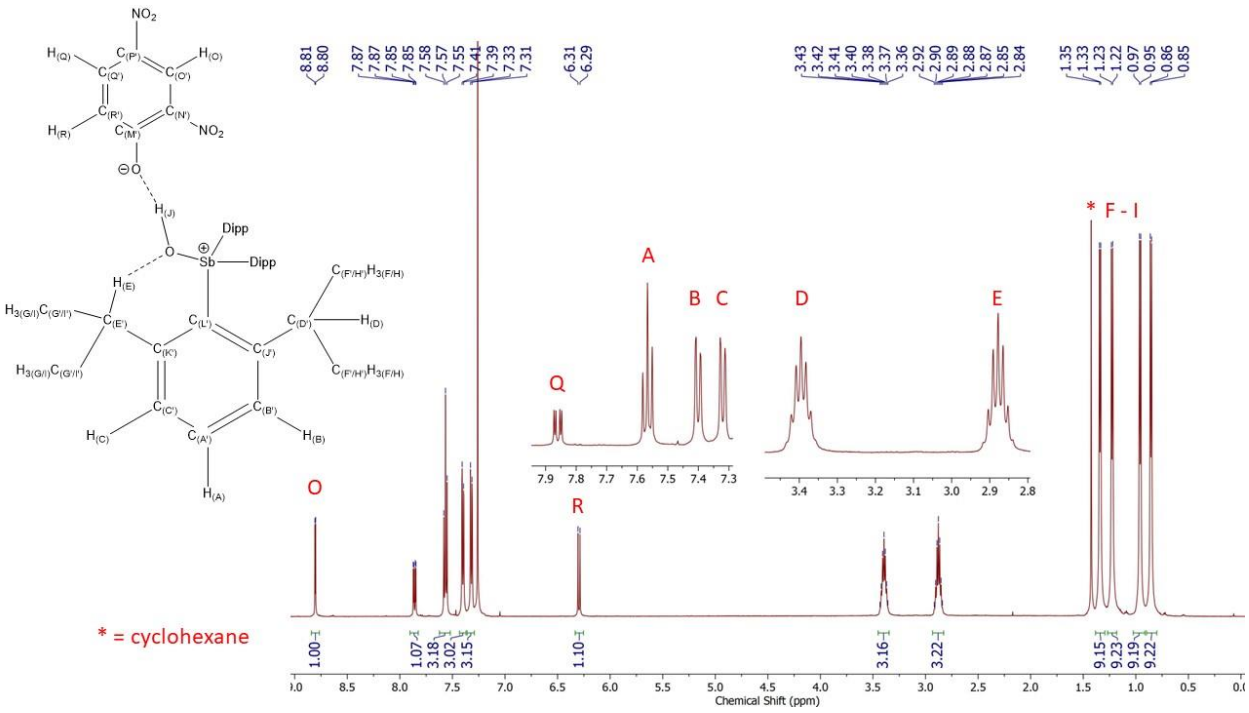

Figure S27. ^{1}H NMR spectrum ($CDCl_3$, 500 MHz) of **5**·2($CHCl_3$) at room temperature.

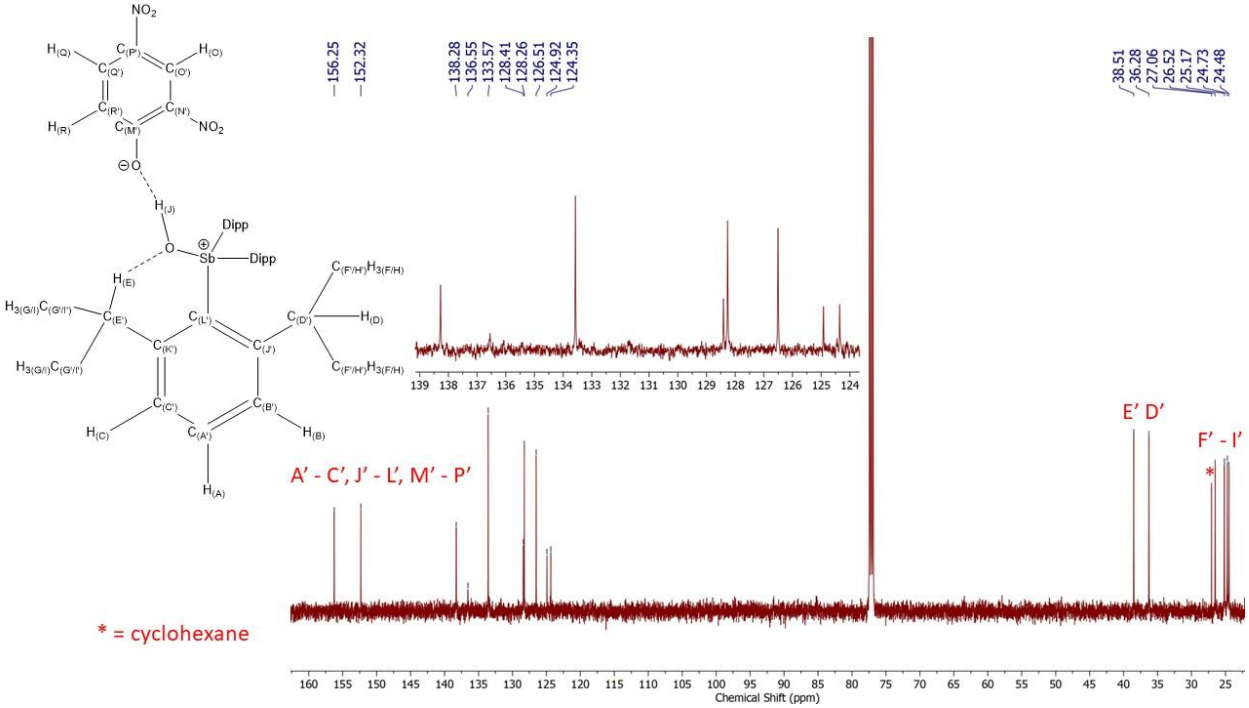

Figure S28. $^{13}C\{^{1}H\}$ NMR spectrum ($CDCl_3$, 125 MHz) of **5**·2($CHCl_3$) at room temperature.

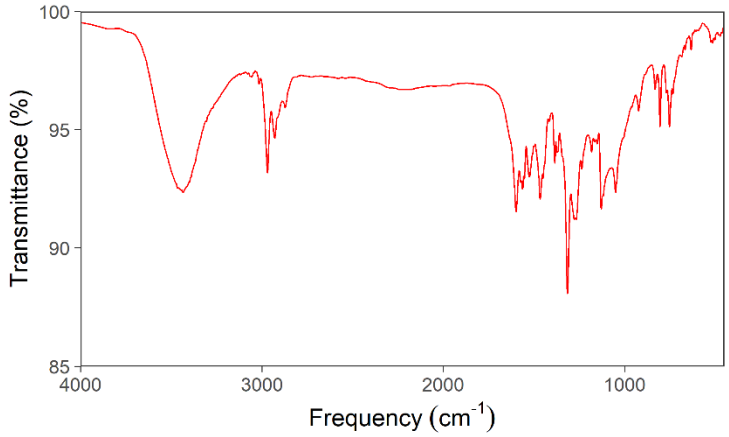

Figure S29. Experimental IR spectrum (KBr pellet) of **5**·2($CHCl_3$).

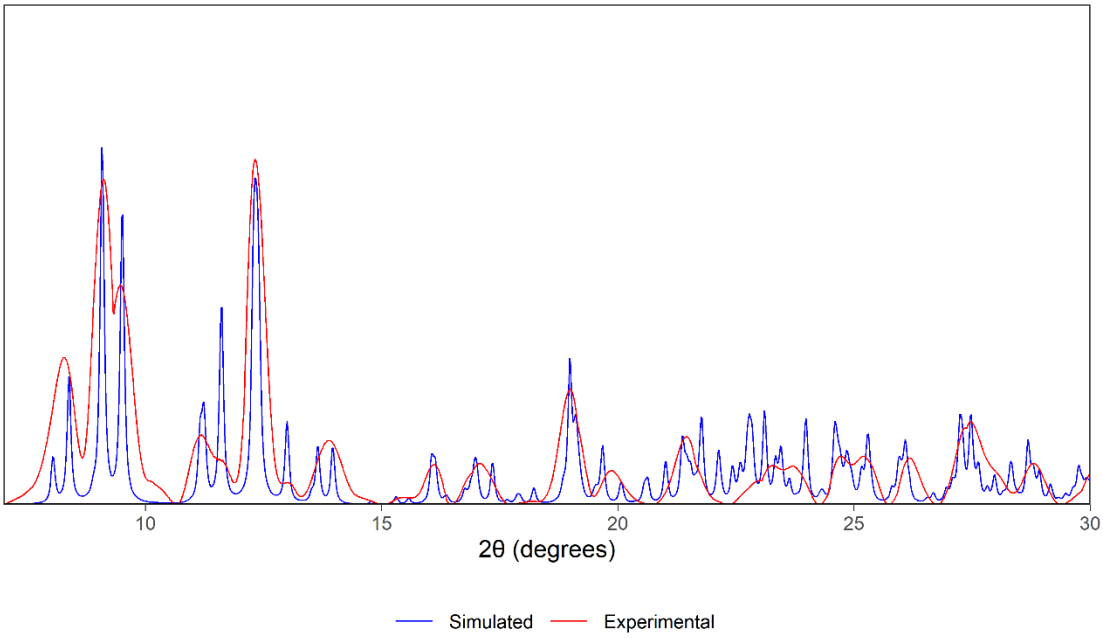

Figure S30. Simulated and experimental PXRD diffractogram of **5**·2($CHCl_3$).

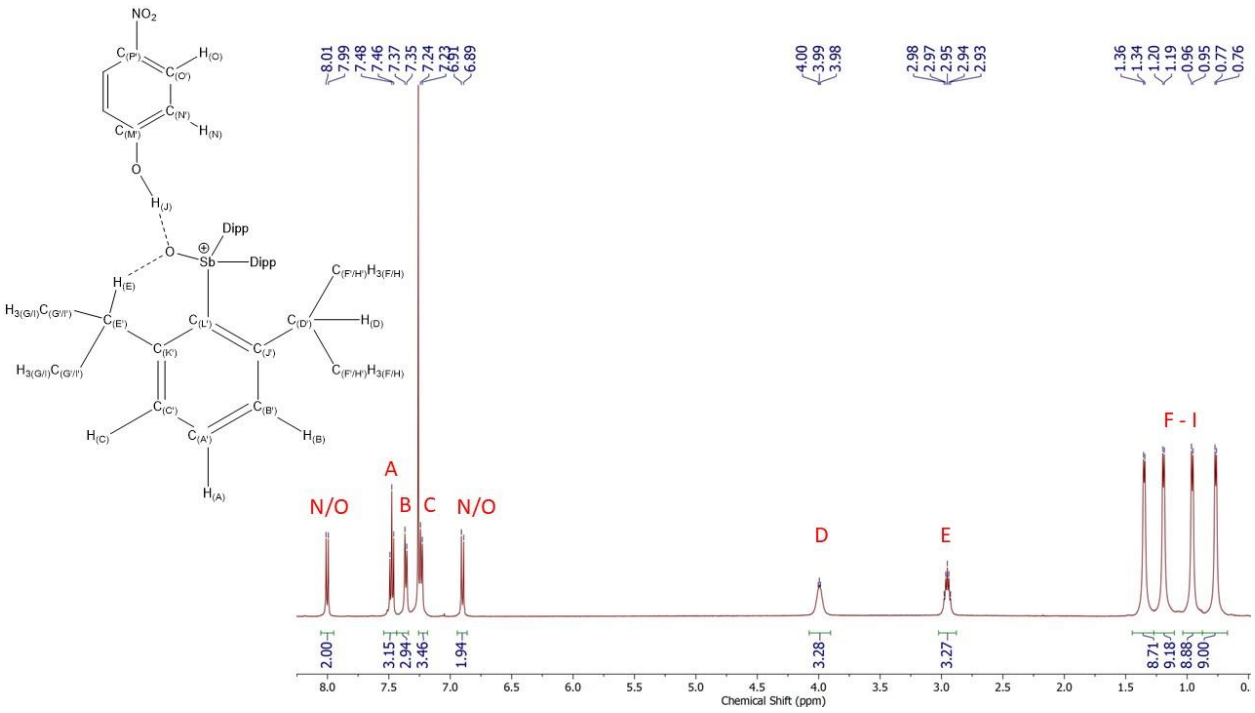

Figure S31. ^{1}H NMR spectrum ($CDCl_3$, 500 MHz) of **6** at room temperature.

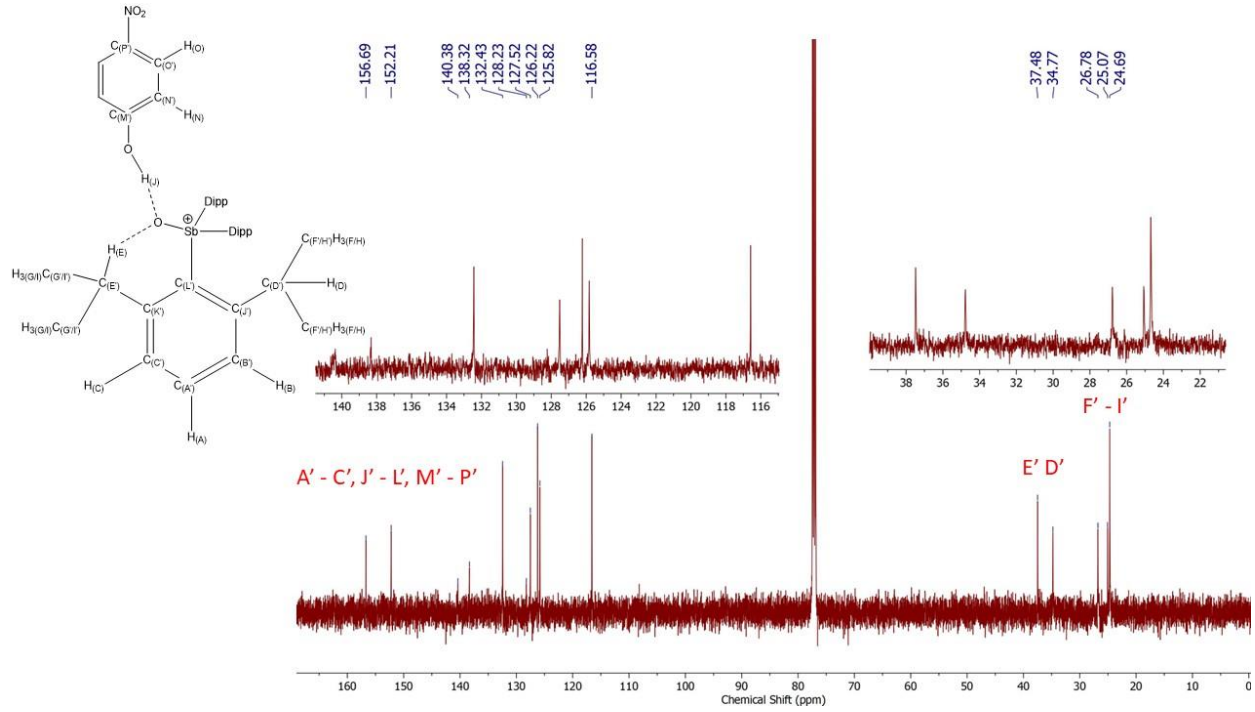

Figure S32. $^{13}C\{^{1}H\}$ NMR spectrum ($CDCl_3$, 125 MHz) of **6** at room temperature.

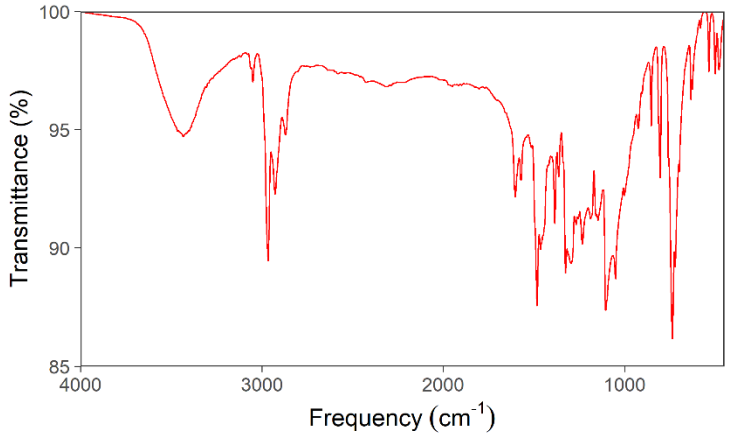

Figure S33. Experimental IR spectrum (KBr pellet) of **6**.

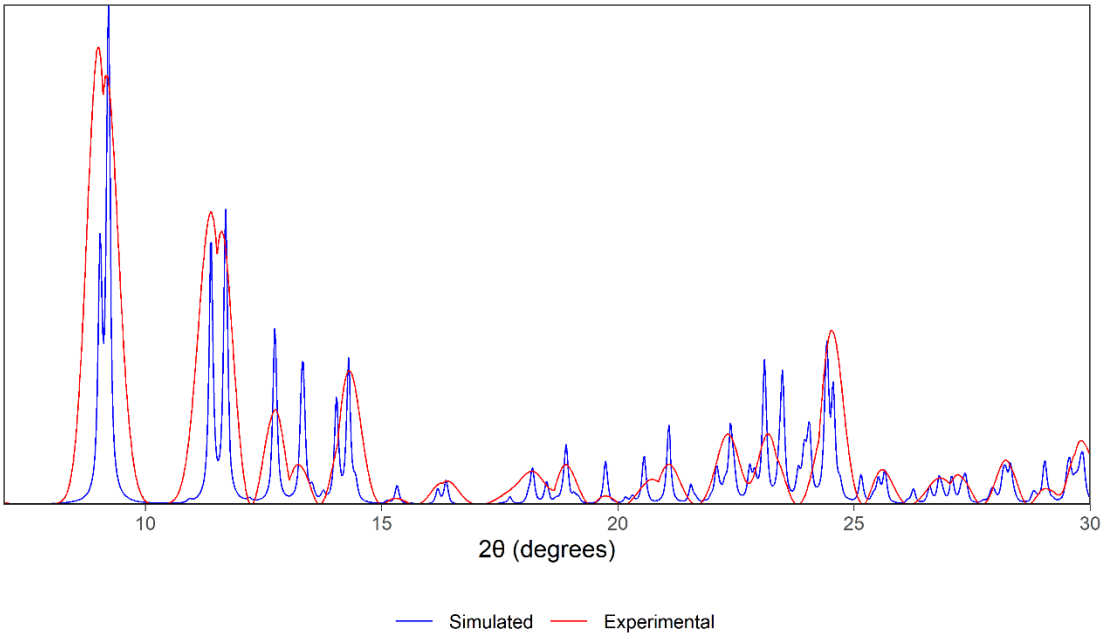

Figure S34. Simulated and experimental PXRD diffractogram of **6**.

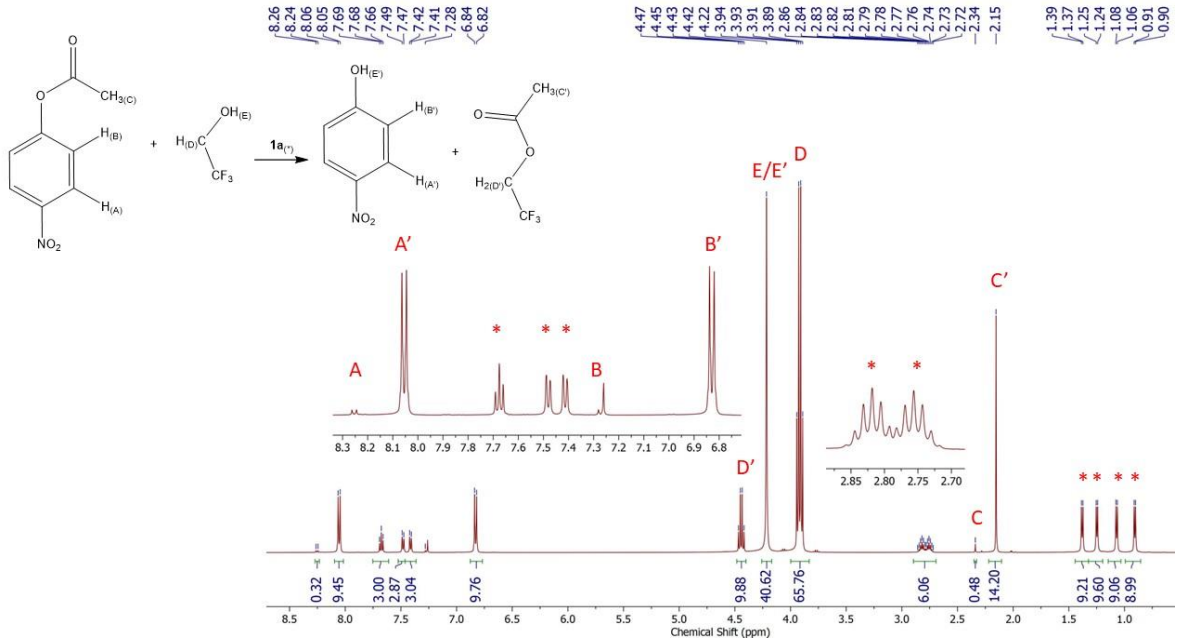

Figure S35. ^{1}H NMR spectrum ($CDCl_3$, 500 MHz) of **1a**-catalyzed transesterification between *p*-nitrophenyl acetate and 2,2,2-trifluoroethanol reaction mixture at room temperature. Signals arising from pnictine oxide catalyst are denoted with an asterisk. The percent conversion was calculated by dividing the integral of peak C by the sum of the integrals of peaks A and A'. We note that a portion of the original 10 equivalents of 2,2,2-trifluoroethanol added to the mixture evaporated during the reaction.

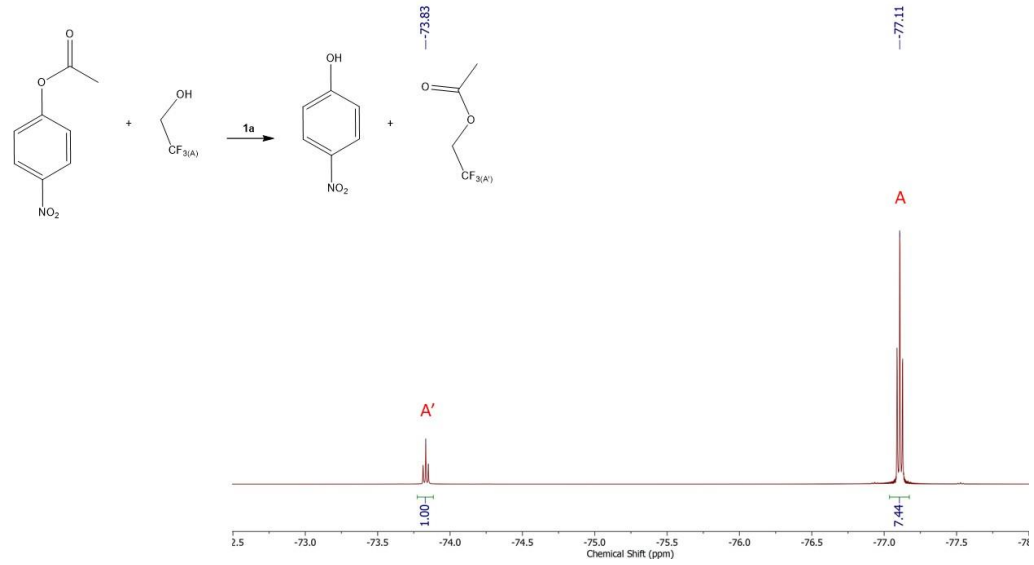

Figure S36. ^{19}F NMR spectrum ($CDCl_3$, 470 MHz) of **1a**-catalyzed transesterification between *p*-nitrophenyl acetate and 2,2,2-trifluoroethanol reaction mixture at room temperature. We note that a portion of the original 10 equivalents of 2,2,2-trifluoroethanol added to the mixture evaporated during the reaction.

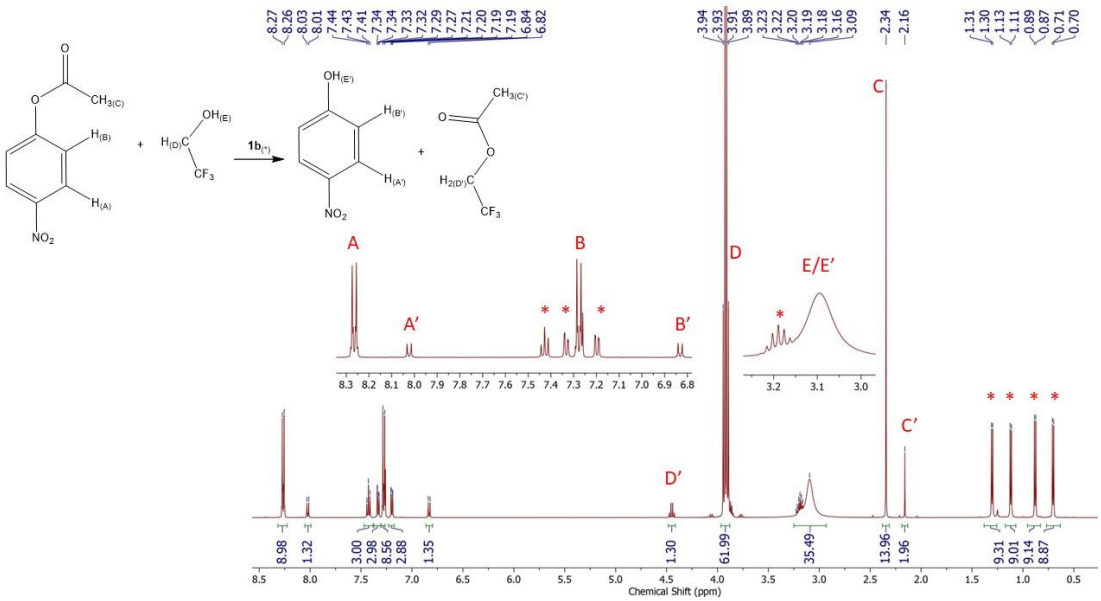

Figure S37. ^{1}H NMR spectrum ($CDCl_3$, 500 MHz) of **1b**-catalyzed transesterification between *p*-nitrophenyl acetate and 2,2,2-trifluoroethanol reaction mixture at room temperature. Signals arising from pnictine oxide catalyst are denoted with an asterisk. The percent conversion was calculated by dividing the integral of peak C by the sum of the integrals of peaks A and A'. We note that a portion of the original 10 equivalents of 2,2,2-trifluoroethanol added to the mixture evaporated during the reaction.

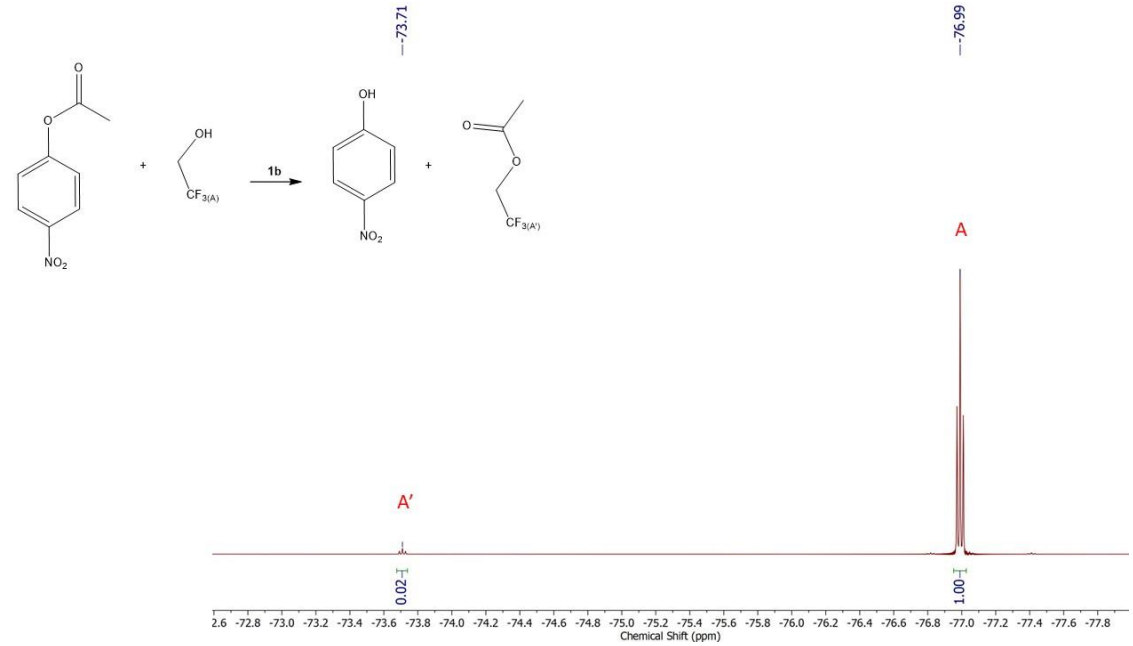

Figure S38. ^{19}F NMR spectrum ($CDCl_3$, 470 MHz) of **1b**-catalyzed transesterification between *p*-nitrophenyl acetate and 2,2,2-trifluoroethanol reaction mixture at room temperature. We note that a portion of the original 10 equivalents of 2,2,2-trifluoroethanol added to the mixture evaporated during the reaction.

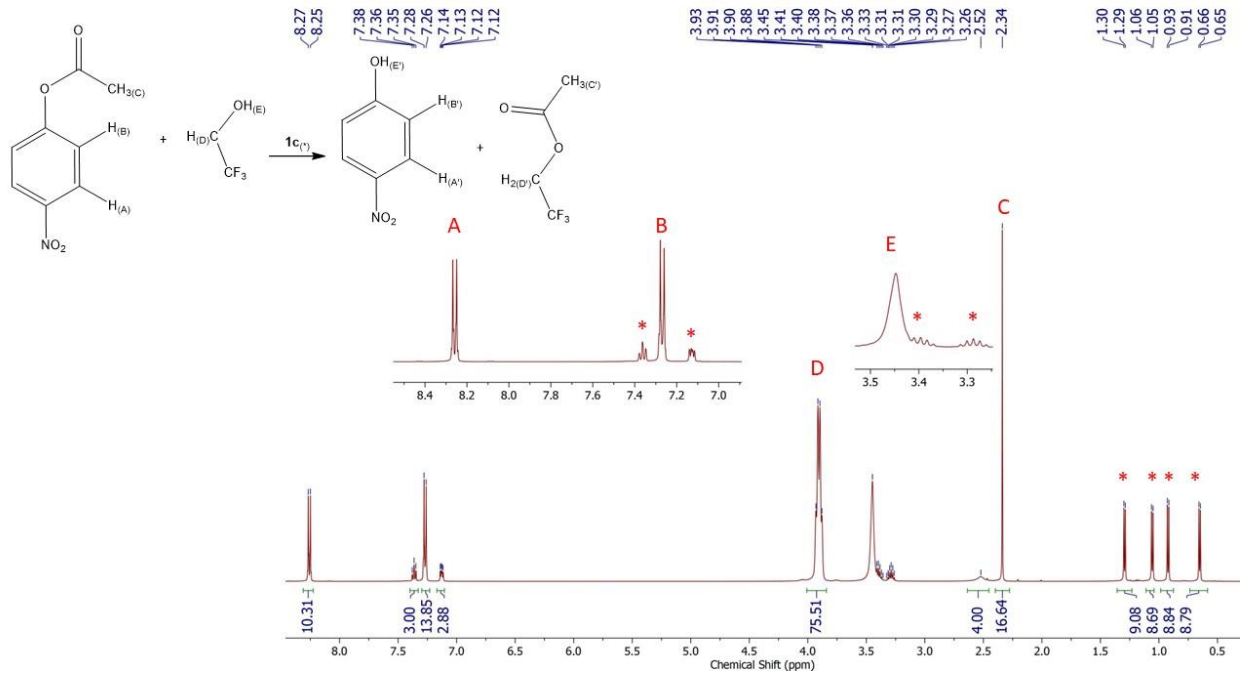

Figure S39. ^{1}H NMR spectrum ($CDCl_3$, 500 MHz) of **1c**-catalyzed transesterification between *p*-nitrophenyl acetate and 2,2,2-trifluoroethanol reaction mixture at room temperature. Signals arising from pnictine oxide catalyst are denoted with an asterisk. The percent conversion was calculated by dividing the integral of peak C by the sum of the integrals of peaks A and A'. We note that a portion of the original 10 equivalents of 2,2,2-trifluoroethanol added to the mixture evaporated during the reaction.

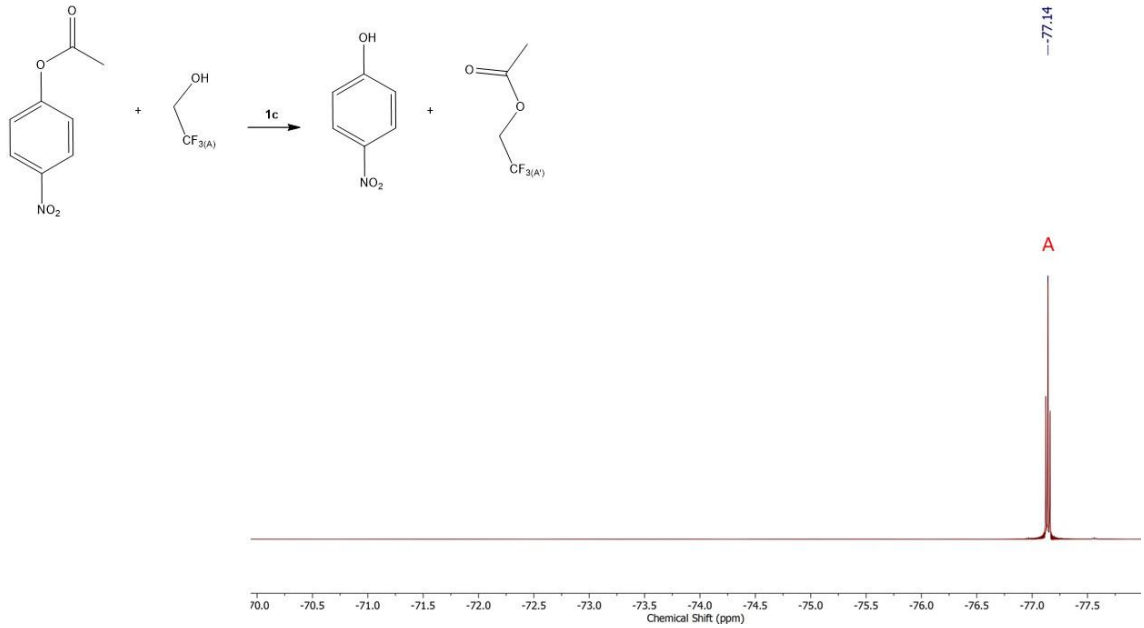

Figure S40. ^{19}F NMR spectrum ($CDCl_3$, 470 MHz) of **1c**-catalyzed transesterification between *p*-nitrophenyl acetate and 2,2,2-trifluoroethanol reaction mixture at room temperature. We note that a portion of the original 10 equivalents of 2,2,2-trifluoroethanol added to the mixture evaporated during the reaction.

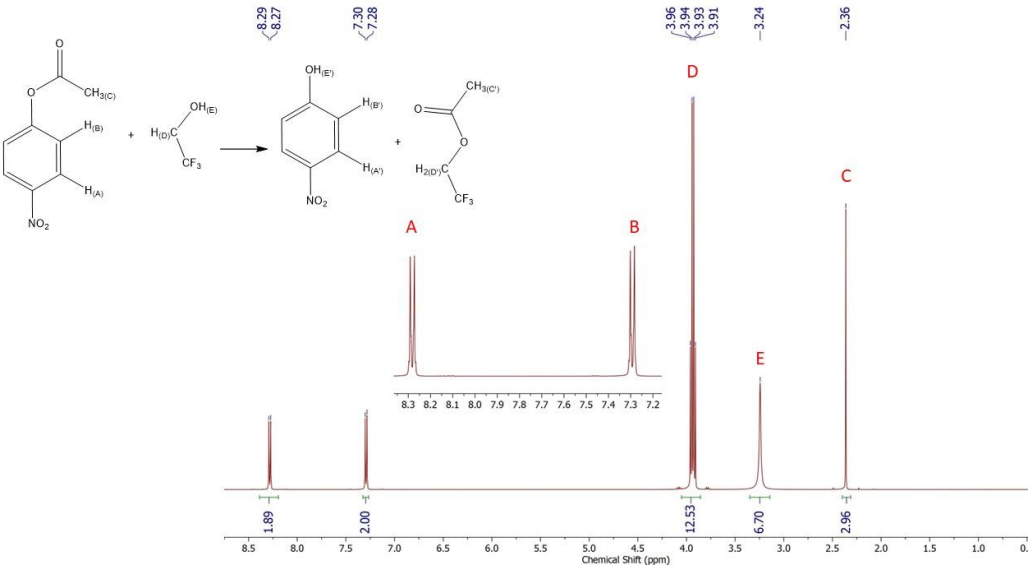

Figure S41. ^{1}H NMR spectrum ($CDCl_3$, 500 MHz) of uncatalyzed transesterification between *p*-nitrophenyl acetate and 2,2,2-trifluoroethanol reaction mixture at room temperature. The percent conversion was calculated by dividing the integral of peak C by the sum of the integrals of peaks A and A'. We note that a portion of the original 10 equivalents of 2,2,2-trifluoroethanol added to the mixture evaporated during the reaction.

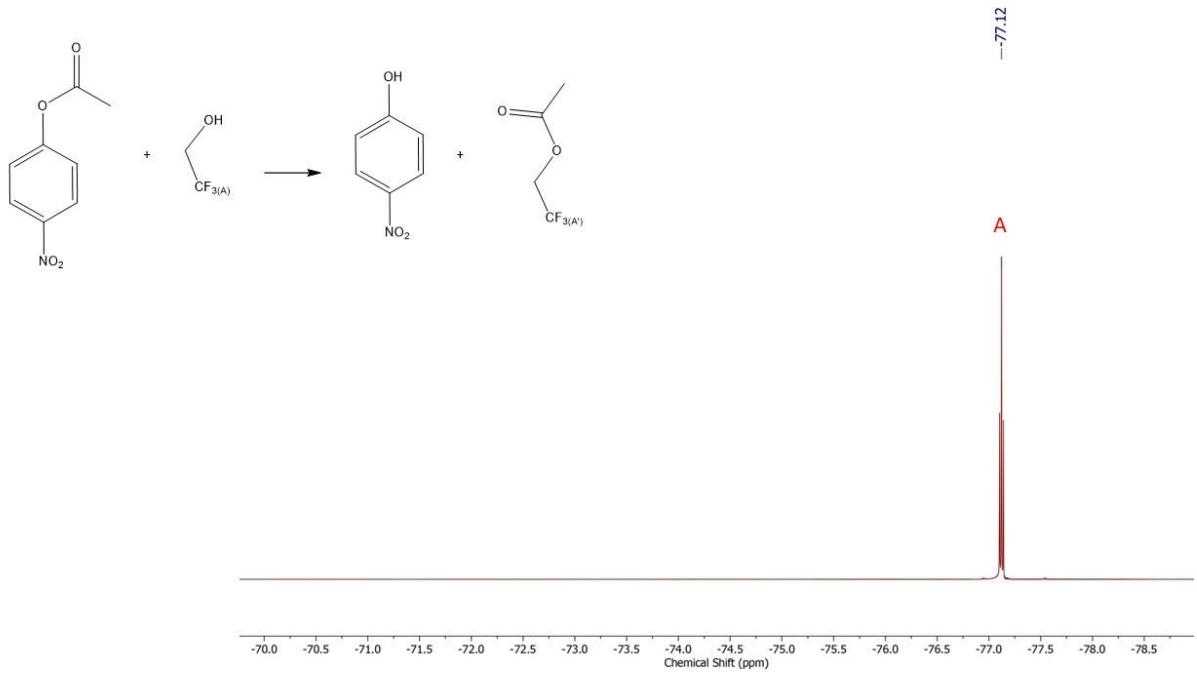

Figure S42. ^{19}F NMR spectrum ($CDCl_3$, 470 MHz) of uncatalyzed transesterification between *p*-nitrophenyl acetate and 2,2,2-trifluoroethanol reaction mixture at room temperature. We note that a portion of the original 10 equivalents of 2,2,2-trifluoroethanol added to the mixture evaporated during the reaction.

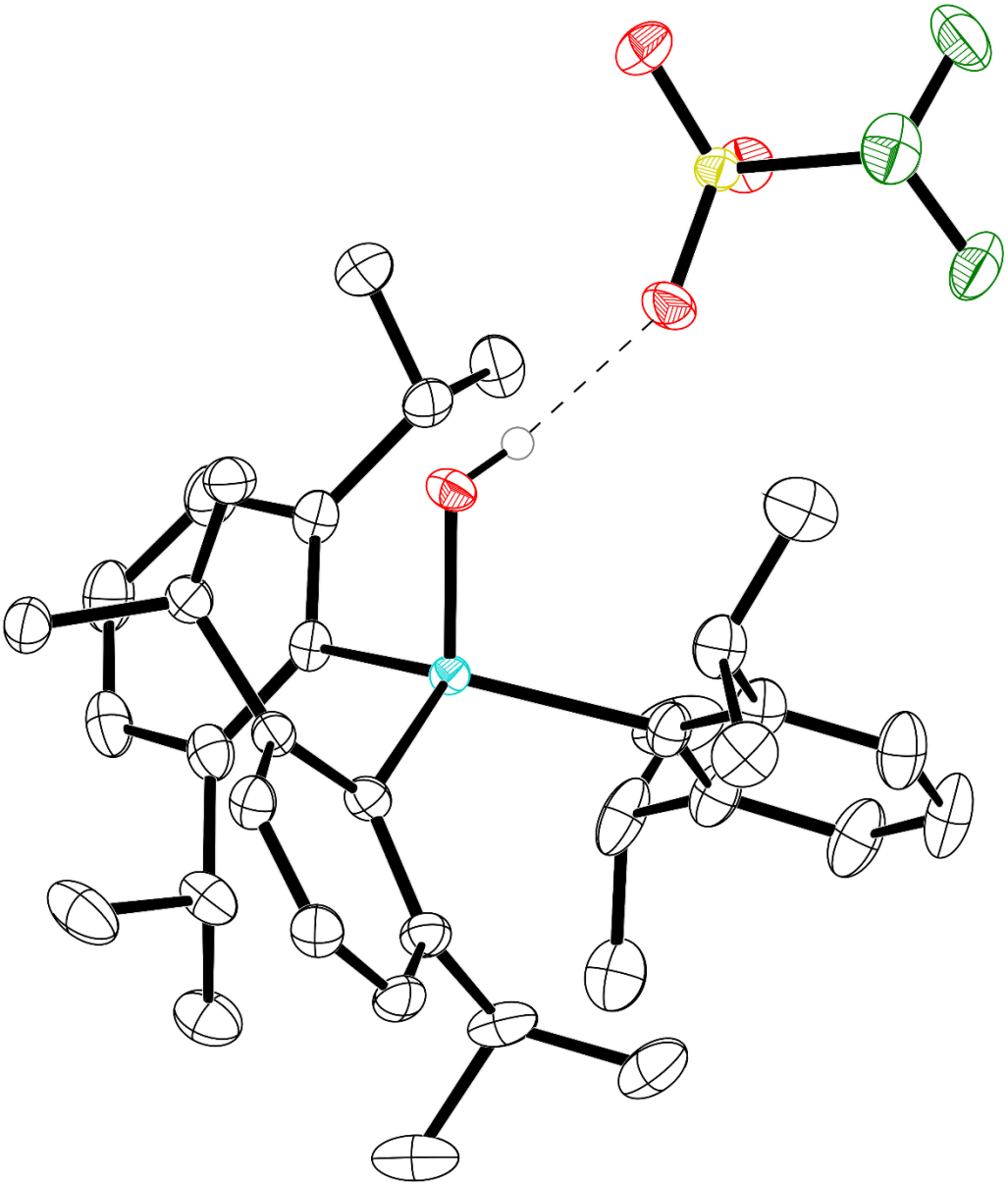

Figure S43. Thermal ellipsoid plot (50% probability) of **2a**. Color code: Sb teal, O red, C black, S yellow, F green, and H grey sphere of arbitrary radius. Non-protic H atoms are omitted for clarity.

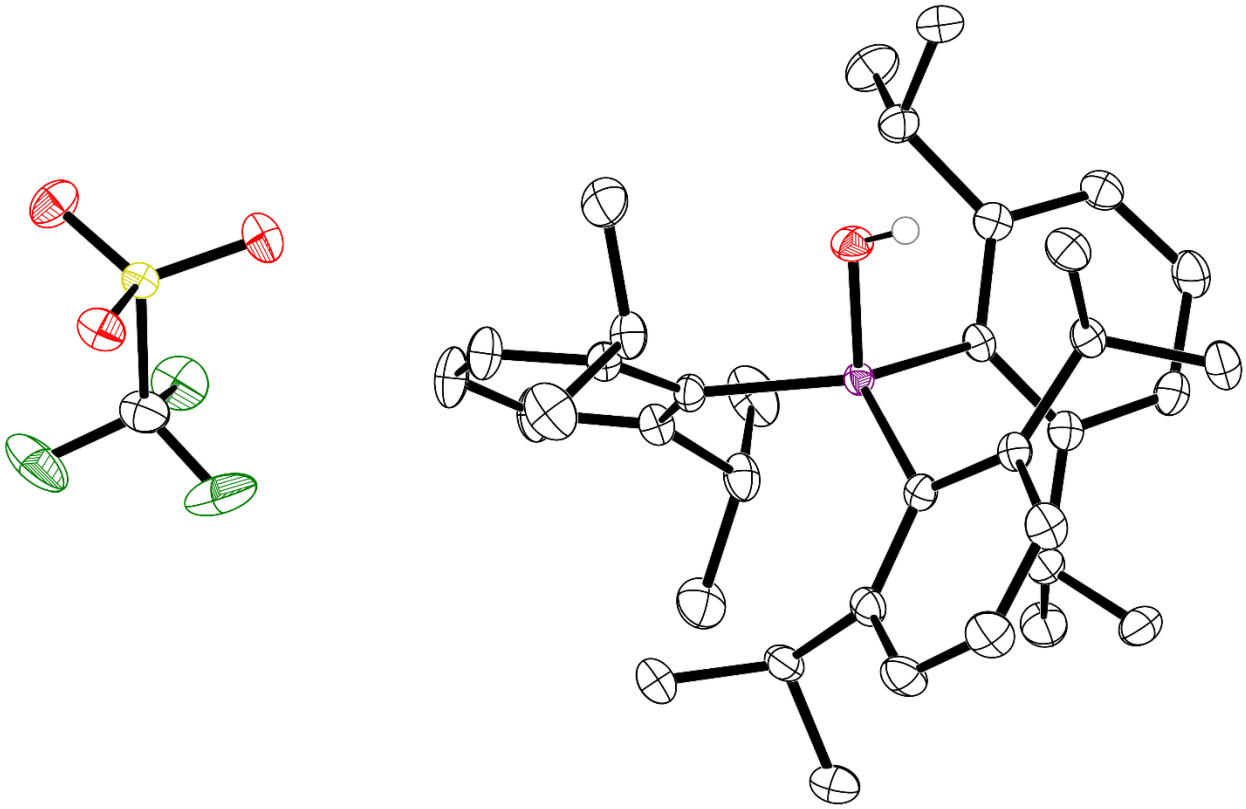

Figure S44. Thermal ellipsoid plot (50% probability) of **2b** triclinic. Color code: As purple, O red, C black, S yellow, F green, and H grey sphere of arbitrary radius. Non-protic H atoms are omitted for clarity.

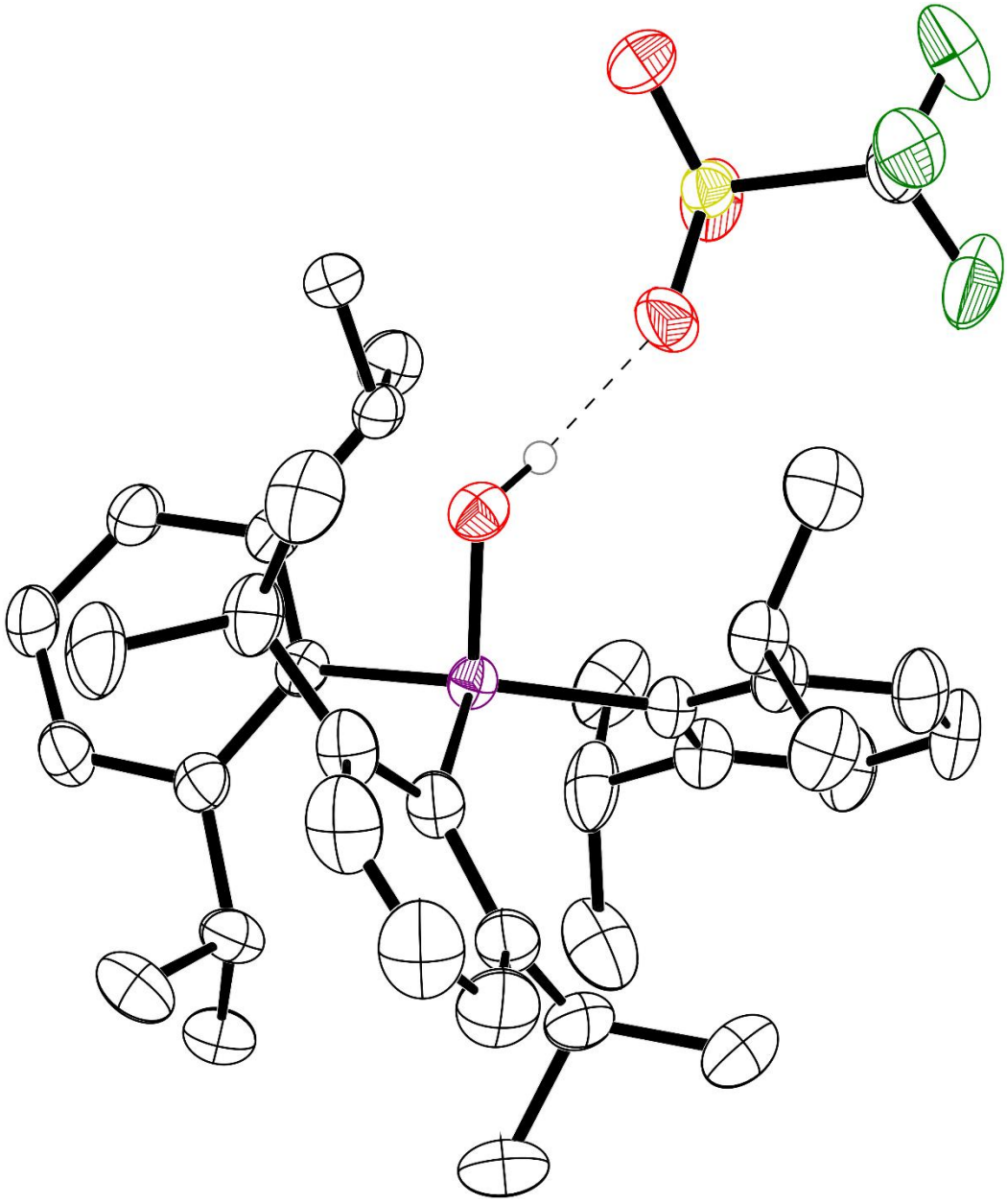

Figure S45. Thermal ellipsoid plot (50% probability) of **2b** monoclinic. Color code: As purple, O red, C black, S yellow, F green, and H grey sphere of arbitrary radius. Non-protic H atoms are omitted for clarity.

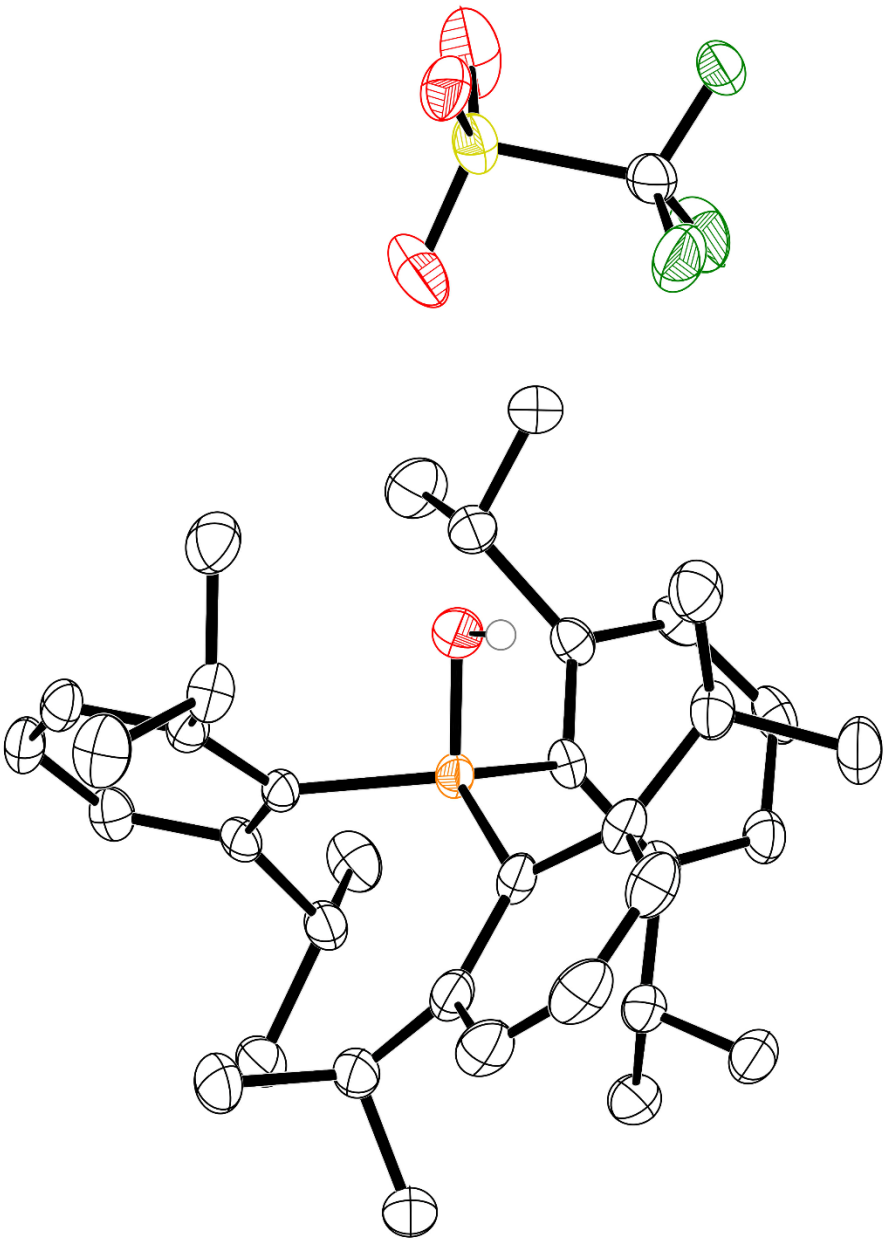

Figure S46. Thermal ellipsoid plot (50% probability) of one of the crystallographically independent copies of **2c** in the asymmetric unit. Color code: P orange, O red, C black, S yellow, F green, and H grey sphere of arbitrary radius. Non-protic H atoms are omitted for clarity.

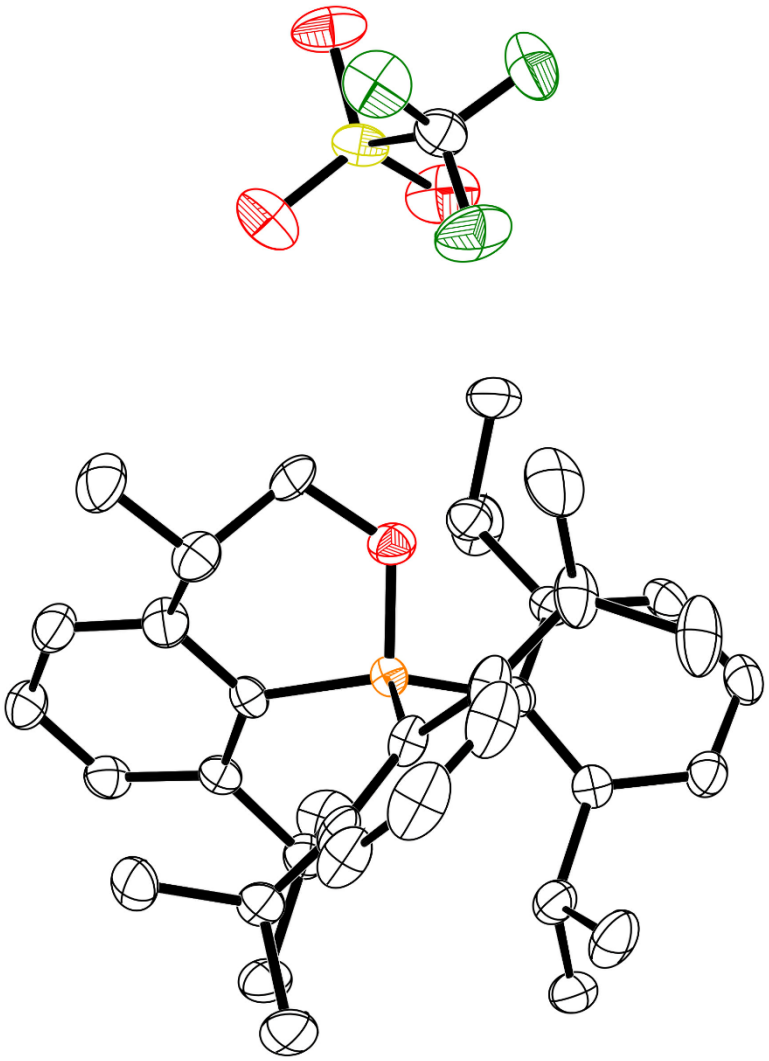

Figure S47. Thermal ellipsoid plot (50% probability) of **3**. Color code: P orange, O red, C black, S yellow, F green. Non-protic H atoms are omitted for clarity.

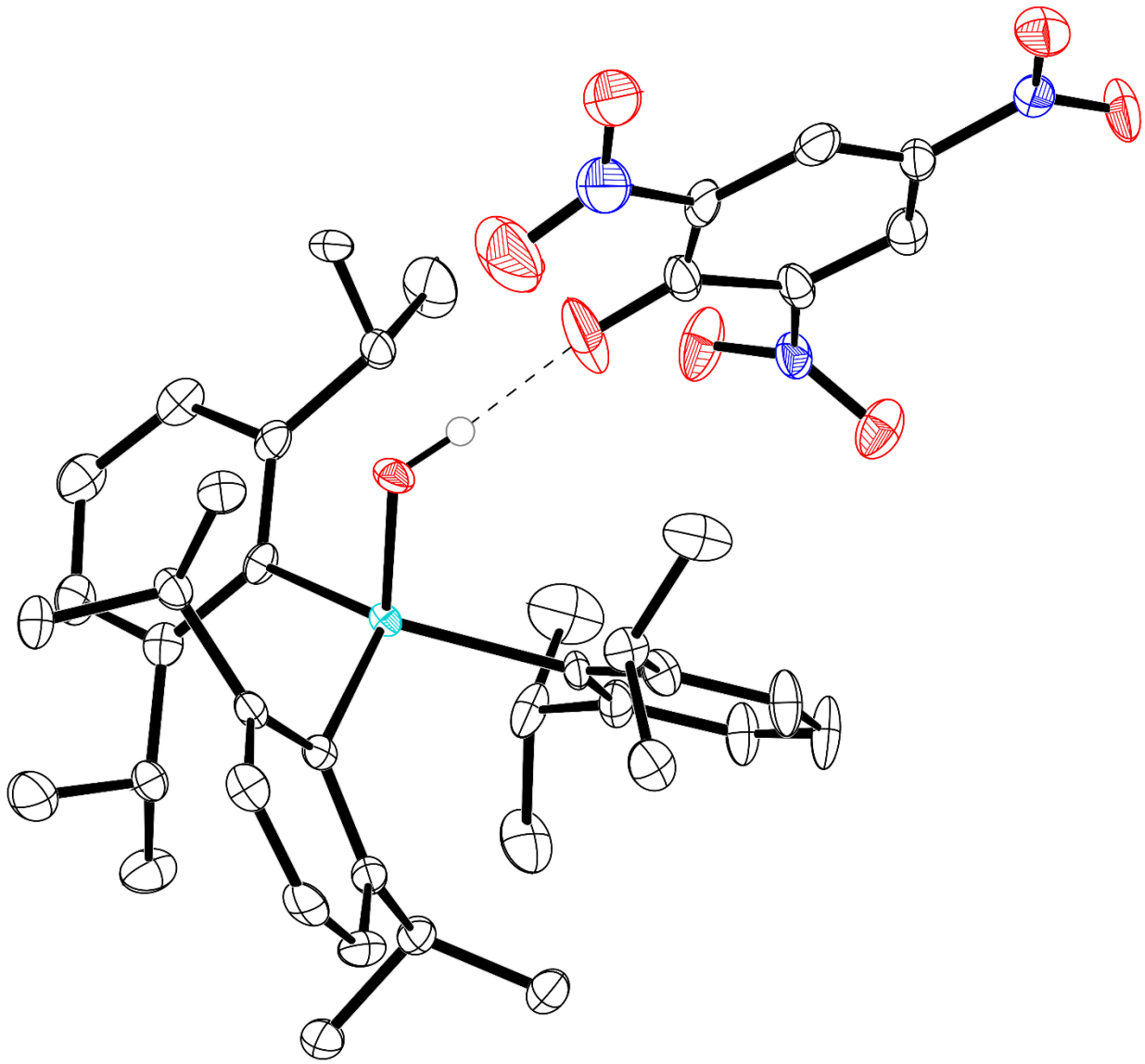

Figure S48. Thermal ellipsoid plot (50% probability) of **4a**. Color code: Sb teal, O red, C black, N blue, and H grey sphere of arbitrary radius. Non-protic H atoms are omitted for clarity.

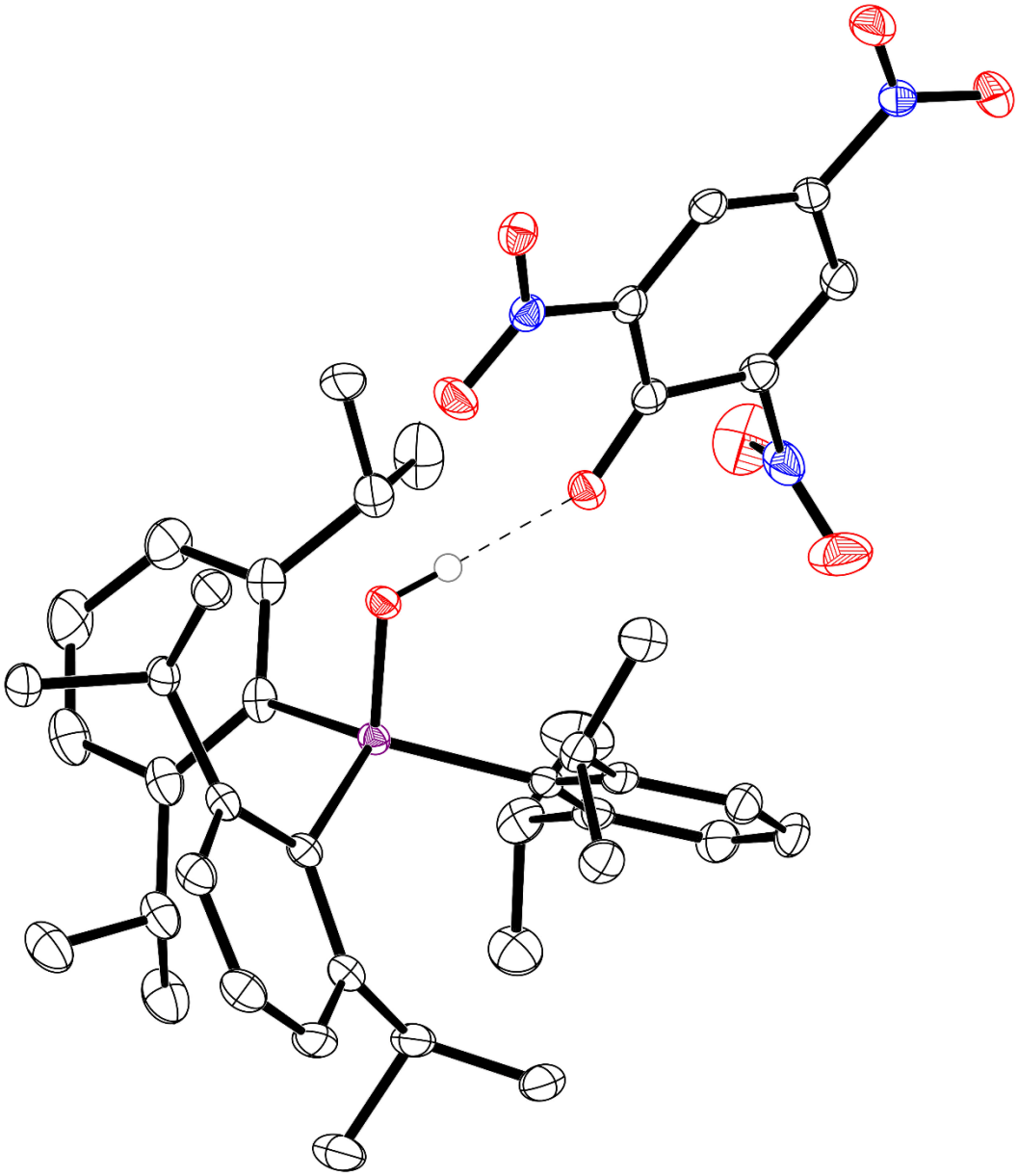

Figure S49. Thermal ellipsoid plot (50% probability) of one of the crystallographically independent copies of **4b** present in the asymmetric unit of crystals of **4b**·¾(C_6H_{12}). Color code: As purple, O red, C black, N blue, and H grey sphere of arbitrary radius. Non-protic H atoms are omitted for clarity.

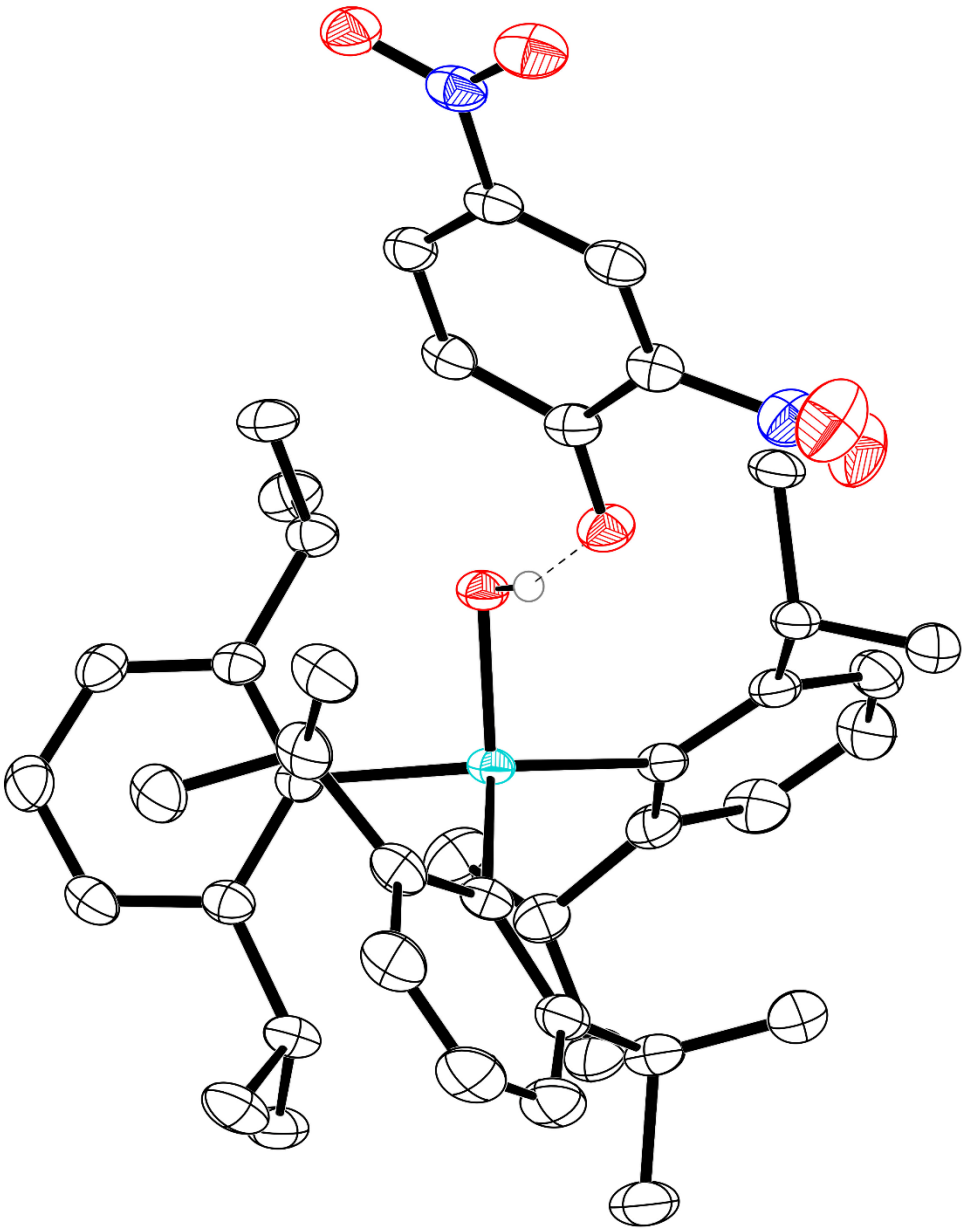

Figure S50. Thermal ellipsoid plot (50% probability) of **5**. Color code: Sb teal, O red, C black, N blue, and H grey sphere of arbitrary radius. Non-protic H atoms are omitted for clarity.

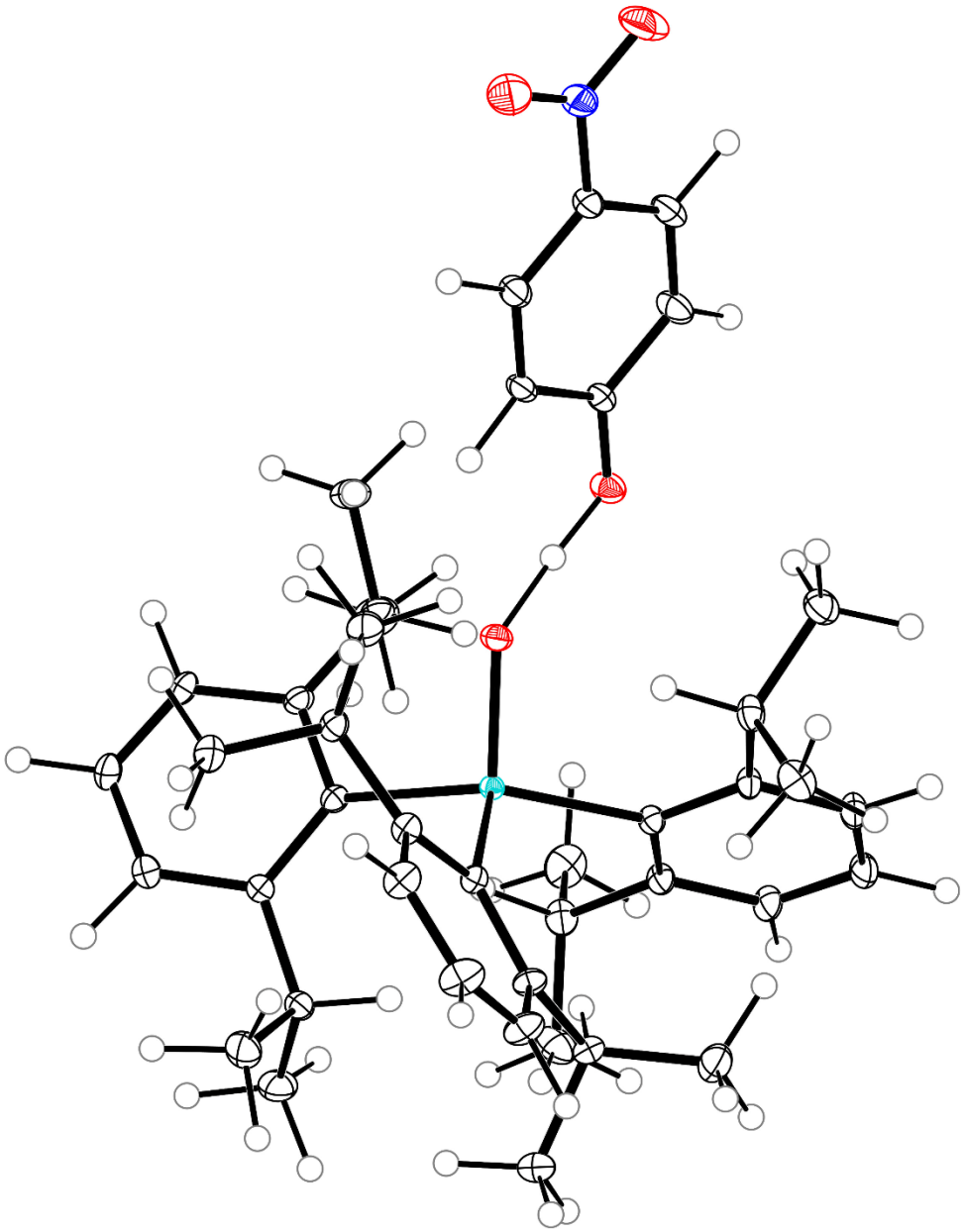

Figure S51. Thermal ellipsoid plot (50% probability) of **6**. Color code: Sb teal, O red, C black, N blue, and H grey spheres of arbitrary radius. Structure was obtained by Hirshfeld atom refinement.

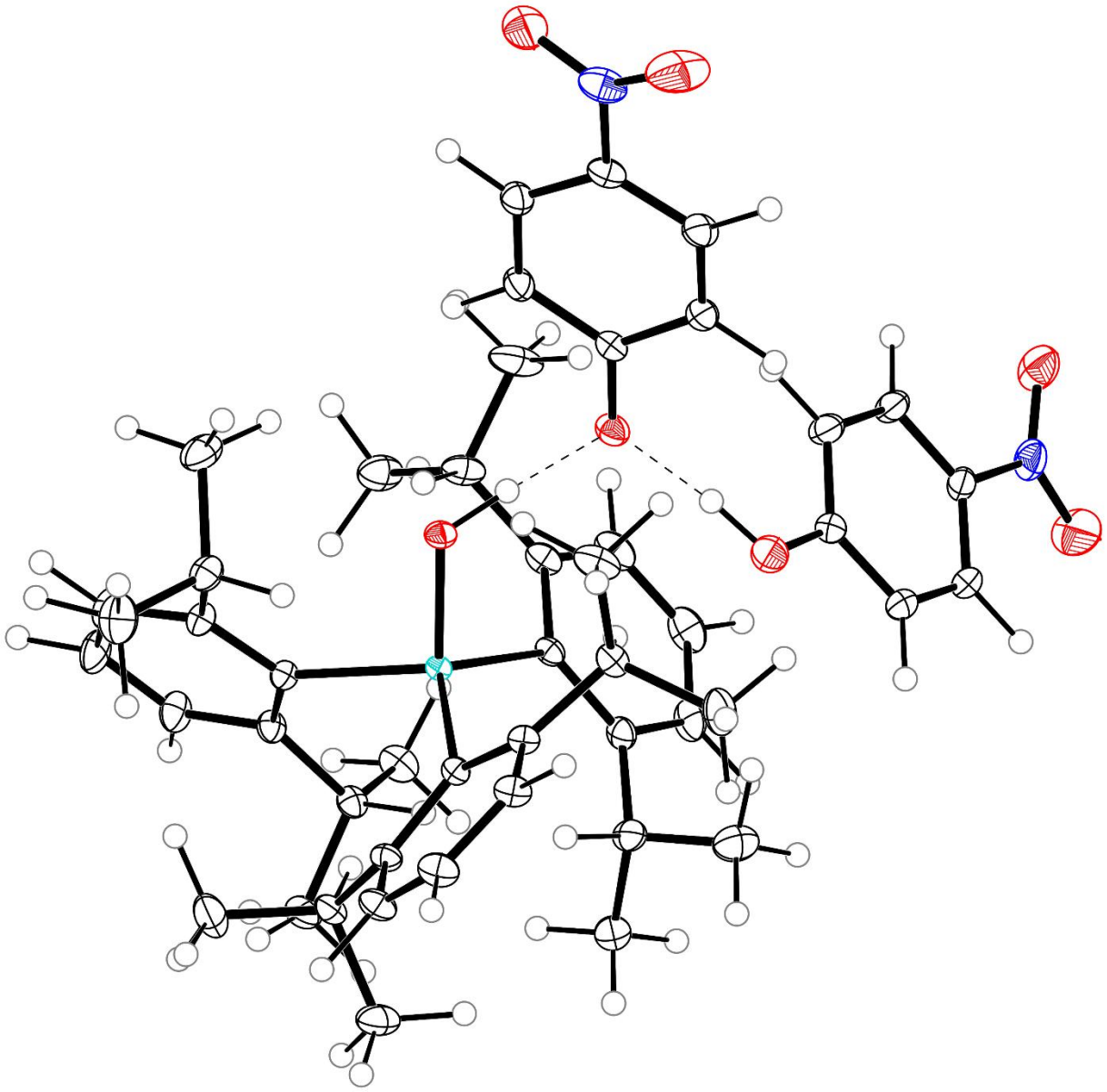

Figure S52. Thermal ellipsoid plot (50% probability) of **6**·*p*-nitrophenol. Color code: Sb teal, O red, C black, N blue, and H grey spheres of arbitrary radius. Structure was obtained by Hirshfeld atom refinement.

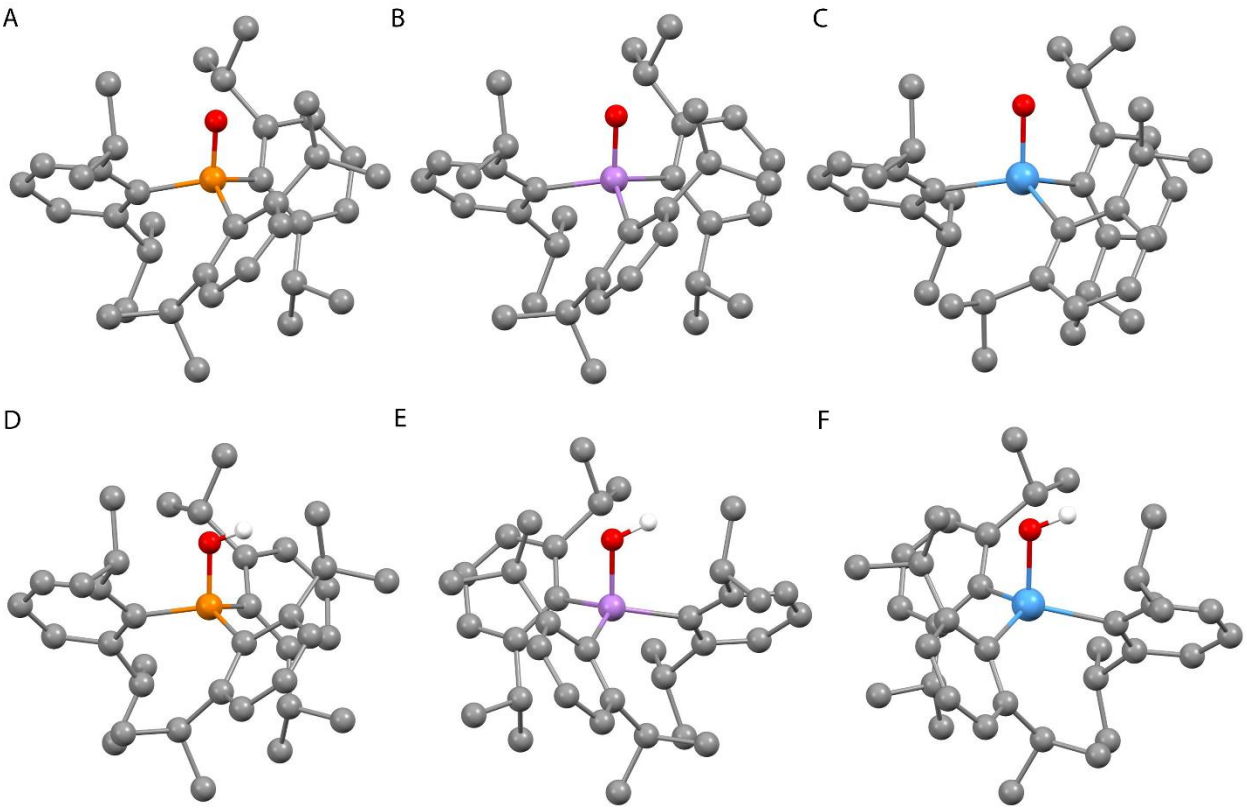

Figure S53. Ball-and-stick representations of atomic coordinates of molecules used in theoretical studies. Geometry optimized (PBE0/def2-TZVPP) structure of (A) **1c**, (B) **1b**, (C) **1a**, (D) **1c**H^+, (E) **1b**H^+, (F) **1a**H^+. Color code: C grey, H white, O red, Sb teal, As violet, P orange. Non-protic H atoms are omitted for clarity.

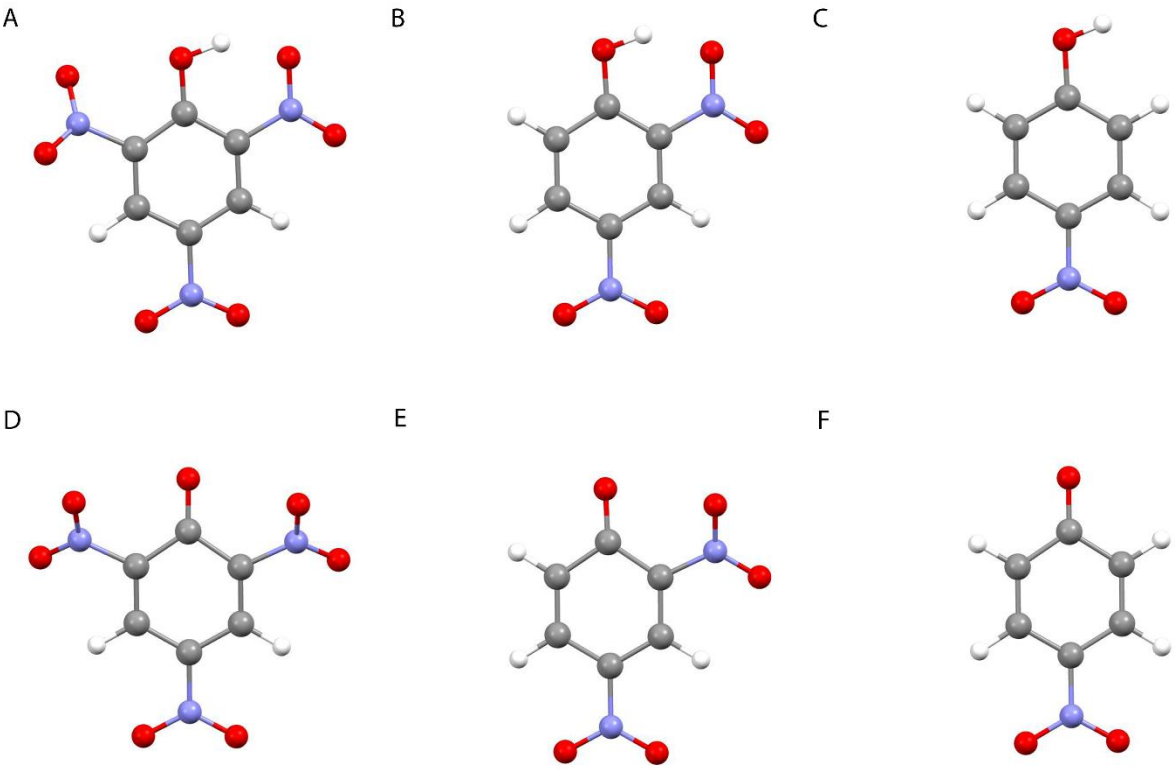

Figure S54. Ball-and-stick representations of atomic coordinates of molecules used in theoretical studies. Geometry optimized (PBE0/def2-TZVPP) structure of (A) 2,4,6-trinitrophenol, (B) 2,4-dinitrophenol, (C) 4-nitrophenol, (D) 2,4,6-trinitrophenoxide, (E) 2,4-dinitrophenoxide, (F) 4-nitrophenoxide. Color code: C grey, H white, O red, N blue.

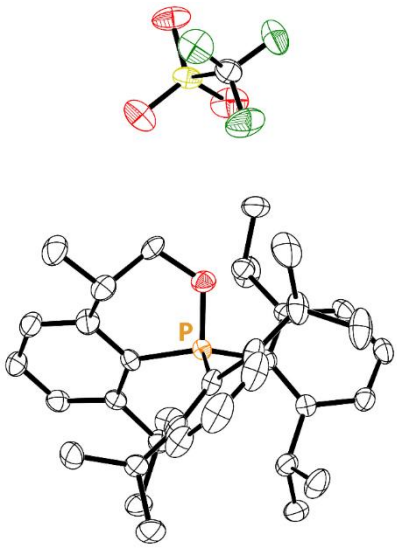

Figure S55. Thermal ellipsoid plot (50% probability) of **3**. Color code: P orange, O red, C black, S yellow, F green. H atoms are omitted for clarity.

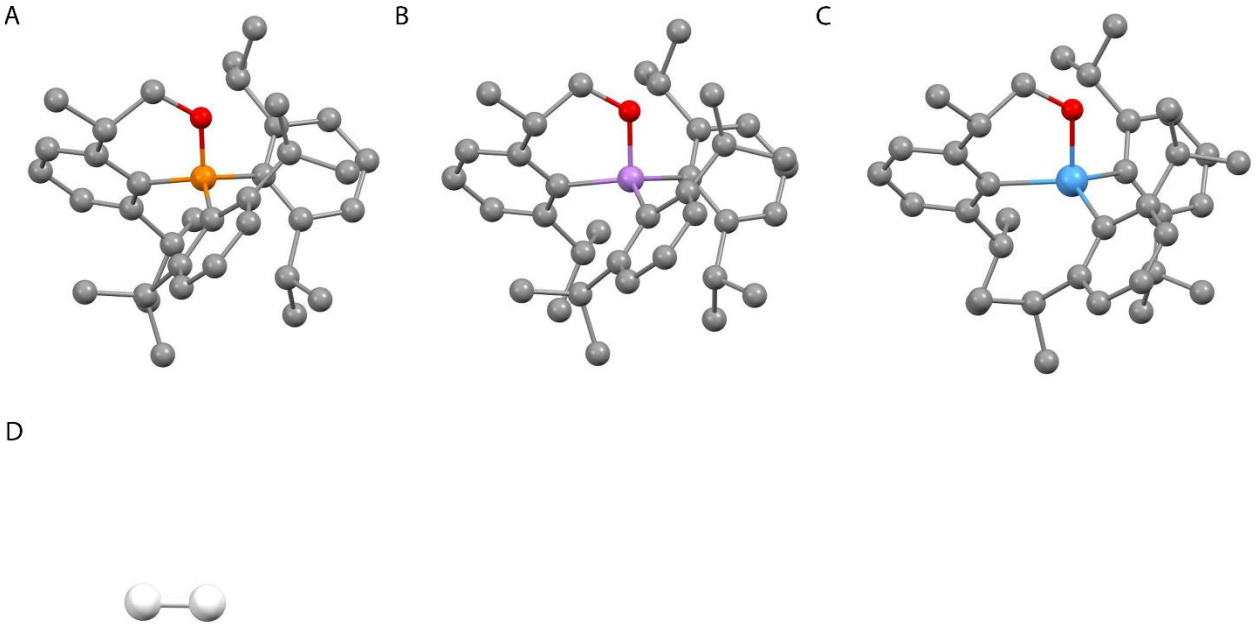

Figure S56. Ball-and-stick representations of atomic coordinates of molecules used in theoretical studies. Geometry optimized (PBE0/def2-TZVPP) structure of (A) **3**$^{+}$, (B) **3**$^{+}$(As), (C) **3**$^{+}$(Sb), and (D) H_2. Color code: C grey, H white, O red, Sb teal, As violet, P orange. H atoms are omitted for clarity from the depictions of the pnictogen compounds.

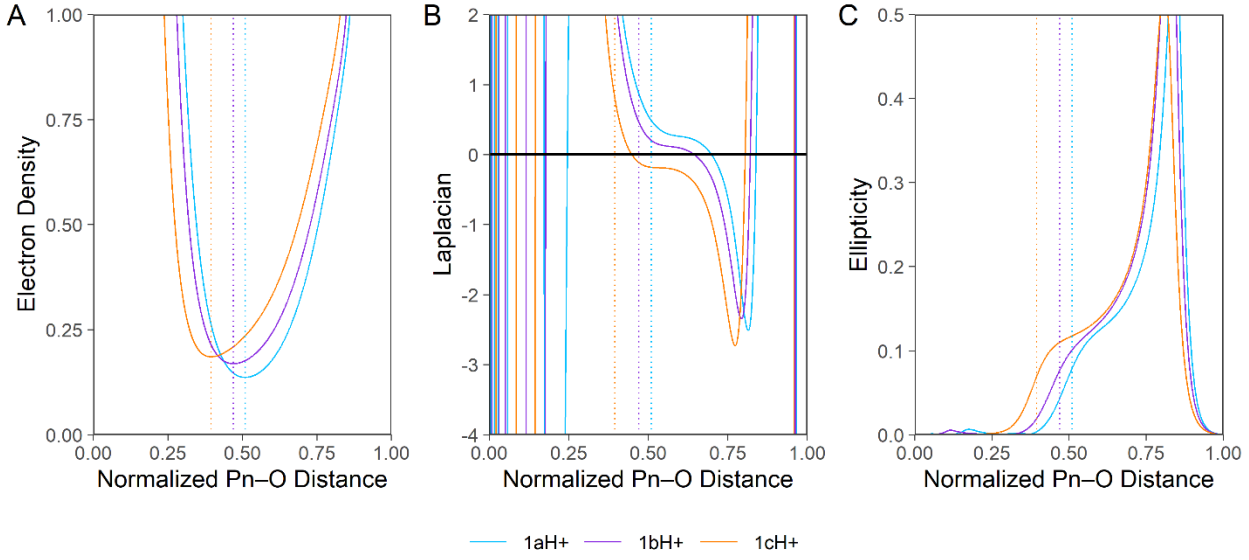

Figure S57. Plots of ρ (e^{-} Å^{-3}), $\nabla^2\rho$ (e^{-} Å^{-5}), and ε along the Pn–O interatomic vector in **1a**-**c**H^{+}.

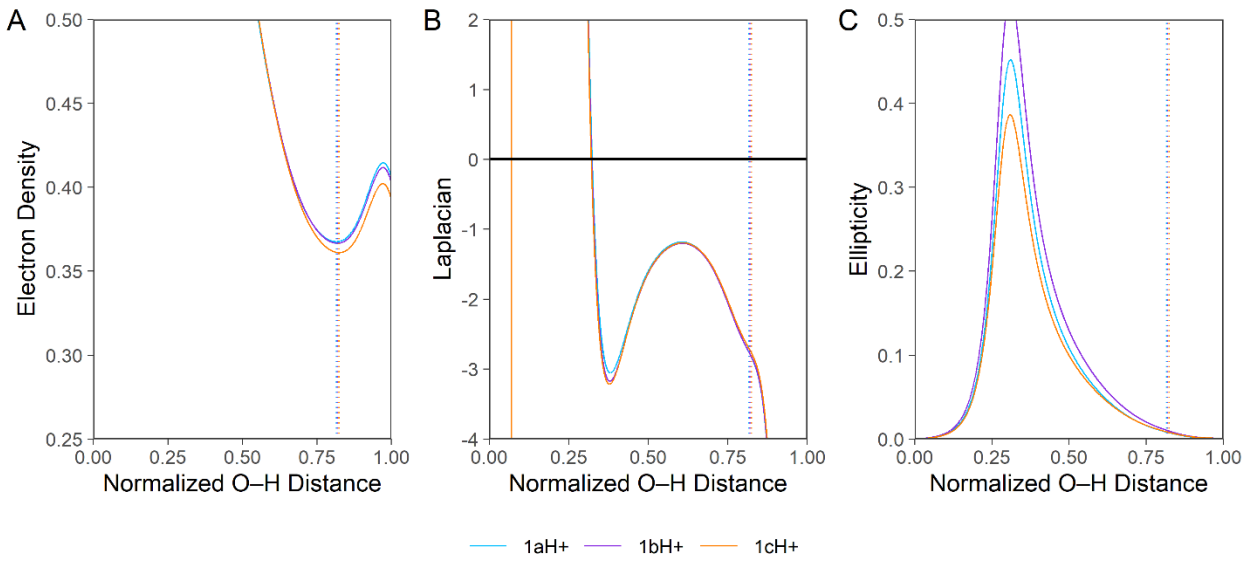

Figure S58. Plots of ρ (e^{-} Å^{-3}), $\nabla^2\rho$ (e^{-} Å^{-5}), and ε along the O–H interatomic vector in **1a**-**c**H^{+}.

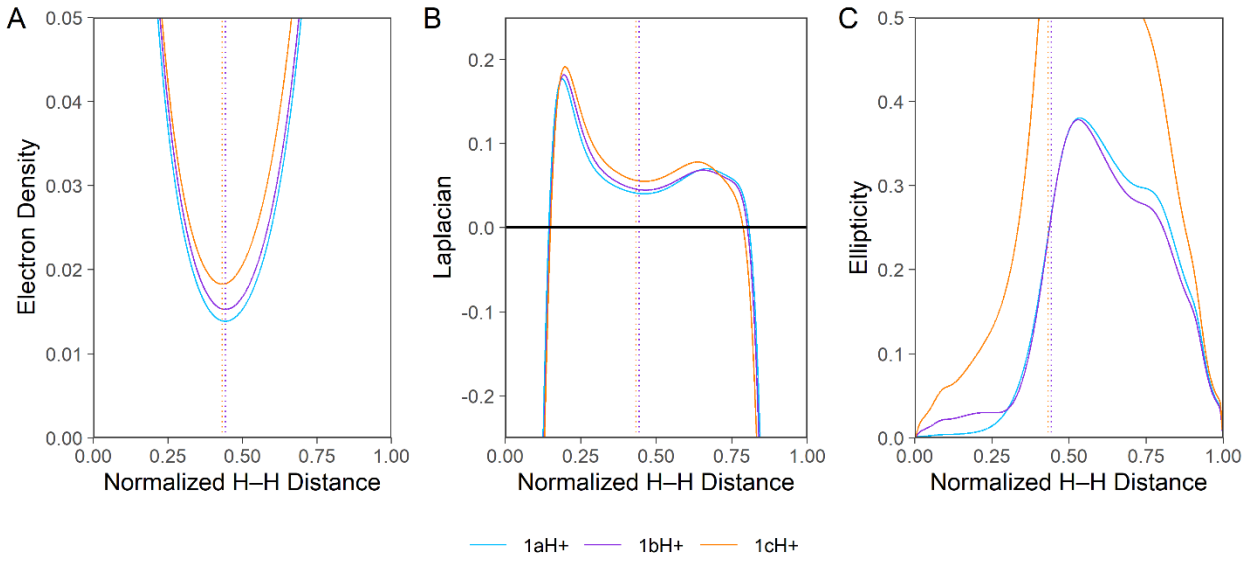

Figure S59. Plots of ρ (e^{-} Å^{-3}), $\nabla^2\rho$ (e^{-} Å^{-5}), and ε along the OH···HC$_{methyl}$ interatomic vector for the primary dihydrogen bonding interaction in **1a**-**c**H^{+}.

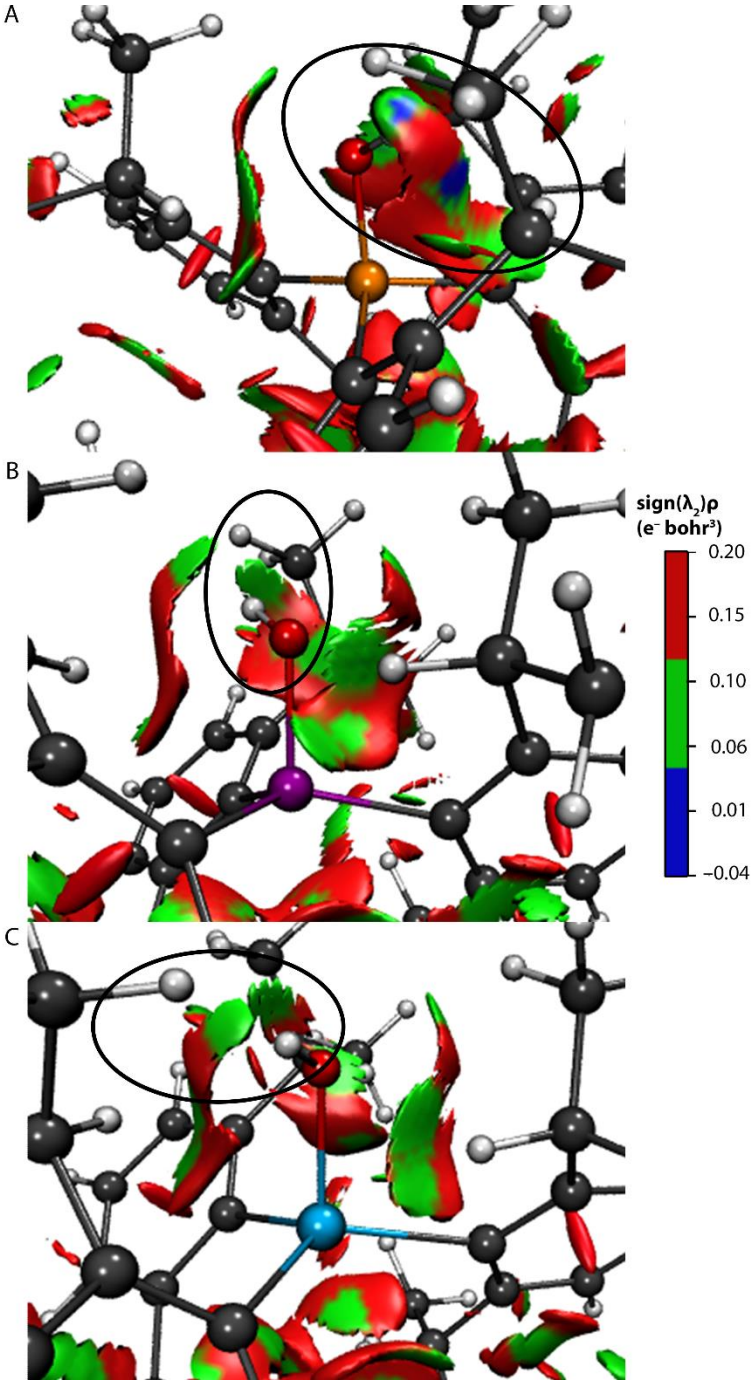

Figure S60. NCI analysis of **1c**H$^+$ (*top*), **1b**H$^+$ (*middle*), and **1a**H$^+$ (*bottom*) depicting reduced gradient surfaces (isovalue = 0.45 a.u.) with the function sign(λ_2)ρ where λ_2 is the second-largest eigenvalue of the Laplacian color-mapped on the surface. Blue is indicative of H-bonding interactions, green is indicative of van der Waals interactions, and red is indicative of steric repulsions. Color code: C black, H grey, O red, Sb teal, As violet, P orange.

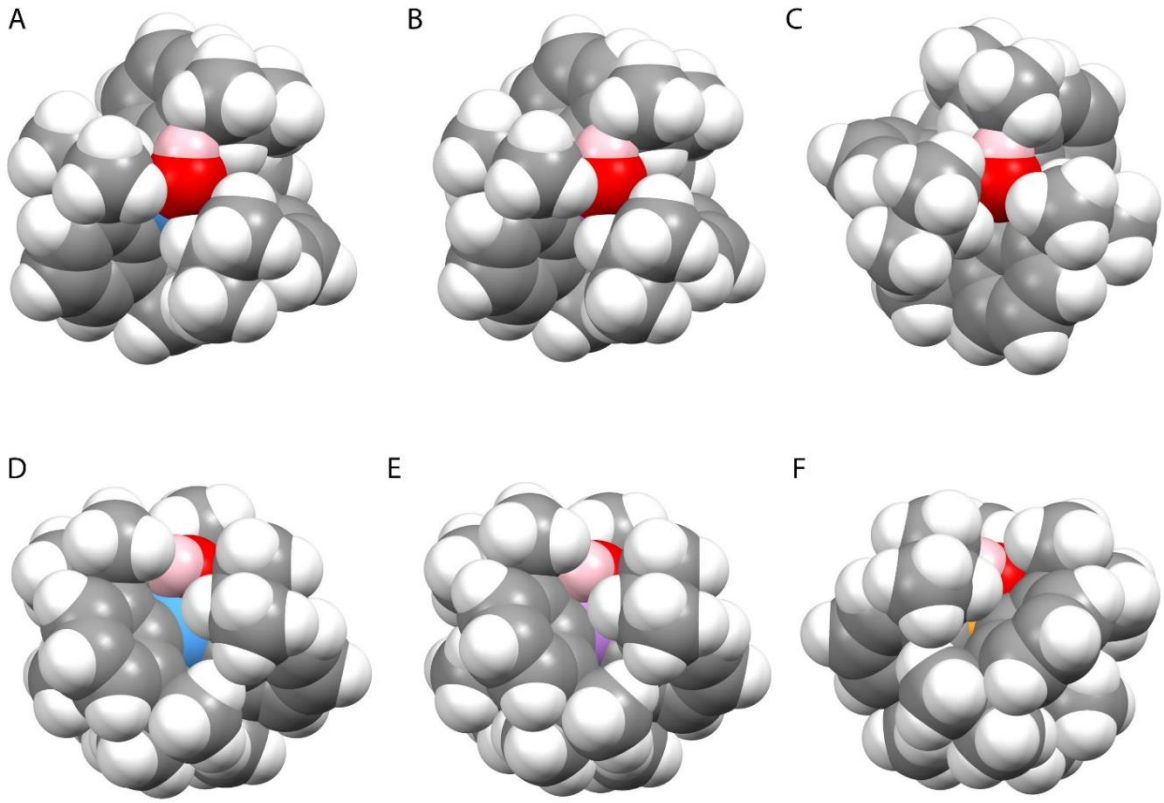

Figure S61. Space-filling diagrams of optimized geometries (PBE0/def2-TZVPP) of **1a**H$^+$ (A, D), **1b**H$^+$ (B, E) and **1c**H$^+$ (C, F) viewed along Pn–O bond axis (A-C) and perpendicular to Pn–O bond axis (D-F) (Pn = Sb, As, P). Color code: Sb teal, As purple, P orange, C grey, H white, protic H atom pink.

Table S1. Calculated reaction enthalpies and Gibbs free energies of elimination of H_2 from hydroxypnictonium cations **1a**-**c**H$^+$ to form cyclized alkoxypnictonium cations **3**$^+$(Sb), **3**$^+$(As), and **3**$^+$, respectively.

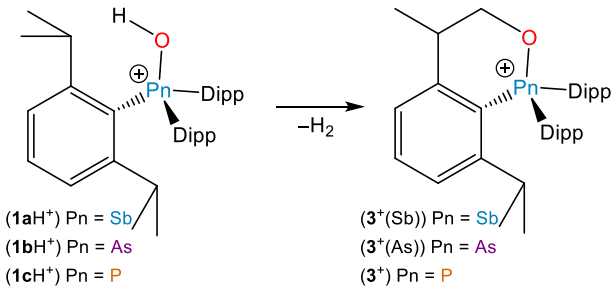

Compound	Δ*H* (kcal/mol)	Δ*G* (kcal/mol)
1aH$^+$	16.3	9.6
1bH$^+$	13.5	6.6
1cH$^+$	12.4	5.3

Table S2. Crystallographic details for **2a**, **2b**·$CHCl_3$ triclinic, **2b**·$CHCl_3$ monoclinic, and **2c**.

Compound	**2a**	**2b**·$CHCl_3$ triclinic	**2b**·$CHCl_3$ monoclinic	**2c**
Empirical formula	$C_{37}H_{52}F_3O_4SSb$	$C_{38}H_{53}F_3Cl_3O_4SAs$	$C_{38}H_{53}F_3Cl_3O_4SAs$	$C_{37}H_{52}F_3O_4SP$
Formula Weight	771.59	844.13	844.13	680.81
Temperature (K)	100.0(1)	100.0(1)	100.0(1)	100.0(1)
Wavelength (Å)	1.54184	1.54184	1.54184	1.54184
Crystal system	Triclinic	Triclinic	Monoclinic	Triclinic
Space group	$P\bar{1}$	$P\bar{1}$	$P2_1/n$	$P\bar{1}$
a (Å)	10.19520(10)	10.1956(2)	10.06410(10)	14.3959(2)
b (Å)	12.58260(10)	14.2779(2)	17.7940(3)	16.0784(2)
c (Å)	14.95020(10)	14.7095(2)	23.5660(3)	16.8118(2)
α (°)	90.2560(10)	92.4510(10)		106.2340(10)
β (°)	98.4430(10)	101.6540(10)	98.6020(10)	99.4490(10)
γ (°)	105.1700(10)	100.5970(10)		97.5890(10)
Volume (Å^3)	1829.10(3)	2054.26(6)	4172.74(10)	3619.84(8)
Z	2	2	4	4
ρ_{calc} (Mg/m^3)	1.401	1.365	1.344	1.249
Crystal size (mm^3)	0.09 × 0.08 × 0.06	0.23 × 0.15 × 0.13	0.23 × 0.06 × 0.05	0.21 × 0.12 × 0.07
θ range (°)	2.991 to 67.073	3.078 to 67.078	3.125 to 67.074	2.801 to 67.078
Total reflections	52573	25894	35950	49143
Unique reflections	6525	7326	7436	12911
Method	IAM	IAM	IAM	IAM
Parameters	431	467	504	928
Completeness	100	100	100	99.9
R_{int}	0.0480	0.0335	0.0394	0.0339
R_1 ($I > 2\sigma$)	0.0198	0.0362	0.0535	0.0435
R_1 (all data)	0.0209	0.0383	0.0573	0.0486
wR_2 ($I > 2\sigma$)	0.0489	0.0942	0.1154	0.1207
wR_2 (all data)	0.0494	0.0957	0.1170	0.1247
Goodness of fit, *S*	1.031	1.056	1.164	1.037

Table S3. Crystallographic details for **3**, **4a**, **4b**·¾(C_6H_{12}), and **5**·$(CHCl_3)_2$.

Compound	**3**	**4a**[†]	**4b**·¾(C_6H_{12})	**5**·$(CHCl_3)_2$
Empirical formula	$C_{37}H_{50}F_3O_4SP$	$C_{42}H_{54}N_3O_8Sb$	$C_{46.5}H_{63}AsN_3O_8$	$C_{44}H_{57}Cl_6N_2O_6Sb$
Formula Weight	678.80	850.63	866.92	1044.36
Temperature (K)	100.0(1)	100.0(1)	100.0(1)	100.0(1)
Wavelength (Å)	1.54184	0.71073	1.54184	1.54184
Crystal system	Monoclinic	Monoclinic	Triclinic	Triclinic
Space group	$P2_1/n$	Pn	$P\bar{1}$	$P\bar{1}$
a (Å)	9.49870(10)	10.4423(2)	11.82030(10)	11.1814(2)
b (Å)	25.1021(3)	20.8325(5)	15.2864(2)	14.1312(3)
c (Å)	14.9869(2)	18.7820(4)	24.9112(2)	16.4708(4)
α (°)			87.8670(10)	79.673(2)
β (°)	101.4440(10)	93.444(2)	80.2660(10)	74.232(2)
γ (°)			88.6100(10)	76.038(2)
Volume (Å^3)	3502.39(7)	4078.44(15)	4432.59(8)	2412.49(10)
Z	4	4	4	2
ρ_{calc} (Mg/m^3)	1.287	1.385	1.299	1.438
Crystal size (mm^3)	0.11 × 0.08 × 0.06	0.27 × 0.21 × 0.14	0.19 × 0.13 × 0.08	0.19 × 0.08 × 0.05
θ range (°)	3.486 to 67.077	2.185 to 25.123	2.893 to 67.077	2.809 to 67.080
Total reflections	48293	32156	60318	30917
Unique reflections	6253	12674	15821	8624
Method	IAM	IAM	IAM	IAM
Parameters	455	1087	1086	621
Completeness	100	99.9	100.0	100.0
R_{int}	0.0372	0.0338	0.0359	0.0457
R_1 ($I > 2\sigma$)	0.0491	0.0310	0.0311	0.0346
R_1 (all data)	0.0524	0.0344	0.0345	0.0367
wR_2 ($I > 2\sigma$)	0.1282	0.0693	0.0779	0.0908
wR_2 (all data)	0.1307	0.0709	0.0799	0.0925
Goodness of fit, *S*	1.039	1.079	1.048	1.048

[†] Flack *x* parameter: -0.008(8)

Table S4. Crystallographic parameters for **6**·*p*-nitrophenol and **6**.

Compound	**6**·*p*-nitrophenol		**6**	
Empirical formula	$C_{48}H_{61}N_2O_7Sb$		$C_{42}H_{56}NO_4Sb$	
Formula Weight	899.788		760.677	
Temperature (K)	100.0(1)		99.95(17)	
Wavelength (Å)	0.71073		0.71073	
Crystal system	Monoclinic		Triclinic	
Space group	$P2_1/n$		$P\bar{1}$	
a (Å)	15.7304(3)		9.8747(2)	
b (Å)	18.4840(3)		12.6935(3)	
c (Å)	15.7610(3)		15.4719(3)	
α (°)			87.478(2)	
β (°)	101.383(2)		77.760(2)	
γ (°)			83.096(2)	
Volume (Å^3)	4492.54(14)		1881.15(7)	
Z	4		2	
ρ_{calc} (Mg/m^3)	1.330		1.343	
Crystal size (mm^3)	0.21 × 0.14 × 0.1		0.22 × 0.08 × 0.06	
θ range (°)	2.32 to 33.73		2.08 to 33.73	
Total reflections	69536		62483	
Unique reflections	17515		15034	
Method	IAM	HAR	IAM	HAR
Parameters	541	706	448	601
Completeness	97.8	97.79	100.0	99.96
R_{int}	0.0388	0.0412	0.0487	0.0515
R_1 ($I > 2\sigma$)	0.0296	0.0255	0.0308	0.0276
R_1 (all data)	0.0403	0.0362	0.0374	0.0341
wR_2 ($I > 2\sigma$)	0.0677	0.0471	0.0664	0.0488
wR_2 (all data)	0.0708	0.0496	0.0720	0.0535
Goodness of fit, *S*	1.059	1.0040	1.061	0.9511

Table S5. Select data from NMR monitoring of titration (replicate 1) of **2a** with triethylamine (TEA).

Volume TEA added (μL)	Chemical Shift (ppm)	Total volume sample (μL)	Deprotonated (%)	[1a] (mM)	[1aH$^+$] (mM)	[TEA] (mM)	Equivalents of TEA added
0.05	2.89	600.5	1.4	0.08	5.32	0.5	0.1
0.1	2.93	601	3.8	0.20	5.19	1.0	0.2
0.15	2.96	601.5	6.3	0.34	5.05	1.4	0.3
0.2	2.98	602	7.5	0.40	4.98	2.0	0.4
0.25	3.01	602.5	9.8	0.53	4.85	2.4	0.6
0.35	3.07	603.5	14.5	0.78	4.59	3.4	0.8
0.5	3.12	605	17.6	0.94	4.41	5.0	1.1
0.75	3.22	607.5	24.8	1.33	4.01	7.5	1.7
1	3.27	610	28.6	1.52	3.79	10.2	2.2
1.5	3.38	610.5	37.1	1.97	3.34	15.7	3.3
2	3.46	611	42.3	2.25	3.06	21.2	4.4
3	3.59	612	51.8	2.74	2.55	32.4	6.6
4.5	3.70	613.5	60.1	3.17	2.11	49.5	10.0
7	3.81	616	68.4	3.60	1.66	77.9	15.5
10	3.90	619	74.6	3.90	1.33	112.0	22.1
15	3.99	624	81.0	4.20	0.99	168.3	33.2
25	4.07	634	87.0	4.45	0.66	278.5	55.4
35	4.11	644	89.9	4.52	0.51	385.4	77.5
45	4.14	654	91.7	4.54	0.41	489.1	99.7
55	4.15	664	93.0	4.54	0.34	589.7	121.8
65	4.17	674	94.0	4.52	0.29	687.4	143.9
85	4.18	694	95.2	4.44	0.23	874.3	188.2

Table S6. Select data from NMR monitoring of titration (replicate 2) of **2a** with triethylamine (TEA).

Volume TEA added (μL)	Chemical Shift (ppm)	Total volume sample (μL)	Deprotonated (%)	[1a] (mM)	[1aH$^+$] (mM)	[TEA] (mM)	Equivalents of TEA added
0.05	2.93	600.5	4.1	0.22	5.17	0.5	0.1
0.1	2.96	601	6.6	0.36	5.03	1.0	0.2
0.15	3.00	601.5	9.3	0.50	4.89	1.4	0.3
0.2	3.02	602	10.7	0.58	4.81	2.0	0.4
0.25	3.05	602.5	12.5	0.67	4.71	2.4	0.6
0.35	3.08	603.5	15.3	0.82	4.55	3.4	0.8
0.5	3.14	605	19.1	1.02	4.33	5.0	1.1
0.75	3.21	607.5	24.8	1.32	4.01	7.5	1.7
1	3.28	610	29.4	1.56	3.75	10.2	2.2
1.5	3.38	610.5	36.9	1.96	3.35	15.7	3.3
2	3.49	611	44.5	2.36	2.94	21.2	4.4
3	3.61	612	53.5	2.83	2.46	32.4	6.6
4.5	3.73	613.5	62.4	3.29	1.99	49.5	10.0
7	3.86	616	71.4	3.75	1.51	77.9	15.5
10	3.94	619	77.3	4.04	1.19	112.0	22.1
15	4.01	624	82.8	4.30	0.89	168.3	33.2
25	4.10	634	89.1	4.55	0.56	278.5	55.4
35	4.14	644	91.7	4.62	0.42	385.4	77.5
45	4.16	654	93.4	4.62	0.33	489.1	99.7
55	4.17	664	94.5	4.61	0.27	589.7	121.8
65	4.18	674	95.3	4.58	0.23	687.4	143.9
85	4.20	694	96.5	4.50	0.16	874.3	188.2

Table S7. Select data from NMR monitoring of titration (replicate 3) of **2a** with triethylamine (TEA).

Volume TEA added (μL)	Chemical Shift (ppm)	Total volume sample (μL)	Deprotonated (%)	[1a] (mM)	[1aH$^+$] (mM)	[TEA] (mM)	Equivalents of TEA added
0.05	2.95	600.5	5.8	0.31	5.08	0.5	0.1
0.1	2.99	601	8.6	0.47	4.93	1.0	0.2
0.15	3.04	601.5	12.0	0.64	4.74	1.4	0.3
0.2	3.07	602	14.1	0.76	4.62	2.0	0.4
0.25	3.10	602.5	16.6	0.89	4.48	2.4	0.6
0.35	3.16	603.5	20.5	1.10	4.27	3.4	0.8
0.5	3.21	605	24.3	1.30	4.06	5.0	1.1
0.75	3.27	607.5	28.6	1.53	3.81	7.5	1.7
1	3.32	610	32.3	1.71	3.60	10.2	2.2
1.5	3.36	610.5	35.6	1.89	3.42	15.7	3.3
2	3.45	611	42.2	2.24	3.06	21.2	4.4
3	3.59	612	51.8	2.74	2.55	32.4	6.6
4.5	3.71	613.5	60.6	3.20	2.08	49.5	10.0
7	3.82	616	69.0	3.63	1.63	77.9	15.5
10	3.91	619	75.0	3.93	1.31	112.0	22.1
15	3.99	624	81.0	4.20	0.99	168.3	33.2
25	4.07	634	87.1	4.45	0.66	278.5	55.4
35	4.11	644	90.1	4.53	0.50	385.4	77.5
45	4.14	654	91.9	4.55	0.40	489.1	99.7
55	4.15	664	93.1	4.54	0.34	589.7	121.8
65	4.17	674	94.0	4.52	0.29	687.4	143.9
85	4.19	694	95.4	4.45	0.22	874.3	188.2

Table S8. Select data from NMR monitoring of titration (replicate 1) of **2b** with acridine (ACR).

Mass ACR added (mg)	Chemical Shift (ppm)	Total volume sample (μL)	Deprotonated (%)	[1b] (mM)	[1bH$^+$] (mM)	[ACR] (mM)	Equivalents of ACR added
0.05	2.79	501	2.3	0.08	3.28	0.5	0.2
0.07	2.82	501.5	4.6	0.16	3.20	0.7	0.2
0.12	2.85	502.5	8.0	0.27	3.08	1.1	0.4
0.17	2.87	503.5	10.1	0.34	3.01	1.6	0.6
0.25	2.90	505	12.7	0.42	2.91	2.3	0.8
0.37	2.94	507.5	16.7	0.55	2.76	3.5	1.2
0.49	2.98	510	20.0	0.66	2.64	4.8	1.6
0.74	3.04	515	25.3	0.83	2.44	7.2	2.5
0.99	3.08	520	29.4	0.95	2.29	9.7	3.3
1.24	3.12	525	33.1	1.06	2.15	12.1	4.1
1.73	3.18	535	39.2	1.23	1.91	16.8	5.7
2.47	3.26	550	45.9	1.41	1.65	23.7	8.2
3.96	3.36	580	55.7	1.62	1.29	36.5	13.1
5.94	3.44	620	62.9	1.71	1.01	51.7	19.7
8.90	3.53	680	72.1	1.79	0.69	71.3	29.5
12.37	3.61	750	79.2	1.78	0.47	90.3	41.0
17.31	3.67	850	84.6	1.67	0.31	112.0	57.4
22.26	3.70	950	88.1	1.56	0.21	129.2	73.8
27.21	3.73	1050	90.6	1.45	0.15	143.2	90.2
32.15	3.75	1150	92.4	1.35	0.11	154.7	106.6
42.05	3.77	1150	94.4	1.38	0.08	202.7	139.4
51.94	3.78	1150	95.6	1.40	0.06	250.7	172.2

Table S9. Select data from NMR monitoring of titration (replicate 2) of **2b** with acridine (ACR).

Mass ACR added (mg)	Chemical Shift (ppm)	Total volume sample (μL)	Deprotonated (%)	[1b] (mM)	[1bH$^+$] (mM)	[ACR] (mM)	Equivalents of ACR added
0.05	2.81	501	4.6	0.15	3.21	0.5	0.2
0.07	2.84	501.5	6.8	0.23	3.13	0.7	0.2
0.12	2.88	502.5	10.9	0.37	2.99	1.1	0.4
0.17	2.91	503.5	13.3	0.44	2.90	1.6	0.6
0.25	2.93	505	15.8	0.53	2.81	2.3	0.8
0.37	2.99	507.5	20.6	0.68	2.63	3.5	1.2
0.49	3.02	510	23.9	0.79	2.51	4.8	1.6
0.74	3.08	515	29.5	0.96	2.31	7.2	2.5
0.99	3.12	520	33.3	1.08	2.16	9.7	3.3
1.24	3.17	525	37.5	1.20	2.01	12.1	4.1
1.73	3.22	535	43.1	1.35	1.79	16.8	5.7
2.47	3.29	550	49.4	1.51	1.55	23.7	8.2
3.96	3.40	580	59.1	1.71	1.19	36.5	13.1
5.94	3.49	620	68.0	1.85	0.87	51.7	19.7
8.90	3.56	680	74.7	1.85	0.63	71.3	29.5
12.37	3.63	750	81.3	1.82	0.42	90.3	41.0
17.31	3.70	850	87.3	1.73	0.25	112.0	57.4
22.26	3.73	950	90.4	1.60	0.17	129.2	73.8
27.21	3.75	1050	92.4	1.48	0.12	143.2	90.2
32.15	3.76	1150	93.3	1.37	0.10	154.7	106.6
42.05	3.78	1150	95.4	1.40	0.07	202.7	139.4
51.94	3.79	1150	96.5	1.41	0.05	250.7	172.2

Table S10. Select data from NMR monitoring of titration (replicate 3) of **2b** with acridine (ACR).

Mass ACR added (mg)	Chemical Shift (ppm)	Total volume sample (μL)	Deprotonated (%)	[1b] (mM)	[1bH$^+$] (mM)	[ACR] (mM)	Equivalents of ACR added
0.05	2.77	501	0.2	0.01	3.35	0.5	0.2
0.07	2.78	501.5	1.6	0.05	3.30	0.7	0.2
0.12	2.81	502.5	3.8	0.13	3.22	1.1	0.4
0.17	2.84	503.5	6.8	0.23	3.12	1.6	0.6
0.25	2.86	505	8.6	0.29	3.05	2.3	0.8
0.37	2.90	507.5	12.4	0.41	2.90	3.5	1.2
0.49	2.93	510	15.1	0.50	2.80	4.8	1.6
0.74	2.98	515	19.7	0.64	2.63	7.2	2.5
0.99	3.02	520	23.7	0.77	2.47	9.7	3.3
1.24	3.05	525	26.5	0.85	2.36	12.1	4.1
1.73	3.12	535	33.1	1.04	2.11	16.8	5.7
2.47	3.18	550	39.0	1.19	1.87	23.7	8.2
3.96	3.29	580	49.2	1.43	1.48	36.5	13.1
5.94	3.39	620	58.3	1.58	1.13	51.7	19.7
8.90	3.48	680	67.5	1.67	0.80	71.3	29.5
12.37	3.55	750	74.1	1.66	0.58	90.3	41.0
17.31	3.63	850	80.8	1.60	0.38	112.0	57.4
22.26	3.67	950	84.6	1.50	0.27	129.2	73.8
27.21	3.70	1050	87.4	1.40	0.20	143.2	90.2
32.15	3.72	1150	89.6	1.31	0.15	154.7	106.6
42.05	3.75	1150	92.1	1.35	0.12	202.7	139.4
51.94	3.77	1150	93.8	1.37	0.09	250.7	172.2

Table S11. Natural population analysis (DKH-PBE0/old-DKH-TZVPP//PBE0/def2-TZVPP) for **1a**-**c**H^+.

Compound	NPA Pn[a] (e^-)	NPA O[b] (e^-)	NPA H[c] (e^-)
1aH^+	2.17761	–1.07558	0.49758
1bH^+	1.84652	–0.98745	0.50877
1cH^+	1.91694	–0.99183	0.53603

[a] Natural population of pnictogen atom. [b] Natural population of O atom. [c] Natural population of protic H atom.

Table S12. Optimized coordinates (PBE0/def2-TZVPP) for **1a**H^+.

Sb	4.857686	3.455658	4.213142
O	5.781276	4.933884	5.05092
C	5.855477	1.81983	5.157928
C	7.152842	1.004911	6.990095
H	7.521315	1.104982	8.003394
C	3.20321	6.432994	4.388681
H	4.029391	6.06504	3.773515
C	7.533061	-0.08743	6.234865
H	8.206765	-0.82586	6.652023
C	5.347469	3.726753	2.145358
C	5.900657	3.116238	7.405674
H	5.159074	3.741067	6.901471
C	6.166257	0.679823	4.397006
C	2.86967	3.89634	4.859413
C	7.096305	4.00072	7.753495
H	7.843621	3.436396	8.315163
H	6.776058	4.837242	8.376893
H	7.570258	4.404315	6.860236
C	2.466086	5.240845	4.967399
C	6.299315	1.981667	6.482806
C	5.56381	0.360859	3.045057
H	4.87471	1.169845	2.774701
C	2.353295	1.375691	5.043859
H	3.285877	1.304749	4.469457
C	2.063065	2.836971	5.306815
C	1.272765	5.492478	5.639078
H	0.93916	6.516617	5.749545
C	7.027358	-0.2564	4.960147
H	7.29335	-1.14031	4.393347
C	6.636466	4.18014	1.804875
C	6.868244	4.509972	0.47225

H	7.847885	4.868382	0.181322
C	0.501881	4.470197	6.157649
H	-0.4161	4.698727	6.685085
C	3.778908	7.324202	5.488734
H	2.975104	7.760534	6.085267
H	4.344343	8.149578	5.051062
H	4.437382	6.769599	6.155138
C	2.30957	7.260068	3.462904
H	1.868149	6.659865	2.667424
H	2.89675	8.055107	3.000074
H	1.495566	7.735997	4.011385
C	1.252832	0.757367	4.180483
H	0.307681	0.718192	4.724175
H	1.515764	-0.2653	3.904437
H	1.083506	1.3286	3.266904
C	4.351757	3.525701	1.175174
C	2.818861	1.620734	0.619119
H	1.893996	1.115422	0.90194
H	3.645156	0.920751	0.748087
H	2.749239	1.85823	-0.44341
C	7.794646	4.329169	2.773724
H	7.504855	3.913852	3.742675
C	8.163692	5.801748	2.972172
H	8.59276	6.215969	2.057801
H	8.903418	5.911357	3.766473
H	7.303845	6.436143	3.211904
C	5.241622	2.600026	8.6847
H	5.936226	2.010144	9.284712
H	4.368756	1.980156	8.479334
H	4.91749	3.44385	9.296156
C	3.007603	2.888554	1.452534
H	2.979443	2.586316	2.506599
C	6.603214	0.263383	1.933641
H	7.345804	-0.50358	2.160401
H	7.126157	1.207138	1.783809
H	6.126355	-0.01009	0.990433
C	4.738357	-0.92567	3.112275
H	4.204713	-1.08367	2.173434
H	4.00959	-0.90197	3.923086
H	5.38209	-1.79184	3.273206
C	9.029696	3.543204	2.335339
H	8.815314	2.480734	2.222892
H	9.816681	3.648005	3.084087
H	9.428654	3.908916	1.388053
C	0.883029	3.155872	5.970979

H	0.248035	2.357885	6.335693
C	5.881167	4.384482	-0.48619
H	6.086467	4.657397	-1.51397
C	2.548084	0.568129	6.322108
H	3.386777	0.939138	6.909617
H	2.741171	-0.47979	6.085195
H	1.654611	0.603708	6.94805
C	1.848944	3.854343	1.23052
H	0.896329	3.363457	1.437702
H	1.823813	4.20226	0.196069
H	1.927569	4.727258	1.877043
C	4.64263	3.881969	-0.13798
H	3.88698	3.748459	-0.90226
H	6.234058	5.499507	4.419825

Table S13. Optimized coordinates (PBE0/def2-TZVPP) for **1b**H^+.

As	6.289453	2.905412	4.344392
O	5.473318	4.237814	3.553247
C	5.323142	1.404029	3.569678
C	4.902389	1.521639	2.226964
C	8.104357	3.177329	3.685703
C	5.914101	3.264246	6.227762
C	4.64512	3.788546	6.568949
C	6.932098	3.118525	7.190626
C	8.229478	2.371248	6.964307
H	8.213554	1.952121	5.955363
C	8.844619	2.069608	3.228417
C	8.561299	4.50172	3.497715
C	6.701118	3.624919	8.465017
H	7.477754	3.53904	9.214626
C	4.931846	0.319215	4.379183
C	7.939822	5.755873	4.090177
H	7.16298	5.461222	4.799085
C	9.706007	4.675272	2.726426
H	10.07226	5.679076	2.553641
C	3.428534	3.869375	5.656167
H	3.645326	3.365663	4.713676
C	3.984628	0.582926	1.764687
H	3.634604	0.654485	0.742724
C	5.497384	4.212858	8.797938
H	5.340167	4.604206	9.795438
C	5.381507	2.565427	1.232451
H	6.161122	3.171411	1.693713
C	8.562025	0.63063	3.607415

H	7.691742	0.613318	4.268412
C	4.479625	4.264753	7.866356
H	3.522101	4.681206	8.152511
C	9.457084	3.269176	7.067218
H	9.447558	4.047414	6.306627
H	10.36762	2.68155	6.936087
H	9.51323	3.748617	8.046242
C	6.010627	1.922482	-0.00458
H	6.868192	1.298123	0.245028
H	6.35471	2.705065	-0.68309
H	5.294994	1.307943	-0.55296
C	9.738746	0.058893	4.403306
H	10.61865	-0.05805	3.768902
H	9.483815	-0.92711	4.796095
H	10.02052	0.700049	5.239446
C	4.003043	-0.57385	3.856587
H	3.673696	-1.40796	4.463733
C	9.975265	2.316781	2.457635
H	10.55037	1.4795	2.08225
C	8.354013	1.195553	7.935942
H	8.495884	1.543573	8.960203
H	9.221286	0.586364	7.675861
H	7.471302	0.55522	7.92439
C	10.38859	3.604671	2.182469
H	11.26664	3.775333	1.571717
C	3.513624	-0.43301	2.572758
H	2.786181	-1.13787	2.189099
C	3.055578	5.324711	5.356317
H	2.697749	5.823617	6.25875
H	2.2598	5.368619	4.611745
H	3.888926	5.934303	4.98999
C	2.213507	3.152265	6.246849
H	2.410008	2.095294	6.420649
H	1.376087	3.224993	5.550858
H	1.89539	3.598191	7.189987
C	8.957115	6.570194	4.893571
H	9.439255	5.981782	5.673305
H	8.453169	7.411767	5.37225
H	9.739175	6.983006	4.255031
C	7.320106	6.643533	3.010071
H	8.094886	7.031348	2.345746
H	6.823883	7.503618	3.464802
H	6.595449	6.104059	2.402864
C	4.511562	0.0275	6.871893
H	4.108369	1.026822	7.026417

H	4.981384	-0.29122	7.80446
H	3.678172	-0.65052	6.678419
C	5.526382	-0.00829	5.734696
H	6.29762	0.732042	5.960494
C	8.252974	-0.26576	2.412771
H	7.337726	0.035121	1.905986
H	8.13114	-1.30056	2.738233
H	9.067917	-0.24716	1.686939
C	4.245332	3.496101	0.811127
H	3.478948	2.948568	0.25865
H	4.62713	4.279537	0.154019
H	3.773244	3.970553	1.66982
C	6.216967	-1.37471	5.697657
H	5.487661	-2.1804	5.601827
H	6.768338	-1.54101	6.624847
H	6.914136	-1.45946	4.86392
H	5.115867	4.861235	4.192602

Table S14. Optimized coordinates (PBE0/def2-TZVPP) for **1c**H^+.

P	8.871935	13.11436	1.997949
O	10.03371	13.73797	2.889692
C	8.504041	14.57381	0.978939
C	6.249361	12.95836	3.06958
C	8.070604	12.03614	4.437406
C	7.612365	12.61648	3.223631
C	8.614216	16.84899	-0.62094
H	8.690013	17.73241	-1.24308
C	9.036313	10.46444	1.009677
C	5.413193	12.85526	4.176055
H	4.372338	13.13555	4.075029
C	9.680701	11.71759	1.153829
C	11.05883	11.86004	0.831759
C	7.178527	11.94611	5.498037
H	7.514311	11.51899	6.434371
C	5.872426	12.38281	5.387569
H	5.204319	12.32007	6.237666
C	8.333645	14.45848	-0.42177
C	8.662883	16.96383	0.754049
H	8.755046	17.94623	1.198494
C	5.594846	13.33069	1.753695
H	6.347822	13.27207	0.967482
C	8.598033	15.85559	1.590686
C	8.613061	16.15188	3.085551
H	8.414819	15.23413	3.637067

C	8.42029	15.60947	-1.19484
H	8.312367	15.52993	-2.2691
C	7.943952	13.18443	-1.14547
H	7.839177	12.38761	-0.40944
C	11.7698	10.70865	0.511722
H	12.82327	10.79357	0.277946
C	9.468646	11.47714	4.687277
H	10.02437	11.44845	3.74501
C	11.8394	13.16711	0.776185
H	11.16278	14.00356	0.937162
C	9.967904	16.70454	3.531835
H	10.78931	16.04068	3.26844
H	9.974076	16.85371	4.613521
H	10.15999	17.6753	3.069964
C	5.021514	14.74305	1.737055
H	4.315734	14.89528	2.555811
H	4.482357	14.91685	0.803839
H	5.803472	15.49567	1.815221
C	4.495957	12.32127	1.40409
H	4.846084	11.29035	1.460165
H	4.133104	12.5041	0.391132
H	3.643599	12.41717	2.078282
C	7.534827	10.25227	1.050735
H	7.055576	11.21743	1.216353
C	9.813081	9.354904	0.699941
H	9.335576	8.387727	0.6056
C	6.575689	13.36098	-1.81361
H	5.822355	13.73733	-1.12093
H	6.228873	12.40545	-2.21127
H	6.633541	14.06162	-2.6477
C	8.965005	12.72325	-2.17992
H	9.170379	13.506	-2.91252
H	8.579903	11.85995	-2.72602
H	9.907673	12.43184	-1.72
C	12.92414	13.22213	1.852026
H	13.68035	12.45195	1.68709
H	12.52202	13.08092	2.854947
H	13.4296	14.18904	1.824802
C	11.17147	9.464566	0.480689
H	11.75855	8.584538	0.247811
C	7.042069	9.731523	-0.30375
H	7.39141	10.3445	-1.13478
H	5.950793	9.717403	-0.32278
H	7.386153	8.711437	-0.48011
C	9.435467	10.02143	5.157477

H	8.915741	9.915249	6.110078
H	10.45586	9.661471	5.299182
H	8.949404	9.372783	4.4305
C	7.513537	17.13905	3.485672
H	7.655643	18.11954	3.029385
H	7.536714	17.28103	4.567738
H	6.518372	16.78548	3.219555
C	10.24114	12.31495	5.716284
H	10.27616	13.38743	5.493789
H	11.26582	11.95345	5.813706
H	9.766916	12.23622	6.69587
C	12.47657	13.38759	-0.59758
H	12.99361	14.34885	-0.60347
H	11.73596	13.40453	-1.39612
H	13.21419	12.62037	-0.83743
C	7.073017	9.311942	2.158751
H	7.576661	8.345589	2.094577
H	6.001172	9.125375	2.068655
H	7.255001	9.728445	3.148346
H	10.21303	13.27149	3.713139

Table S15. Optimized coordinates (PBE0/def2-TZVPP) for *p*-nitrophenol.

O	11.33395	10.01982	8.156644
H	10.56261	9.640683	8.583652
O	10.22561	8.781734	2.159532
O	12.118	9.792252	2.010708
N	11.18103	9.352491	2.644543
C	10.1565	9.027604	4.848025
H	9.335955	8.527676	4.352994
C	11.25741	9.837114	6.824381
C	11.20594	9.520945	4.091593
C	10.1836	9.186219	6.219297
H	9.369111	8.804352	6.82556
C	12.28066	10.17046	4.681044
H	13.08024	10.54144	4.05549
C	12.30656	10.32898	6.049876
H	13.13029	10.83032	6.5406

Table S16. Optimized coordinates (PBE0/def2-TZVPP) for *p*-nitrophenoxide.

O	11.30498	9.975346	8.141701
O	10.21904	8.780122	2.146187
O	12.11221	9.803221	1.989992

N	11.17824	9.359612	2.665552
C	10.16001	9.024365	4.858222
H	9.336234	8.524747	4.364111
C	11.2759	9.836869	6.904521
C	11.20825	9.51894	4.062087
C	10.18747	9.173987	6.214135
H	9.379064	8.792793	6.828996
C	12.28874	10.17388	4.679444
H	13.08539	10.54856	4.049117
C	12.32516	10.32875	6.034416
H	13.1588	10.8335	6.511

Table S17. Optimized coordinates (PBE0/def2-TZVPP) for 2,4-dinitrophenoxide.

O	6.083273	11.73542	6.876694
O	6.877526	12.41523	2.923155
O	1.167935	10.24006	3.422735
O	7.572447	12.45163	4.952385
O	2.502744	10.86709	1.854652
N	6.70983	12.22837	4.09976
N	2.228177	10.666	3.017049
C	5.437052	11.71508	4.555889
C	5.198114	11.49872	5.929822
C	4.468727	11.44576	3.6006
H	4.67253	11.61798	2.553706
C	2.981129	10.73386	5.363384
H	2.010886	10.34878	5.645035
C	3.254463	10.95765	4.014774
C	3.942027	11.00264	6.30457
H	3.760035	10.83885	7.358273
H	6.890721	12.07182	6.425699

Table S18. Optimized coordinates (PBE0/def2-TZVPP) for 2,4-dinitrophenoxide.

O	6.127129	11.68551	6.852463
O	6.760229	12.67159	2.915998
O	1.160534	10.29019	3.426521
O	7.765341	11.90973	4.655477
O	2.490732	10.92459	1.855459
N	6.757286	12.10927	4.007764
N	2.248703	10.71125	3.039069
C	5.494916	11.64795	4.532107
C	5.303401	11.44358	5.970949
C	4.495863	11.43366	3.609212

H	4.688159	11.62865	2.564318
C	3.005694	10.70943	5.373375
H	2.031112	10.3348	5.65753
C	3.257621	10.95766	4.00666
C	3.973558	10.94223	6.294121
H	3.79361	10.76541	7.348216

Table S19. Optimized coordinates (PBE0/def2-TZVPP) for 2,4,6-trinitrophenol.

O	6.997438	3.555826	10.28335
O	6.51942	5.615749	11.9503
O	7.571542	1.242428	9.472688
O	9.367461	0.253237	10.10184
N	8.619071	1.192469	10.11962
O	12.38459	2.287312	13.14263
N	7.716904	5.753361	11.90637
O	8.322346	6.799038	11.983
C	8.100951	3.46676	10.97676
C	8.956331	2.339161	10.94286
C	8.531224	4.537859	11.78539
C	10.13221	2.277337	11.66791
H	10.75385	1.394457	11.62302
N	11.73475	3.305998	13.20949
C	9.711056	4.501444	12.48659
H	10.02093	5.35501	13.07379
O	12.01853	4.285332	13.86136
C	10.49369	3.359016	12.43532
H	6.914601	2.707239	9.783846

Table S20. Optimized coordinates (PBE0/def2-TZVPP) for 2,4,6-trinitrophenoxide.

O	7.213539	3.627223	9.99123
O	6.552728	5.654361	11.75563
O	7.509566	0.877335	9.934185
O	9.604801	0.445926	9.720113
N	8.678163	1.139481	10.11707
O	12.34863	2.264832	13.20057
N	7.754798	5.752113	11.86921
O	8.334755	6.798323	12.1265
C	8.124653	3.504032	10.79203
C	9.002511	2.328087	10.88047
C	8.55684	4.553238	11.72645
C	10.14419	2.27724	11.62858
H	10.76355	1.392057	11.60561

N	11.67556	3.286322	13.24029
C	9.700009	4.495837	12.47098
H	9.97543	5.329942	13.10031
O	11.96055	4.250557	13.93816
C	10.50146	3.357063	12.43257

Table S21. Optimized coordinates (PBE0/def2-TZVPP) for **3**$^{+}$.

P	1.517571	16.0625	10.61671
O	0.581484	17.31536	10.33881
C	3.277606	15.13647	8.633907
C	2.918345	16.80137	11.51992
C	0.421532	14.96228	11.5576
C	0.327287	13.56824	11.3878
C	1.43951	15.62663	6.591065
H	0.730254	15.77421	5.786891
C	1.950944	15.53268	8.938991
C	3.655368	15.0877	7.298288
H	4.670332	14.80555	7.048531
C	0.992006	15.70366	7.90504
C	-0.72796	12.90667	12.01126
H	-0.82459	11.83614	11.88143
C	3.4182	16.27237	12.73261
C	2.759893	15.36404	6.284536
H	3.08187	15.33368	5.250751
C	-0.48626	15.64801	12.4009
C	1.330335	12.72463	10.6345
H	2.145851	13.37384	10.3178
C	-1.63694	13.57396	12.80516
H	-2.44411	13.02994	13.28023
C	3.389612	18.05161	11.0309
C	-1.5048	14.93655	13.01344
H	-2.20463	15.44712	13.6599
C	3.134659	14.88022	13.26202
H	2.536579	14.34293	12.52714
C	4.292449	14.62882	9.645134
H	3.830319	14.62822	10.63411
C	2.348593	14.90672	14.57099
H	2.910577	15.41932	15.35397
H	2.155288	13.8896	14.91724
H	1.388374	15.4117	14.46255
C	4.284308	17.05535	13.48769
H	4.656346	16.67026	14.42854

C	4.663801	13.17664	9.321269
H	5.272383	13.12085	8.417542
H	3.787597	12.54717	9.164734
H	5.250498	12.75212	10.13805
C	1.930447	11.64636	11.53939
H	1.186874	10.89325	11.80409
H	2.3296	12.05961	12.46632
H	2.741847	11.13348	11.02021
C	4.432977	14.09002	13.44323
H	5.026947	14.0613	12.52859
H	4.206877	13.06247	13.73391
H	5.056369	14.51896	14.22879
C	-0.49919	15.93783	8.097184
H	-0.74557	15.83156	9.153419
C	3.043368	18.68872	9.690351
H	2.39172	18.02831	9.124096
C	-0.91401	17.33544	7.636975
H	-0.75097	17.45088	6.56358
H	-0.35356	18.1186	8.145865
H	-1.97851	17.49298	7.822109
C	-1.3346	14.89121	7.355939
H	-2.3915	15.0492	7.57846
H	-1.08077	13.87318	7.650036
H	-1.21758	14.9665	6.274043
C	0.734502	12.08732	9.383147
H	1.476882	11.45615	8.890706
H	0.406669	12.83956	8.667546
H	-0.1211	11.45586	9.630306
C	5.563503	15.46752	9.732182
H	6.283087	14.98375	10.39545
H	5.369169	16.46526	10.12089
H	6.038444	15.5662	8.754201
C	4.694575	18.30001	13.05713
H	5.366087	18.89345	13.66552
C	4.270269	18.77068	11.83075
H	4.633099	19.72755	11.47787
C	4.28981	18.90592	8.830216
H	5.006296	19.57439	9.310383
H	4.000775	19.36265	7.881923
H	4.798383	17.96899	8.607331
C	2.307851	20.01551	9.875366
H	1.411562	19.90569	10.48476
H	2.01115	20.41801	8.905235
H	2.945134	20.75918	10.35767
C	-0.35294	17.1385	12.59979

H	0.641855	17.34196	13.01518
C	-1.37857	17.77258	13.52382
H	-1.17998	18.8405	13.623
H	-1.33635	17.33883	14.52289
H	-2.39561	17.65643	13.14365
C	-0.41168	17.80976	11.24288
H	-1.38487	17.64766	10.77149
H	-0.24233	18.88289	11.3329

Table S22. Optimized coordinates (PBE0/def2-TZVPP) for **3**$^{+}$(As).

As	1.542823	16.03719	10.61796
O	0.517359	17.42601	10.33048
C	3.304847	15.09004	8.524603
C	3.019531	16.87136	11.57843
C	0.330011	14.91123	11.62266
C	0.256106	13.5201	11.47532
C	1.471845	15.56977	6.473255
H	0.764201	15.71744	5.667361
C	1.985399	15.49949	8.80826
C	3.681683	15.00563	7.189398
H	4.692893	14.70496	6.945124
C	1.026543	15.67835	7.787384
C	-0.79509	12.86543	12.11353
H	-0.88447	11.79087	12.01355
C	3.528651	16.30983	12.7643
C	2.786318	15.27222	6.172033
H	3.105	15.21138	5.138637
C	-0.57566	15.62826	12.42933
C	1.268103	12.68971	10.72113
H	2.077503	13.35278	10.40535
C	-1.71121	13.55243	12.88396
H	-2.51631	13.01664	13.37169
C	3.470358	18.1188	11.09184
C	-1.59434	14.92225	13.05288
H	-2.30517	15.44361	13.67856
C	3.209825	14.91874	13.27115
H	2.581879	14.41539	12.53301
C	4.306218	14.61651	9.561315
H	3.839466	14.67441	10.54913
C	2.436748	14.94904	14.5874
H	3.023626	15.42901	15.3728
H	2.210033	13.93375	14.91822
H	1.494672	15.4909	14.49591
C	4.429053	17.06756	13.50593

H	4.821888	16.66393	14.43074
C	4.653054	13.14446	9.316414
H	5.244452	13.03092	8.406632
H	3.764019	12.52235	9.209021
H	5.247929	12.75576	10.14496
C	1.884975	11.61706	11.6191
H	1.147496	10.86129	11.89331
H	2.290212	12.03632	12.54078
H	2.693511	11.10675	11.09305
C	4.481438	14.08142	13.41726
H	5.059655	14.05229	12.49254
H	4.226995	13.05626	13.69208
H	5.130697	14.47479	14.20076
C	-0.45476	15.94094	7.994699
H	-0.68079	15.86533	9.059049
C	3.057788	18.77494	9.783762
H	2.397696	18.10778	9.23173
C	-0.85154	17.33682	7.516155
H	-0.6926	17.43536	6.440364
H	-0.2771	18.115	8.016557
H	-1.91231	17.51289	7.705758
C	-1.31559	14.89022	7.290725
H	-2.36699	15.06413	7.526679
H	-1.06675	13.87507	7.59967
H	-1.21413	14.94352	6.205819
C	0.672386	12.05665	9.467535
H	1.421529	11.45032	8.954707
H	0.314729	12.81212	8.769328
H	-0.1648	11.40284	9.719417
C	5.584935	15.44646	9.609046
H	6.287763	15.00978	10.32107
H	5.39551	16.47398	9.914723
H	6.076924	15.46415	8.634769
C	4.844531	18.31271	13.07835
H	5.544914	18.88577	13.67348
C	4.384892	18.81452	11.87688
H	4.743704	19.77613	11.53224
C	4.257687	19.04788	8.876233
H	4.975666	19.72494	9.341609
H	3.915388	19.51938	7.953292
H	4.782456	18.13146	8.607405
C	2.289747	20.07056	10.04079
H	1.425855	19.90741	10.68409
H	1.938522	20.49353	9.097971
H	2.926458	20.81701	10.51999

C	-0.45037	17.12601	12.57941
H	0.553027	17.35043	12.96522
C	-1.45861	17.76513	13.51965
H	-1.25644	18.83286	13.61
H	-1.40279	17.33419	14.51935
H	-2.48188	17.65056	13.15573
C	-0.54678	17.77553	11.20822
H	-1.49526	17.50634	10.73098
H	-0.51049	18.8624	11.30775

Table S23. Optimized coordinates (PBE0/def2-TZVPP) for **3**$^{+}$(Sb).

Sb	1.575269	16.04027	10.62815
O	0.430463	17.58398	10.4121
C	3.331053	15.00889	8.354546
C	3.19324	16.95923	11.66451
C	0.203432	14.84589	11.707
C	0.172197	13.45399	11.58581
C	1.480991	15.47654	6.311214
H	0.767636	15.62795	5.510558
C	2.027835	15.45452	8.635452
C	3.68412	14.85699	7.017788
H	4.682763	14.51905	6.768847
C	1.064856	15.64494	7.6292
C	-0.87874	12.78139	12.20635
H	-0.93552	11.70212	12.13441
C	3.735203	16.35133	12.80649
C	2.778167	15.11178	6.005234
H	3.077409	14.99711	4.970567
C	-0.7542	15.56925	12.44213
C	1.215745	12.65247	10.84279
H	2.0167	13.33827	10.5374
C	-1.84229	13.46742	12.91833
H	-2.65012	12.92412	13.39322
C	3.627631	18.21098	11.19534
C	-1.77783	14.84631	13.042
H	-2.53546	15.36056	13.61652
C	3.340962	14.97765	13.30297
H	2.699539	14.50867	12.54679
C	4.337621	14.59302	9.407796
H	3.883642	14.72828	10.39833
C	2.529098	15.05959	14.59341
H	3.124617	15.49686	15.3972
H	2.213957	14.06449	14.91272
H	1.635707	15.67335	14.46876

C	4.698452	17.06091	13.51659
H	5.128134	16.62628	14.41073
C	4.665633	13.10457	9.275061
H	5.203778	12.90644	8.346809
H	3.766635	12.48654	9.273135
H	5.303732	12.78274	10.10011
C	1.852727	11.589	11.73524
H	1.127966	10.81912	12.00457
H	2.244675	12.01392	12.66026
H	2.672604	11.09481	11.21121
C	4.552822	14.06444	13.47453
H	5.143731	13.99952	12.55934
H	4.232771	13.05703	13.74601
H	5.210523	14.41847	14.26978
C	-0.39042	15.98426	7.878504
H	-0.5753	15.9508	8.955973
C	3.112857	18.90124	9.947393
H	2.425257	18.2326	9.42118
C	-0.73553	17.38839	7.388013
H	-0.59297	17.46709	6.308199
H	-0.1177	18.14457	7.871389
H	-1.78255	17.61622	7.597601
C	-1.32271	14.95158	7.244133
H	-2.35737	15.1747	7.510244
H	-1.09925	13.93792	7.578158
H	-1.25577	14.96614	6.155131
C	0.646079	12.02317	9.574603
H	1.419082	11.46605	9.041897
H	0.244597	12.77763	8.898163
H	-0.1575	11.32529	9.817444
C	5.614641	15.42595	9.382602
H	6.313125	15.07142	10.14282
H	5.415546	16.4792	9.575836
H	6.113112	15.34597	8.414767
C	5.123488	18.30686	13.09526
H	5.874647	18.84199	13.6632
C	4.602608	18.86525	11.94385
H	4.958729	19.83323	11.6137
C	4.234447	19.23124	8.963561
H	4.960863	19.92044	9.396867
H	3.817407	19.7118	8.076899
H	4.769834	18.33846	8.639421
C	2.326063	20.16036	10.30554
H	1.501953	19.93606	10.98198
H	1.914027	20.61638	9.403621

H	2.969719	20.8995	10.787
C	-0.68415	17.07838	12.56178
H	0.296137	17.34275	12.98422
C	-1.74465	17.68806	13.46556
H	-1.57626	18.76108	13.56055
H	-1.71665	17.25927	14.46733
H	-2.74955	17.54525	13.06211
C	-0.74666	17.73827	11.18521
H	-1.6119	17.35593	10.62959
H	-0.88026	18.81592	11.31016

Table S24. Optimized coordinates (PBE0/def2-TZVPP) for H_2.

H	1.213722	16.39218	10.49317
H	0.776893	16.97779	10.34751